HEAT TRANSFER IN CRYOGENIC VAPOUR COLUMNS

J. BOARDMAN

A THESIS SUBMITTED FOR THE DEGREE OF
DOCTOR OF PHILOSOPHY
OF THE UNIVERSITY OF SOUTHAMPTON

DEPARTMENT OF PHYSICS
JANUARY 1974

ABSTRACT

But a literate age,unbenighted by creed,
Can find on two boards all it wishes to read;
For the back of the cover shows somebody shot
And the front of the cover will tell you the plot.

Commercial Candour
G.K. Chesterton

ABSTRACT

FACULTY OF SCIENCE

PHYSICS

Doctor of Philosophy

HEAT TRANSFER AND FLUID FLOW IN CRYOGENIC VAPOUR COLUMNS

by John Boardman

The complex fluid flow and heat transfer mechanisms in the cryogenic vapour column above both boiling liquid nitrogen and liquid helium are investigated by visual and non visual methods.

It has been found that the vertical upward flow in the vapour column is contained within a thermally induced boundary layer attached to the wall, while the major portion of the vapour column suffers a small reverse flow with a non-uniform negative velocity profile. The experimental detail and results on vertical temperature profiles, boundary layer thickness, and negative peak velocities are presented. A Bessel solution is extended to the free convection limit to describe the almost linear variation of boundary layer thickness with vertical distance and the off-axial position of, and near uniform velocity of, the peak reverse flow. Thermosyphoning effects and the existence of a turbulent zone above the liquid are briefly described.

The heat transfer from a small heated surface within the vapour column has also been investigated, and the experimental detail and results are presented. An analysis is sought which describes the effects of both free convection and gaseous conduction.

CONTENTS

INTRODUCTION

I mean to write with all my strength
(It lately has been sadly waning)
A ballad of enormous length-
Some parts of which will need explaining.

Dedicatory Ode
H. Belloc

INTRODUCTION

In the study and analysis of problems concerned with the heat transfer between a cryogenic vapour and a solid surface, it has been previously assumed that the heat exchange was either "perfect" or could be described by an overall coefficient. This is the case, for example, in the problem of the minimisation of heat inleak for vapour cooled cryogenic support tubes, and the optimum design of current leads to superconducting solenoids (Scott[1], Williams, Donnadieu and Dammann). The detailed fluid flow behaviour and heat transfer mechanisms in the cryogenic vapour column do not seem to have been explicitly considered.

Although these assumptions have been shown to be justifiable in terms of overall experimental results, the lack of fundamental information and understanding must lead to either an uncertainty in the predicted behaviour of more complex systems, or unresolved experimental features, such as the distribution of heat fluxes and the existence of horizontal temperature profiles (Lynam and Scurlock (1968)).

Initially it was hoped in this investigation to try to establish a meaningful heat transfer coefficient which could be used in detailed design studies. For this purpose a series of experiments on isolated heaters in the vapour column were designed which would show the variation of heat transfer with heat flux, temperature level, and vapour property and geometric effects. However, on looking at the environment to the heater it was observed that the column of vapour in the dewar appeared to be stationary; and later complex flows were observed. This led to a further series of experiments which investigated this curious and interesting behaviour.

Owing to the scope of the experimentation required and the complexity of the interacting factors it has not been possible to investigate all the various influences on the heat transfer nor to make an accurate quantative analysis. Rather an attempt has been made to gather sufficient information, within the time available, to characterise the problem, both for an understanding of the behaviour of these types of systems and as a broad base for the design of future experiments.

CHAPTER 1

"If the Lord Almighty had consulted me before embarking on the creation, I should have recommended something simpler."

Alphonso X of Castile

LITERATURE SURVEY

Breadth of Review

The effect of natural convection on temperature and flow fields has been extensively investigated for many physical situations. Of particular relevance are the cases of heated plane surfaces and enclosed spaces, vertical forced flow, and stratification in cryogenic vessels. By reviewing and extending certain features of these three cases it is possible to gain an understanding of the behaviour of vapour above cryogenic liquids.

The first section deals with the important limiting case of free convection from heated flat plates, and presents some of the underlying assumptions and conclusions. The second section deals with natural convections in tubes showing the influence of the boundaries and possible temperature stratification. The last section describes the effects of mixed free and forced convections and presents a useful Bessel solution for flow problems.

I - Free Convections from Plane Surfaces

Theoretical Analysis

Following the work of Lorenz, Schmidt and Beckmann investigated the behaviour of laminar free convections around heated plates in air. They used a quartz fibre deflection anemometer to measure the air velocities and fine thermocouples to measure the temperatures. With these results and with the aid of Pohlhausen they solved the partial differential equations governing the temperature and velocity fields.

In two dimensions, with vertical x axis, and D_x representing partial differentiation with respect to co-ordinate x etc, we have

$$D_x U + D_y V = 0$$

$$U D_x U + V D_y U = \nu (D_x^2 U + D_y^2 U) + g\beta t(T_s - T_o)$$

$$U D_x V + V D_y V = \nu (D_x^2 V + D_y^2 V)$$

$$U D_x t + V D_y t = \alpha (D_x^2 t + D_y^2 t)$$

where

$$t = \frac{T - T_o}{T_s - T_o}$$

with T_o as the environment temperature

T_s as the surface temperature

the boundary conditions are:

$$y = 0 \quad U = 0 \quad V = 0 \quad t = 1$$

$$y = \infty \quad U = 0 \quad t = 0$$

Under the approximations

$$D_x^2 U \ll D_y^2 U$$

$$D_x^2 t \ll D_y^2 t$$

$$V \ll U$$

the equations reduce to the following

$$D_x U + D_y V = 0$$

$$U D_x U + V D_y U = \nu D_y^2 U + g\beta t(T_s - T_o)$$

$$U D_x t + V D_y t = \alpha D_y^2 t$$

These equations represent the motion of a two dimensional incompressible fluid flowing up a vertical heated plate, with a laminar boundary layer whose thickness is negligible in comparison to its length. No allowance has been made for property changes due to temperature, except in the buoyancy term. Also the fluid has been assumed to enter the boundary layer horizontally.

If the stream function E is introduced where:

$$U = D_y E$$

$$V = - D_x E$$

then the equation of continuity is automatically satisfied.

Pohlhausen suggested introducing the new variables

$$p = C_1 y (x)^{-\frac{1}{4}}$$

$$C_1 = (g(T_s - T_o)\beta/(4\nu^2))^{\frac{1}{4}}$$

and

$$X(p) = t(x,y)$$

$$W(p) = (E(x,y)/(4\nu C_1^4)).x^{-\frac{3}{4}}$$

On substitution, the set of partial differential equations reduce to two ordinary differential equations (prime denotes ordinary differentiation).

$$W''' + 3W W'' - 2(W')^2 + X = 0$$

$$X'' + (3\nu/\alpha)W X' = 0$$

with the boundary conditions

$$W = 0 \quad W' = 0 \quad X = 1 \quad p = 0$$

$$W' = 0 \quad W'' = 0 \quad X = 0 \quad p = \infty$$

Pohlhausen expanded the terms of the differential equation into a convergent series and numerically integrated using the experimentally determined values of $W'' = 0.675$ and $X' = -0.508$ at $p = 0$ $(y=0)$.

The heat transfer coefficient may be calculated from

$$h_c = - k(D_p X)_{y=0} (D_y p)_{y=0}$$

$$= - k X_o' C_1 x^{-\frac{1}{4}}$$

and using the value $X_o' = -0.508$ and integrating we obtain

$$h_{c_{mean}} = 0.479 \frac{k}{L} (g L^3 (T_s - T_o) \beta / \nu^2)^{\frac{1}{4}}$$

or

$$N_{u_m} = 0.479 G_{r_L}^{\frac{1}{4}}$$

which differs only in the constant (0.507) from Lorenz's earlier result. This work has been extended by both Sparrow (1956) and Ostrach (1952) to cover the range $0.00835 \leqslant P_r \leqslant 1000$.

The agreement of the analysis with experiment for the heat transfer was excellent in the case of small plates and within 4% for the large plates. Jakob[1] mentions that the work of Lorenz and the later work of Weise show a shift of 25% above the Schmidt and Beckmann analysis. This, he comments, may be due to the motions of the air around the edges of the plate. Schmidt and Beckmann observed that even a small disturbance around the edges increased the heat transfer by appreciable percentages.

Constant Flux and Constant Temperature Boundary Conditions

Sparrow and Gregg (1956(ii)) used a similar form of analysis to compare the constant flux boundary condition with that of the constant temperature wall. Using a modified form of the Grashof number (the product of Grashof and Nusselt) they compared the value of the average constant flux Nusselt number, based on either the mean temperature difference or the temperature halfway along the plate, with the value as obtained from the constant temperature wall analysis by Ostrach (1953). The analyses differed by less than 8%, and in particular for a Prandtl number of unity were 6.6% different using an averaged temperature difference, and 1.5% different using the midpoint temperature difference.

They also comment that if a comparison between the two analyses is made of local Nusselt numbers, where either the fluxes are equal, or the temperature differences are equal, then the agreement is better

than 15%. This suggests that the upstream variations of temperature or flux only moderately affect the local heat transfer.

A more detailed account of temperature and flux variation effects is given by Sparrow (1955) who uses a von Karman-Pohlhausen method to solve the equations. This integral method will be demonstrated in a later section which deals with free convection in stratified fluids.

Turbulent Free Convections

Griffiths and Davis using a combined resistance thermometer and hot wire anemometer plotted the temperature and velocity field close to a heated plate. They carefully examined the influence of vertical height and the temperature excess on the heat transfer. Through dimensional analysis they were able to reduce the data to a single line. The curve had a point of inflection and they found that this point of minimum heat loss was followed by a region where the heat loss was independent of the height. They concluded that the air was in rolling motion above a critical height, and this height was dependent on the boundary conditions.

Unlike laminar flow, tubulence is difficult to analyse theoretically. A recent paper by Kwang-tzu Yang and Nee points out that, although some progress has been made in establishing a theory of overall heat transfer by such methods as those employed by Eckert and Jackson, it has not been possible to predict detailed behaviour of the turbulent layer. They go on to say their own work shows that the turbulent free convection layer is characterised by convection, diffusion, generation and decay of turbulence. They further suggest that the behaviour of the boundary layer can be described by three regions, a viscous sublayer next to the wall, an inner layer characterised by an approximate balance between turbulent generation and decay, and an outer layer governed mainly by turbulent convection and diffusion. Increasing the Grashof number (natural convection influence) is seen to influence turbulent generation

and decay more than diffusion and convection.

Unheated Starting Lengths

In their paper Sparrow and Gregg (1956(i)) comment that futher information is required on the effects of unheated starting lengths on the heat transfer from a vertical plate. From the results of Dotson and the work of Sparrow (1955) they suggested that non-uniform heat flux distributions were felt principally in the neighbourhood of the leading edge. Bevans, using interferometric methods, examined this question and concluded that for $10^3 < G_r < 10^8$ there was no noticeable difference between the heat transfer with and without an unheated starting length. He did notice secondary flows along the edges of the test plate but was unable to quantify these precisely owing to lack of knowledge of the heated path length. From the sharpness of the image he considered that the effect was small.

Variable Property Effects

Finally, Sparrow and Gregg (1958) examined the variable fluid property problem in free convection. They used the normal stream function type solution but retained the temperature dependent terms within the dependent and independent variables of the differential equation. These were then solved numerically for gases having prescribed temperature dependent properties. The thermal conductivity and viscosity were considered to vary either as power laws or according to a Sutherland type formula with the specific heat and Prandtl number constant, except for one case, where a linear variation in specific heat was considered. The solutions were then compared with the constant property solution. With a suitable choice of reference temperature at which to evaluate the properties of the gas, it was possible to make the solutions agree closely. Four reference temperatures were chosen; wall, ambient, arithmetic mean or

film temperature and a special one defined:

$$T_r = T_s - 0.38(T_s - T_o)$$

In the range $\frac{1}{4} \leqslant T_s/T_o \leqslant 4$ the deviation of the two solutions for power law variations and constant specific heat and Prandtl number was 0.6% when evaluated at the special reference temperature. The film temperature gave results which were within 1% at the higher temperature ratios. The other reference temperatures gave errors of five to ten per cent.

II - Free Convections in Tubes

Closed Ended Convections - Thermosyphons

The problem of free convection in closed isothermal tubes has been solved theoretically, for the special case of thermosyphons, by Lighthill using the Karman-Pohlhausen technique. Martin and Cohen and later Martin describe experiments on thermosyphons designed to test the validity of Lighthill's predictions on both laminar and turbulent flow for a range of length to diameter ratios and Prandtl numbers. Lighthill shows that the variation of laminar heat transfer with increasing modified Rayleigh number (based on the radius) is characterised by three flow regimes.

The first flow regime, which applies for low values of the modified Rayleigh number, is called impeded similarity flow. That is, the velocity and temperature profiles are similar at each section, retaining their shape and only changing linearly in magnitude with vertical distance. The similarity solution gives a unique value of the modified Rayleigh number, and for values less than this (e.g. longer tube) the flow will not fill the whole length of the tube. The excess length will in fact be filled with stagnant fluid.

At higher values of the modified Rayleigh number a second flow regime is predicted, where the flow, as before, fills the whole width of the tube, but variation of the profile shape is permitted in the vertical direction. This is described as 'non-similarity with boundary layer filling the tube' or 'impeded non-similarity'. The Nusselt variation is for the most part linear with modified Rayleigh number as it is in the first regime. However impeded non-similarity goes through a maximum in the Nusselt number and shortly afterwards ends abruptly. The Nusselt number has a mathematical discontinuity between this regime and the third regime. This can be seen by reference to Figure 1.

The final regime is described as having 'flow with boundary layer not filling the tube'. This is unimpeded flow, in that the cool fluid

FIGURE 1 NUSSELT NUMBER VERSUS MODIFIED RAYLEIGH NUMBER

THERMOSYPHONS--(LIGHTHILL)

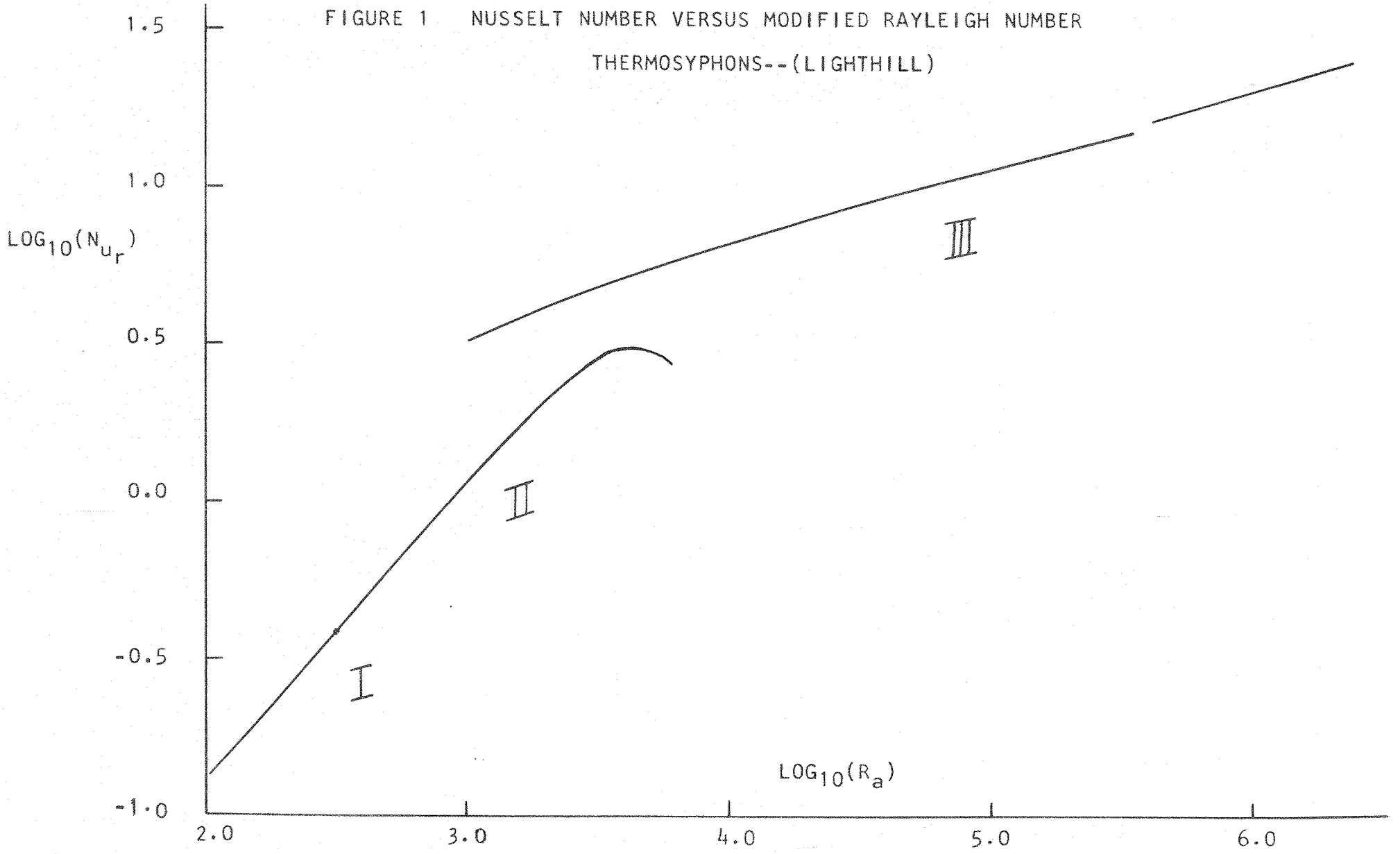

entering the thermosyphon penetrates to the closed end of the tube before being drawn into the boundary layer and warmed. The Nusselt number varies initially as a 0.27 power law of modified Rayleigh number, and extends in the limit to a 0.25 power law, similar to free convection from a vertical plane surface.

Lighthill briefly discusses the transition from impeded non-similarity to free boundary layer flow, and comments that this will occur at the earliest opportunity when the temperature profile has a flat portion in the centre. However, Martin and Cohen showed experimentally that the transition across the mathematical discontinuity is resolved in practice by a long period oscillation which is not attributable to turbulence. It is said to be an oscillation between boundary layer flow and impeded non-similarity flow, and occurs in the following manner. The establishment of a boundary layer with its higher fluid velocities leads to a rapid intake of fluid into the tube, and consequently a reduction in the pre-heating time of fluid near the orifice. The heat transfer is therefore reduced and the boundary layer flow begins to decay. This allows the incoming fluid to mingle with boundary layer and is thereby warmed. The heat transfer is enhanced and the boundary layer flow is restored, thus completing the cycle.

Lighthill also analysed the transition to turbulence and the resulting heat transfer. He concluded that the transition would arise in laminar impeded flow and the turbulent mixing of the hot and cold streams would markedly reduce the heat transfer, increasing only at high modified Rayleigh numbers, when a turbulent boundary layer would be formed. Martin,however, found that turbulence could arise either from laminar impeded flow or boundary layer flow, depending on the Prandtl number. The characteristic was that for the former transition the whole fluid became turbulent simultaneously, whereas in the latter case turbulence occurred at the edge of the boundary layer. Both types lead to a stable

'fully mixed' turbulent flow where the fluid was turbulent from entry. Unlike Lighthill's prediction, the turbulent boundary layer appeared as a transition mode rather than an end point.

The experimental work has been extended from the isothermal case by Hartnett and Welsh to include the constant flux boundary condition. Their own limited results are in agreement with those of Martin, and noting that both Sparrow and Gregg (1956(i)) for free convections and Seban and Shimazaki for forced convections obtained similar results for both boundary conditions, they conclude that Martin's results can be applied generally to the constant flux boundary condition.

Open Ended Convections

At the other extreme to Lighthill, Elenbaas has analysed the problem of free convections in open ended tubes for uniform wall temperature conditions. He assumes velocity and temperature profiles, and determines the constants by substitution into a set of simplified, partial differential, boundary layer equations. He then evaluates the temperature profile at the wall and integrates over the height of the tube. The resulting Nusselt equation is then found to be exponentially dependent on height and Grashof number. Because of the assumptions made the constant in the exponential term has to be adjusted to give the correct asymptotic behaviour. That is a parabolic velocity distribution and a horizontal temperature profile for narrow tubes, and a free convection boundary layer flow for large diameter tubes.

Restricted Convections

Dyer, using a finite different scheme very similar to that used by Bodoia and Osterle, numerically solved the problem of free convections in tubes with open upper ends and varying degrees of flow restriction at the lower end. He found that, depending upon the size of the

FIGURE 2 NUSSELT NUMBER VERSUS MODIFIED RAYLEIGH NUMBER

RESTRICTED DUCTS--(DYER)

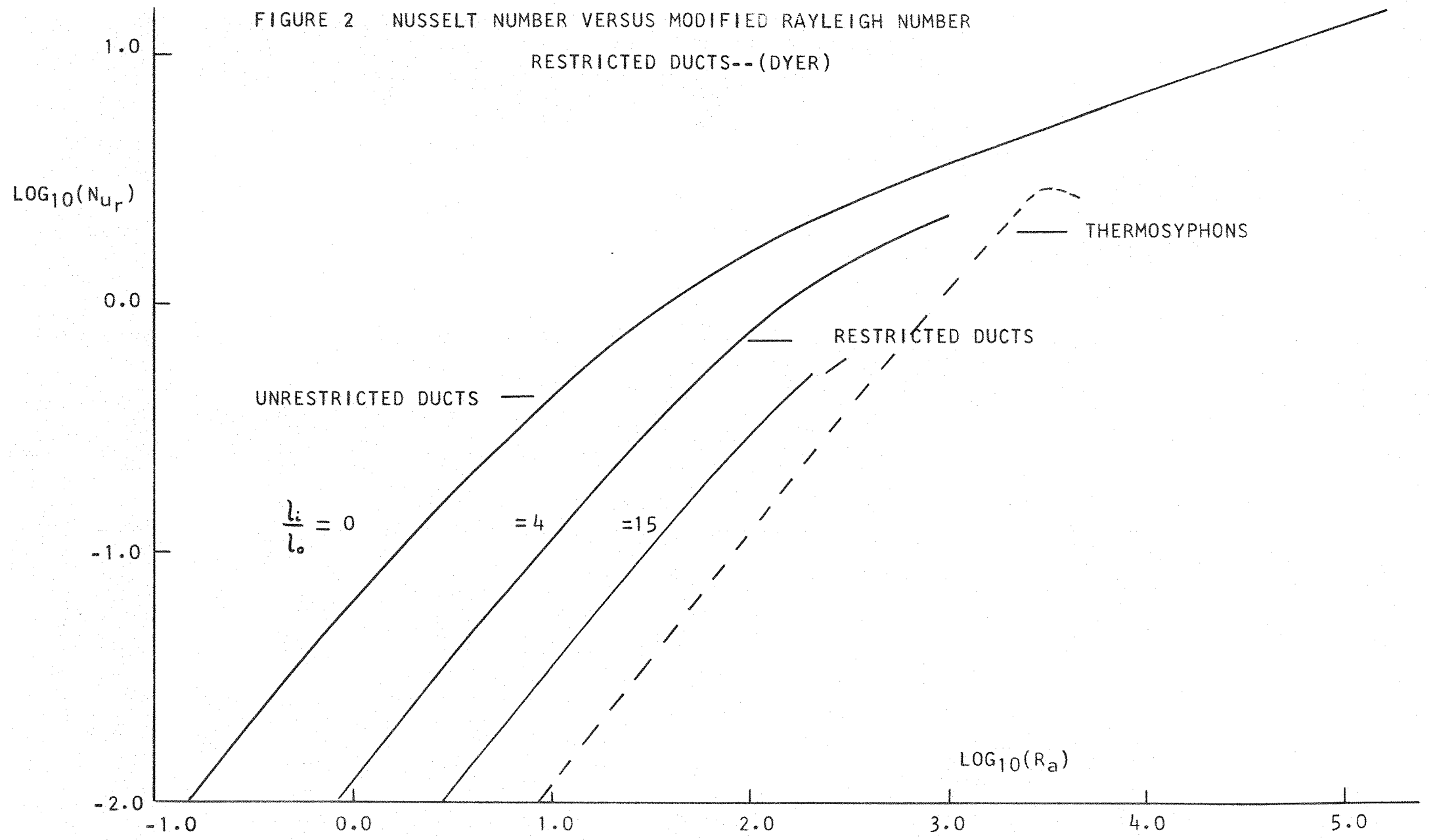

restriction, naturally convective forces caused fluid to enter at the bottom alone or at the bottom and top together. His analysis bridged the work of Elenbaas and Lighthill, although he was not able to describe all the possibilities. The row by row relaxation technique employed was unsuitable for situations in which the velocity became negative. This limitation meant that the thermosyphoning effects which produced negative velocities in the upper part of the tube, as the restriction became too great, could not be analysed. In general, Dyer considers that when the flow is supplemented by thermosyphoning a rather complicated and unstable flow will be produced at the upper end.

However, unlike the work of Lighthill, his analysis does not produce a discontinuity in the Nusselt number and no long period oscillations are reported in the experimentation.

The Nusselt variation between the convection limits of Elenbaas and Lighthill, as given by Dyer, can be seen in Figure 2.

Boundary Layers in Stratified Environments

A further feature of naturally convective flows arises in the study of heat transfer and fluid flow in stratified fluids. Schwind and Vliet investigated the behaviour of water between heated vertical plates using both temperature measurements and Schlieren photography. They demonstrated the formation of a boundary layer at the wall and a reverse shear layer close to the boundary between stratified and unstratified fluid. This 'reverse shear layer' consisted of fluid pealing away from the normal direction of the boundary layer and reversing its flow direction. In the stratified fluid the boundary layer was seen to become thinner with vertical distance.

Their conclusions are mainly qualitative and hinge around the expected behaviour of boundary layers in adverse temperature gradients. If the temperature outside the boundary layer is reasonably uniform

the boundary layer will grow in width and increase in velocity. In this case the rate of diffusion of heat across the boundary layer is sufficient to warm additional mass and to set it in motion. However if the temperature outside the boundary layer increases owing to stratification there will be a loss of buoyancy, and hence the rate of acceleration on the outer layers will be changed. The resulting flow is dependent upon the degree of adverse gradient and Schwind and Vliet describe three cases. The first shows the flow in moderate adverse gradients where the deceleration due to loss of buoyancy is exactly counterbalanced by the acceleration due to heating. That is, the rate of growth due to heating and the rate of decay due to temperature gradient are exactly matched. This results in a boundary layer which does not grow with vertical distance. If the temperature gradient is increased the decelerating force will dominate and the boundary layer will be seen to lose mass and become thinner with vertical distance. The fluid decelerates and simultaneously comes to rest in a region where it is in temperature equilibrium. The situation can however be envisaged where the adverse temperature gradient is so large (and possibly sudden) that the momentum of the fluid causes it to overshoot its own equilibrium temperature level, and the resulting downward force will result in reverse flow.

Evans, Reid and Drake have investigated the flow in closed containers both experimentally and analytically. They use a similar model in their analysis to that used by several authors where the flow is divided into three regions. These are; a thin boundary layer rising along a heated wall, a mixing region at the top where the boundary layer discharges and mixes with the upper core fluid, and a main core region which slowly falls in plug flow. The core temperature is assumed to vary in the vertical direction but not in the horizontal direction. These assumptions have been shown to be justified (Tatom and Carlson, Barakat and Clark).

An important part of their analysis is the solution of the free convection equations for a varying bulk temperature. Their formulation of the problem is similar to that used by Sparrow using an integral form of the boundary layer equations due to von Karman and polynomial approximations to the temperature and velocity profiles due to Pohlhausen. Unlike Sparrow, however, the authors consider an extra term in the energy equation which results from the bulk temperature variation.

As before we have

$$D_x U + D_y V = 0$$

$$U D_x U + V D_y U = \vartheta D_y^2 U + g\beta(T - T_o)$$

$$U D_x T + V D_y T = \alpha D_y^2 T$$

Integrating the momentum equation over the width of the boundary layer and combining the product rule of differentiation and the equation of continuity we have

$$\int U D_x U\, dy + \int V D_y U\, dy = \int \vartheta D_y^2 U\, dy + \int g\beta(T - T_o)dy$$

now $$\int V D_y U\, dy = V U\Big| - \int U D_y U\, dy$$

and $$D_y V = - D_x U$$

hence $$2\int U D_x U\, dy = \int g\beta(T - T_o)dy + \vartheta \int d D_y U$$

and since $2U D_x U = D_x(U^2)$

then $$D_x \int U^2\, dy = \int g\beta(T - T_o)\, dy + \vartheta \left[D_y U\right]_o$$

Similarly we can write

$$D_x \int U(T - T_o)dy = q/\rho C_p - \int U D_x(T_o)dy$$

where the last term arises from the assumed variation of the bulk temperature T_o.

If we now assume temperature and velocity profiles defined by

$$(T - T_o) = (q\delta)/(2k).(1 - y/\delta)^2$$

$$U = (\omega y)/\delta .(1 - y/\delta)^2$$

which satisfy the boundary conditions as follows

$$y = 0 \qquad D_y T = -(q/k) \qquad U = 0$$
$$y = \delta \qquad T = T_o \qquad U = 0$$
$$D_y T = 0 \qquad D_y U = 0$$

The equations are now written in dimensionless form with

$$X = C.x$$
$$M^* = (\omega^2 \delta)/(C_2 \vartheta^2 C_M)$$
$$\theta_\infty' = (k/q).(d T_o/dX)$$
$$E^* = (\omega \delta^2 C_2)/(C_E \vartheta)$$
$$C_2 = ((g \beta q)/(k \vartheta^2))^{\frac{1}{4}}$$
$$C_M = (60/P_r)^{4/5}.(10/(4/5 + P_r))^{3/5}$$
$$C_E = (60/P_r)$$

the equations then become

$$dM^*/dX = (7/5 + (7.P_r)/4)((E^*)^{4/3}/(M^*)^{2/3}) - (7.P_r.M^*)/(4E^*)$$
$$dE^*/dX = 1 - 5.(60/P_r)^{3/5}(10/(4/5 + P_r))^{1/5}(E^*.M^*)^{1/3}\,\theta_\infty'$$

with initial conditions

$$X = 0 \qquad M^* = 0 \qquad E^* = 0$$

In practice, in order to avoid numerical problems, it would appear that the starting values of E^* and M^* should be small but non-zero, such that $M^* = (E^*)^{7/5}$.

In terms of the new variables the boundary layer thickness δ and the velocity constant ω are given by

$$\delta = \left[(C_E^2.(E^*)^2)/(C_M M^*)\right]^{1/3}/C_2$$
$$\omega = C_2 \vartheta \left[(C_M^2 (M^*)^2)/(C_E E^*)\right]^{1/3}$$

The pair of ordinary differential equations in M^* and E^* are solved numerically and graphs are presented for the variation of the momentum and energy variables for different linear vertical temperature gradients and Prandtl numbers. The zero gradient case of $M^* = (X)^{7/5}$ and $E^* = X$ is also given.

A feature of this family of curves is that both E^* and M^* for a

given Prandtl number reach asymptotically limiting values with vertical distance. This is the condition reached where the boundary layer has grown to such an extent that the rate of diffusion of energy across it is just sufficient to keep the average temperature level of the boundary layer fluid increasing at the same rate as the bulk temperature.

These limiting asymptotic values can be obtained from the differential equations by setting the derivatives to zero.

Thus

$$E_{\infty}^{*} = (0.582)/((P_r)^{1/4}.(\theta_{\infty}')^{5/4})$$

$$M_{\infty}^{*} = (0.471)/((P_r)^{7/20}.(\theta_{\infty}')^{7/4}).\left[(11/5 + P_r)/P_r\right]^{3/5}$$

The authors also suggest that the presence of an axial temperature gradient will delay the transition to turbulence. They suggest that the criteria $E^{*} = 500$ should be used which reduces to the conventional Grashof turbulence criteria of 10^9 for zero gradient.

This analysis of a free convection layer within a bulk environment provides one view of this type of problem. An alternative analysis by Prandtl shows a further interesting feature.

In his discussion of "mountain and valley winds in stratified air" Prandtl considers a different formulation of the boundary layer equations. Assuming the flow to be fully developed he combines the energy and velocity equations to give a fourth order differential equation of the type

$$((\frac{d}{dx})^4 + W^4)y = 0$$

The solution of this equation is shown by substitution to be the product of an exponential and an oscillatory term. In any practical situation the damping effect of the exponential would not permit more than two maxima. However it is clear that, for example, the velocity profile has a juxtapositioned positive and negative flow in a damped sinusoidal form.

This approach will be discussed in a later section, where a comparison will be made between the solution as presented by Prandtl and a Bessel solution to mixed free and forced convection in a tube. Similar results will be obtained at high Grashof numbers.

III - Mixed Convections

Extent of Mixed Regime - Plane Surfaces

The influence of free convection effects on forced flow in vertical tubes has been extensively investigated and numerous methods and simplifying assumptions have been used. Little work, however, seems to have been carried out for the opposite case of forced convection effects on free convection flow. It will, therefore, be necessary to look first at flat plate analyses in order to determine the extent of a mixed regime and its influence on the Nusselt number.

(a) Effect of Free Convection on Forced Convection

Sparrow and Gregg (1959) extended the Blasius solution of forced convection over a plate by introducing extra terms in the stream and temperature functions. These terms in $G_r/(R_e)^2$ were shown by Acrivos to be the characteristic parameter in this type of analysis for Prandtl number equal to or less than unity.

We have

$$\psi = (\vartheta . U_o)^{\frac{1}{2}} \left(f_o(s) + (G_r/R_e^{\,2})\, f_1(s)\right)$$

$$t = \frac{T - T_o}{T_s - T_o} = \theta_o(s) + (G_r/R_e^{\,2})\theta_1(s)$$

with

$$s = (y/(2x))((x\, U_o)/\vartheta)$$

$$G_r = (g\rho(T_s - T_o)x^3)/\vartheta^2$$

$$R_e = (U_o\, x)/\vartheta$$

On substitution into the boundary layer equations and grouping terms in power of $G_r/R_e^{\,2}$ the resulting ordinary differential equations are numerically solved for θ and f. In terms of $\theta_o'(0)$ and $\theta_1'(0)$ (prime denoting differentiation) the heat transfer is given as

$$q = (k(T_s - T_o))/2.(U_o/\vartheta.x)^{\frac{1}{2}}.(\theta_o'(0) + (G_r/R_e^{\,2})\theta_1'(0))$$

In order to compare this equation with a later one it is necessary to

write it in terms of the Nusselt number and to evaluate $\theta_o'(0)$ and $\theta_1'(0)$. We have the local Nusselt number based on the distance along the plate x:

$$N_u = (hx)/k = (qx)/\left[(T_s - T_o)k\right]$$

$$= -(R_e^{\frac{1}{2}}/2)(\theta_o'(0) + (G_r/R_e^{\,2})\theta_1'(0))$$

where the pure forced condition is given by the first term. For a Prandtl number close to unity, Sparrow and Gregg (1959) give:

$$\theta_1'(0)/\theta_o'(0) = 0.816$$

Roshenow and Chow give the empirical relation

$$N_u = 0.332\ P_r^{\,0.343}\ R_e^{\frac{1}{2}}$$

which closely fits the numerical work of Pohlhausen for flow over flat plates. This suggests on comparison with the pure forced solution

$$-\theta_o'(0)/2 = 0.332\ P_r^{\,0.343}$$

hence

$$\theta_o'(0) = -0.590$$

$$\theta_1'(0) = -0.482$$

we can then write

$$N_u = (R_e^{\frac{1}{2}}/2)(0.590 + (G_r/R_e^{\,2}).0.482)$$

(b) Effect of Forced Convection on Free Convection

Siavash Eshghy considered the other asymptotic case, and solved the free convection equations for a forced flow perturbation. He solved the two sets of equations (the unperturbed and perturbed) using fifth order profiles for the velocity and temperature. He gives the Nusselt number as

$$N_u = -(0.51(G_r)^{1/4})/2^{\frac{1}{2}}.(1 + 0.126(G_r^{\frac{1}{2}}/R_e) \ \ldots\ )$$

These two analyses may now be plotted and the results are compared in Figure 3. The dotted lines give the region of inapplicability of the

FIGURE 3 MIXED CONVECTIONS---PLANE SURFACES

(SPARROW AND GREGG--ESHGHY)

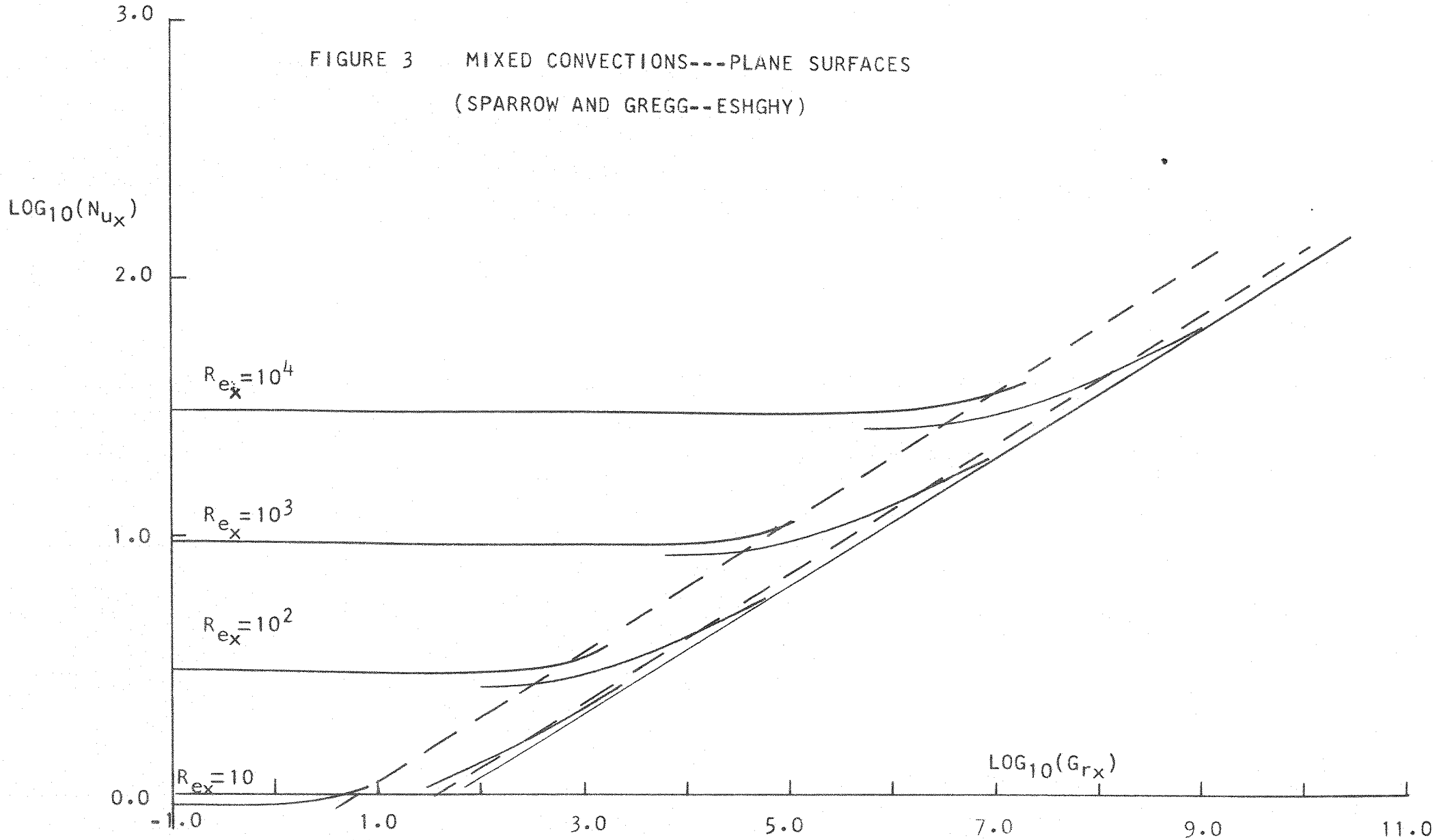

analyses, and the full curves represent the mixed flows and forced and free convection limits.

As mentioned, Acrivos has solved this problem by an approximation method and concludes that, because the mixed region is small, the pure forced or pure free solution may be used without a great loss of accuracy.

Turbulent Mixed Convections - Plane Surfaces

Turbulent mixed convections from heated plates has been briefly discussed by Hall and Price and they attempt both a general discussion of the salient features and possible flow model, and an experimental comparison.

They consider the turbulent boundary layer to be composed of two parts, an inner and an outer layer. The inner layer, whose boundary coincides with the peak in the velocity distribution, takes little part in the convection of heat from the surface. The outer layer is responsible for the majority of the convected heat transfer. With superimposed forced flow the inner layer is not greatly affected, but the outer layer is compared to a mixed layer between two streams of different velocities. These he calls the wall layer velocity and the free stream velocity. Turbulence is generated by the difference in velocity between the streams, and hence, one can expect that the turbulence will first decrease and then increase as the free stream velocity approached and exceeded the wall layer velocity. This minimum in the heat transfer would not be experienced in laminar flows. They present experimental evidence of this minimum at the predicted condition of

$$G_r/R_e^2 = 10$$

where both dimensionless numbers are based on distance along the plate.

Mixed Convections in Tubes

Martinelli and Boelter were among the first to attempt a solution of the problem of forced convection with superimposed free convection in

vertical tubes. They considered three idealised systems, which were of increasing complexity. The final system allowed for buoyancy effects due to a linear variation in density with temperature and also a variation in the mixed mean fluid temperature along the tube. In a manner similar to that used by Leveque, they assume that the heat transfer is determined by the fluid flow close to the wall, with the flow distribution in the centre of the pipe being considered relatively unimportant. Pigford, using a similar approach, allowed for variations both in the density and viscosity, and presents similar graphs of heat transfer versus Graetz number for various wall to bulk viscosity ratios, as those of Martinelli and Boelter. It is not possible by this method, however, to investigate the behaviour of the velocity and temperature profiles across the tube. It is necessary to seek an alternative method for this information.

The solution of the partial differential equations governing the vertical flow of fluid in heated tubes is discussed in some detail by Ostroumov. They are homogeneous, non linear, partial differential equations both owing to their structure and the non linear properties of the physical parameters of the fluid. It is possible to simplify this set of equations by assuming constant properties (independent of temperature and pressure), and by eliminating non-linear terms if these are physically small. This is termed as parametric and structured linearisation.

Several authors (e.g. Ostroumov, Hallman, Morton, Hanratty) have treated the case of fully developed flow under a linear vertical temperature gradient with constant heat flux at the walls. This flow is characterised by a velocity profile which is invariant in the direction of flow, and by pressure and temperature changes which are linear with distance downstream.

In polar co-ordinates the equations of momentum, continuity and

energy may be written:

$$\rho(V\,D_r\,U + U\,D_z\,U) = -D_z\,P - \rho g + \mu(D_r^2 U + \frac{1}{r} D_r\,U + D_z^2\,U)$$

$$\rho(V\,D_r\,V + U\,D_z\,V) = -D_r\,P + \mu(D_r^2\,V + \frac{1}{r} D_r\,V - \frac{V}{r^2} + D_z^2\,V)$$

$$D_r\,V + \frac{V}{r} + D_z\,U = 0$$

$$\rho C_p\,(V\,D_r\,T + U\,D_z\,T) = k(D_r^2\,T + \frac{1}{r} D_r\,T + D_z^2\,T)$$

and the assumptions

$$V,\ D_z\,U,\ D_z^2\,U,\ D_r\,P,\ D_z^2\,T = 0$$

with

$$D_z\,T = \text{constant} = A$$

$$D_z\,P = \text{constant}$$

the momentum and energy equations become

$$D_z\,P + \rho g = \frac{\mu}{r} D_r\,(r\,D_r\,U)$$

$$U\rho\,C_p\,D_z\,T = k(D_z^2\,T + D_r^2\,T + \frac{1}{r} D_r\,T)$$

If we consider the density to vary as

$$\rho = \rho_o(1 - \beta(T - T_o))$$

then we can write the differential equations with $\Theta = (T - T_o)$

$$\frac{1}{r}\frac{d}{dr}(r\frac{du}{dr}) + \frac{\rho\beta\Theta}{\mu} = \frac{1}{\mu}(\frac{dP}{dz} + \rho_o g)$$

$$\frac{1}{r}\frac{d}{dr}(r\frac{d\Theta}{dr}) - \frac{\rho\,C_p\,A\,U}{k} = 0$$

If heat generation within the fluid is to be considered then a term will appear on the right hand side of the energy equation (i.e. $-q/k$ where q is the flux).

By substitution, the equations can be non-dimensionalised and in a manner similar to Hallman we let:

$$R = 2r/D$$

$$U_d = U/U_m$$

$$R_a = (\rho^2\,g\,\beta\,C_p\,D^4\,A)/(16\mu\,k)$$

$$\phi = (2k\,\Theta)/(\rho\,U_m\,C_p\,D^2\,A)$$

$$C = \left[-(dP/dz + \rho_o g)D^2\right]/32\mu U_m$$

then we obtain

$$1/R \; d/dR \; (R \frac{dU_d}{dR}) + 2 R_a \phi = -8C$$

$$1/R \; d/dR \; (R \frac{d\phi}{dR}) - U_d/2 = 0$$

by differentiating the first equation twice with respect to R, ϕ can be eliminated from the equations to give

$$\nabla^4 U_d + R_a U_d = 0$$

where

$$\nabla^2 = \left(\frac{d^2}{dR^2} + 1/R \; d/dR\right)$$

The general solution of this equation can be expressed by the ordinary and modified Bessel functions of complex argument and zero order

hence

$$U_d = a^* J_o (R_a^{1/4} (iR)^{\frac{1}{2}}) + b^* Y_o(R_a^{1/4} (iR)^{\frac{1}{2}}) + c^* I_o(R_a^{\frac{1}{4}} (iR)^{\frac{1}{2}}) + d^* K_o(R_a^{\frac{1}{4}} (iR)^{\frac{1}{2}})$$

since the velocity is finite for R = 0 then

$$b^*, d^* = 0$$

The constants a^* and b^* are complex and may be written

$$U_d = (a + ib)J_o(R_a^{\frac{1}{4}}(iR)^{\frac{1}{2}}) + (c + id)I_o(R_a^{\frac{1}{4}}(iR)^{\frac{1}{2}})$$

The real and imaginary parts of the Bessel functions have been tabulated and are the Kelvin functions ber and bei. Noting that J_o and I_o are complex conjugates i.e.

$$J_o = ber_o - i\, bei_o$$

$$I_o = ber_o + i\, bei_o$$

then (dropping subscript)

$$U_d = A^* ber(R_a^{\frac{1}{4}} R) + B^* bei(R_a^{\frac{1}{4}} R)$$

with $A^* = a + c$

$B^* = b - d$

The constants are determined from the boundary conditions. For no slip at the wall R = 1, $U_d = 0$ then

$$A^* = (-B^* \text{bei } R_a^{\frac{1}{4}})/\text{ber}(R_a^{\frac{1}{4}})$$

A further boundary equation is required and this is chosen to be constant volume flow. Morton does consider an alternative of constant pressure drop.

For constant volume flow

$$\int_0^1 U_d R \, dR = \tfrac{1}{2}$$

and noting that for a variable z

$$\int z \, J_0(z) = z \, J_1(z)$$

$$\int z \, I_0(z) = z \, I_1(z)$$

then the velocity becomes for zero order Kelvin functions

$$U_d = \frac{R_a^{\frac{1}{4}}}{2} \left[\frac{\text{ber}(R_a^{\frac{1}{4}} R)\text{bei}(R_a^{\frac{1}{4}}) - \text{bei}(R_a^{\frac{1}{4}} R)\text{ber}(R_a^{\frac{1}{4}})}{\text{ber}(R_a^{\frac{1}{4}})\text{ber}'(R_a^{\frac{1}{4}}) - \text{bei}(R_a^{\frac{1}{4}})\text{bei}'(R_a^{\frac{1}{4}})} \right]$$

where prime denotes differentiation.

The temperature solution can now be found from the second of the original dimensionless differential equations, and is

$$\phi = \left[\frac{1}{4R_a^{\frac{1}{4}}} \cdot \frac{\text{ber}(R_a^{\frac{1}{4}}R)\text{berR} + \text{bei}(R_a^{\frac{1}{4}}R)\text{bei}(R_a) - (\text{ber}^2(R_a^{\frac{1}{4}}) + \text{bei}^2(R_a^{\frac{1}{4}}))}{\text{ber}(R_a^{\frac{1}{4}})\text{ber}'(R_a^{\frac{1}{4}}) + \text{bei}(R_a^{\frac{1}{4}})\text{bei}'(R_a^{\frac{1}{4}})} \right]$$

These solutions are shown in Figure 4 for various Rayleigh numbers ($l = R_a^{\frac{1}{4}}$). It is interesting to note the dimpling effect of natural convection in the velocity profile, resulting in almost zero flow at the axis, and reverse flow just off axis. Also the bulk of the flow is increasingly concentrated near the wall. The temperature profile also exhibits a tendency towards the formation of a boundary layer. This is demonstrated by the almost horizontal temperature distribution, for high Rayleigh number, across the tube with the temperature rise occurring close to

FIGURE 4 MIXED CONVECTIONS IN TUBES

(HALLMAN)

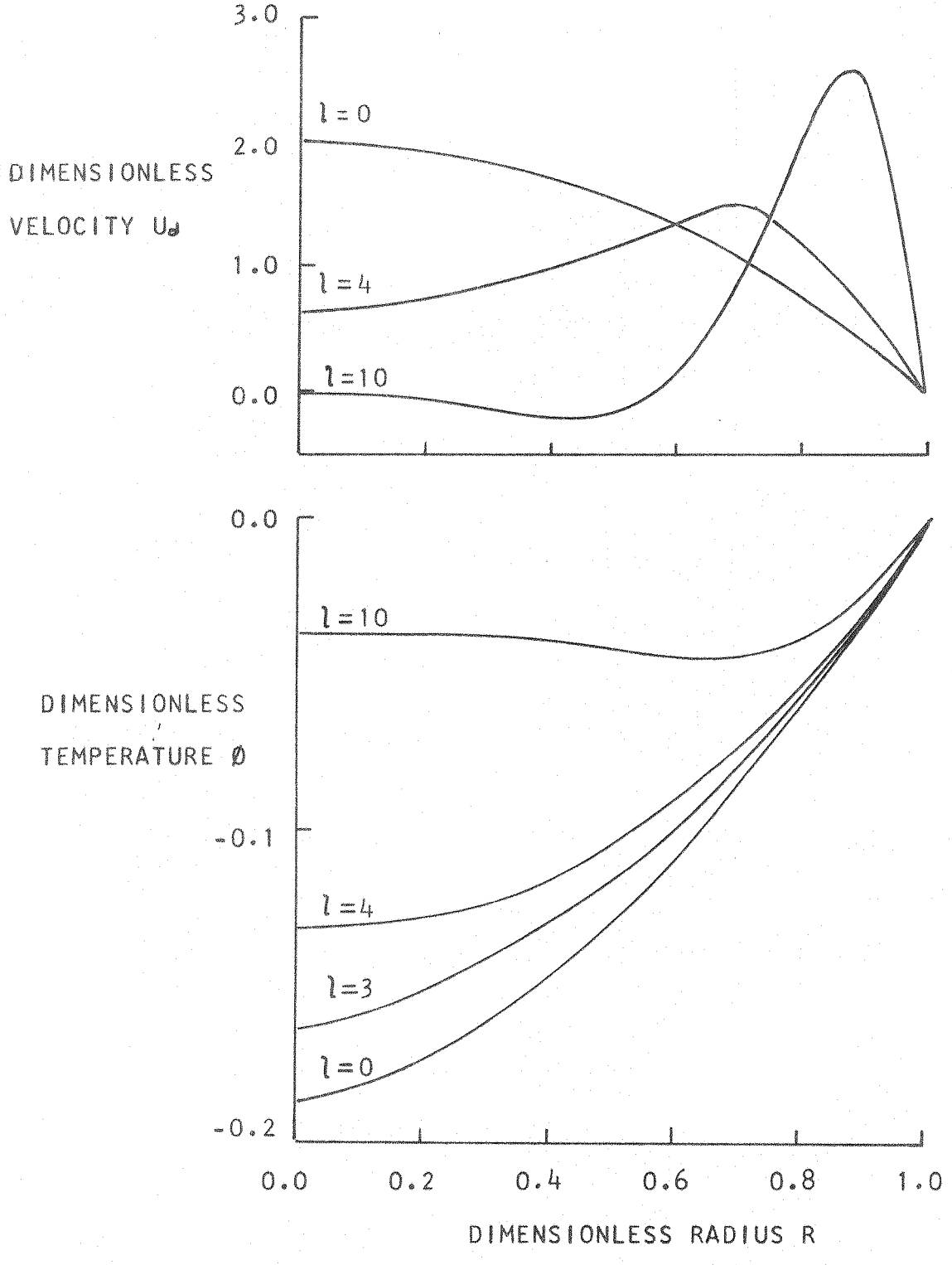

the wall. The pure forced condition ($R_a = 0$) is shown as the Poiseuille parabolic distribution of velocity.

The Nusselt number is shown in Hallman's paper to increase from the forced convection limit of 48/11 with increased Rayleigh number. This variation can be represented by the following equation:

$$N_u = 1.4\ R_a^{0.28}$$

Morton's results are similar to those presented by Hallman, with two notable differences. For constant pressure drop the volume of flow is at first only slightly affected by increased Rayleigh number, but then drops quickly at higher Rayleigh numbers. Also the Nusselt number variation is said to be represented by a 0.25 power law above a Rayleigh number of 10^3.

Effects in Mixed Flow

Other features of mixed flow in tubes are discussed in some detail in the quoted papers. These are the problems associated with development lengths, parametric temperature effects, and transition to turbulence.

Development or entrance length effects have been investigated by Hallman, Rosen and Hanratty, and Lawrence and Chato, covering both experimental and theoretical work. Because of the numerical finite difference scheme used by Lawrence and Chato it is difficult to draw conclusions which are not explicitly made in the publications. They solve particular cases which are considered typical and do not cover large variations of Grashof to Reynolds ratios. A further complication arises in comparing the work of Hallman (1961) with the above authors since there appear to be wide discrepancies in the quoted development lengths. This may be resolved qualitatively by considering the difference in the development length of a velocity profile and the Nusselt number. Hallman is interested in the development only in so far as it affects the Nusselt number; and since Collins, for example, notes that the

development depends on the diffusion rate of heat from the wall to the centre line, then the velocity at the wall will be developed sooner than the centre-line velocity. The velocity gradient at the wall characterises the heat transfer and so one would expect the Nusselt number to be developed sooner than the full velocity profile. In general the conclusions of the authors suggest that development lengths become shorter with increasing Grashof to Reynolds ratios.

In order to simplify the boundary layer equations the physical properties of the fluid are often considered to be constant or to vary only in a limited way. Both Morton and Hallman comment that a temperature change should only have a secondary effect on the profile shape. Hallman allows for these parametric effects by applying the theory locally. That is, he considers that at each section the flow is fully developed, and can be described by evaluating the Rayleigh number at that temperature level. There is satisfactory agreement between applying the theory in this way and the quoted experimental results.

The transition to turbulence is described in a similar manner in all the papers quoted. It is seen to happen as a consequence of the instability of the velocity profile shape and is therefore interrelated with its development length and the growth rate of inherent disturbances. Transition will occur at some axial position if the tube is long enough, and also after the velocity profile has developed an inflection point where the centre line velocity is less than that at some radial position. The profile is then said to be unstable to disturbances, and these are amplified into turbulent flow. For a fixed Grashof number the turbulence transition point will move upstream with decreasing Reynolds number and the development length will become shorter.

Correlation of Convections in Tubes

Finally, it is interesting to look at the correlation work of Eckert and Diaguila, and Metais and Eckert, who try to establish the extent of the free, mixed, and forced regimes for both laminar and turbulent conditions. The criteria they use is 'that the actual heat flux under the combined influence of convection forces does not deviate by more than 10% from the heat flux that would be caused by the external forces alone (forced convection) or by the body forces alone (free convection)'. Their compounded graph is presented in Figure 5.

FIGURE 5 MIXED CONVECTION REGIME

(METAIS AND ECKERT)

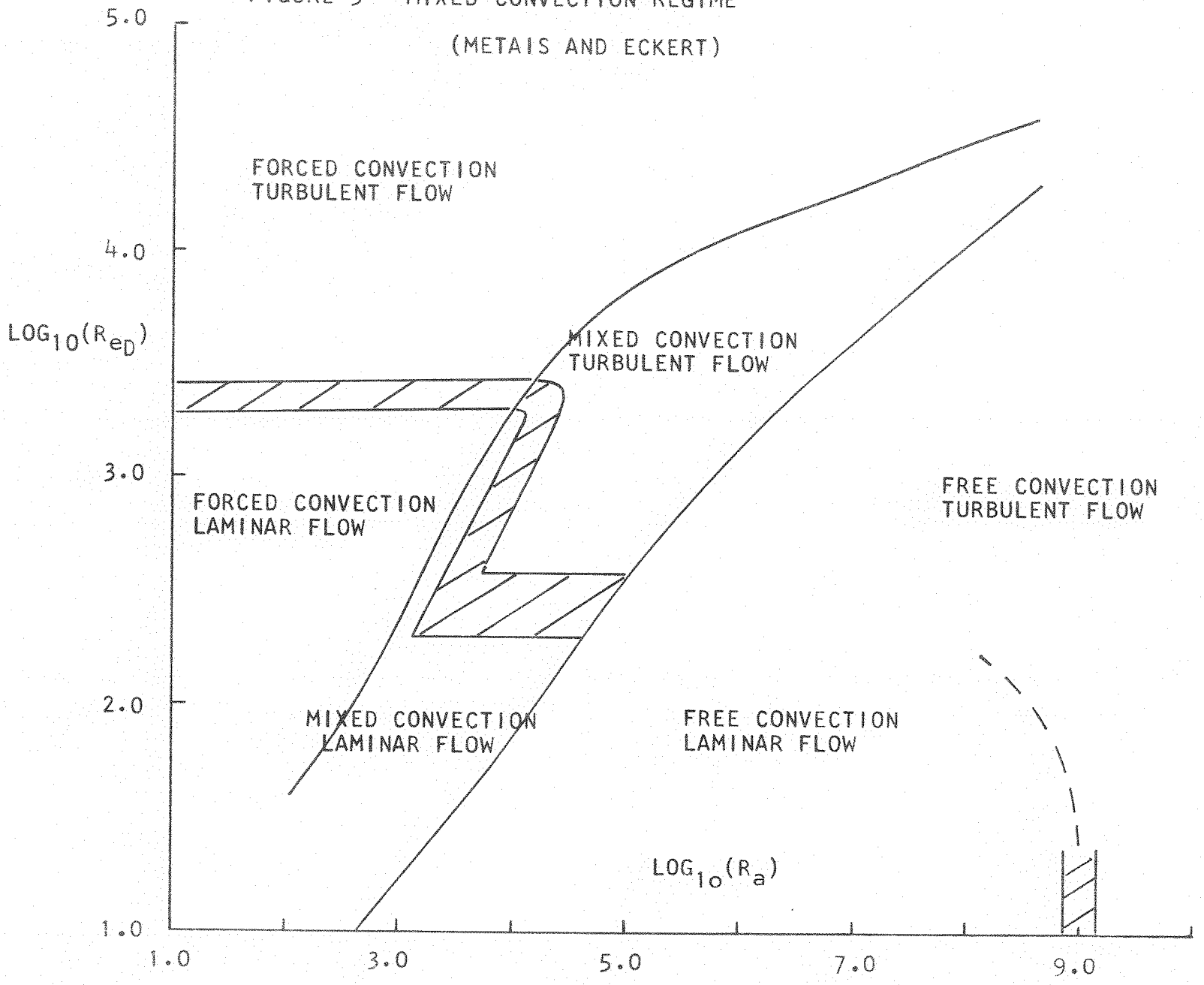

CHAPTER 2

Between, that the book may be handily padded,
Some pages of mere printed matter are added,
Expanding the theme, which in case of great need
The curious reader might very well read

Commercial Candour
G.K.Chesterton

APPARATUS

Modular Helium Dewar

The dewar was designed to enable heat transfer measurements to be made relatively easily and quickly in the helium vapour column, for various boundary conditions. The geometry could be changed by replacing the whole helium section with an alternative while retaining the same nitrogen shielding and vacuum jacket. Also the temperature gradient in the vapour column could be varied by adjustment of the position of the nitrogen shield collar.

The construction was therefore broken down into three independent but interlocking sections; a vacuum jacket, a nitrogen shield, and a helium neck and container. The dewar is shown in Figure 6. The vacuum jacket (1) was a seam welded aluminium tube with welded flanges and two side access ports, one used for a vacuum pump connection, and the other a bursting disc. The shield (2) was a full length, copper, liquid nitrogen container, with an 8.9 litre capacity and 240 cc liquid/hr evaporation rate, resulting in a 37 hour life. It was suspended from three stainless steel, fill/vent tubes from the top flange via re-entrant tubes. The helium section used in these experiments (3), consisted of a 675 mm long stainless steel tube of approximately 76 mm diameter and 0.25 mm wall thickness, connected to a brass "diffuser" (4) and copper helium container with a 2.5 litre capacity (5). This assembly was suspended from a flange which was bolted to the nitrogen shield flange.

The "diffuser" was designed to prevent excessive "turning" of the gas flow, and also to prevent vapour bubbles from being trapped when the liquid level was high, and hence steady gas flows were produced.

FIGURE 6 HELIUM DEWAR

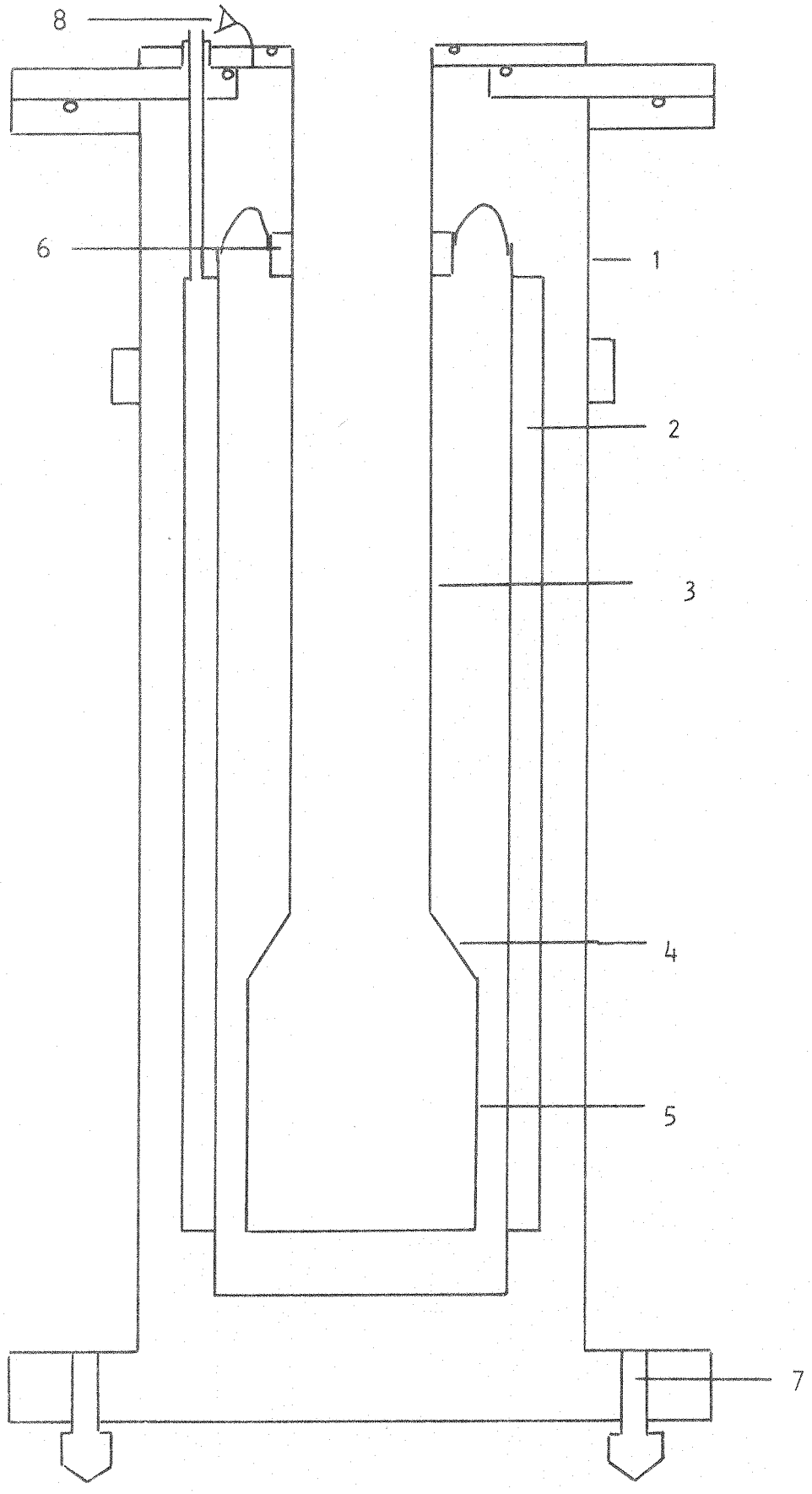

A copper collar (6) was clamped to the helium neck approximately 10 cm from the top and connected via six 12.5 mm wide flexible braidings to the liquid nitrogen shield. Good thermal contact with the neck was achieved using either "j" oil or vacuum grease between the collar and the neck. The space between the shield and the collar was covered with aluminium foil to prevent room temperature radiation from reaching the helium container.

The dewar had four adjustable feet (7) in order to arrange that the dewar be vertical, and it also had a nine-channel feed-through seal (8) which fed wires into the common vacuum space.

The brass "diffuser" and copper container maintained the temperature at the bottom of the helium neck constant and therefore a steady evaporation rate was produced of approximately 19 $cm^3 hr^{-1}$ of liquid helium giving a working life of four days.

Vacuum System

This was a conventional Edwards system with an E02 diffusion pump and an ES35 gas ballast rotary pump. It was connected via a 1" flexible coupling and isolation valve to the dewar. Vacuum was generally maintained to better than 2×10^{-5} torr as measured at the inlet to the dewar. However, on the warming up of the dewar after a helium run the vacuum was lost for a time. This occurred around 20 K and was thought to be due to the desorbtion of hydrogen from the cold surface and which could have originated from inclusions in the aluminium (Scott[2]).

Top Plate Assembly

Figure 7 shows schematically the structure of the top plate assembly. It was comprised of three basic parts. That is, two probes with their associated gearing and position indicators (A, B), three tubes (C) which carried thermocouple and electrical wires and which also supported

FIGURE 7 TOP PLATE ASSEMBLY

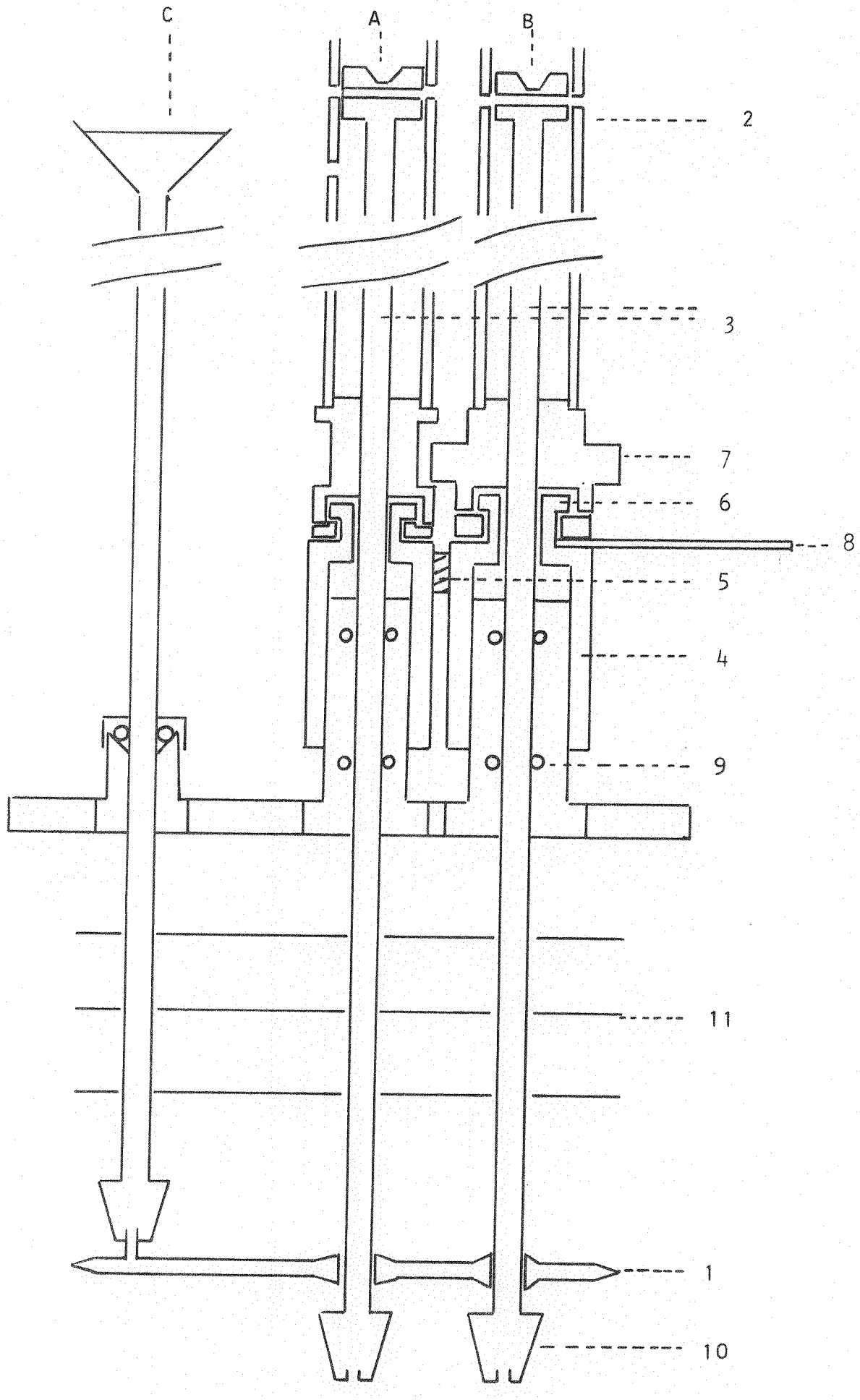

a "spacer" (1) designed to be a close fit to the helium neck, and lastly gas outlet and helium syphon inlet tubes.

It was intended to be able to take measurements of the temperature field in the neck at any vertical position and also to scan the horizontal plane from the centre (where there might be a heated surface) to the wall. The extensive vertical travel required (> 700 mm) meant that continuous positioning of the 6.3 mm O.D., 0.56 mm thick by 900 mm long stainless steel tubes (3) would be difficult to achieve, and hence it was decided to divide the operation into fixed interval positioning, and continuous positioning within any interval. The 25.4 mm I.D. stainless steel tubes (2) were used as guide tubes, in order to keep the probes straight and prevent damage, and were also used to position the probes vertically in steps of 20 mm. The tubes were supported at their upper ends from a tripod mounted on the dewar flange. The brass lifting gears (4) were designed to move the guide tubes and the probes through 30 mm. They were screw-cut on the inside with a 2 mm pitch thread and vertical grooves were milled on the outside. A third gear (5) milled in the same way connected the two lifting gears together, and was driven through 1:1 right angled crossed helical gears from an Amphenol 10:1 geared counting dial. The rotation of the lifting gears was prevented from being transmitted to the guide tubes by the coupling (6). The guide tubes could not rotate freely being fixed by either a gear (7) or an anti-rotation collar connected to the top of the tripod. The 36:1 worm gear (7) was driven by a 10:1 Amphenol counting dial mounted on an arm (8) which was restrained to move only vertically, and rotated the guide tube and one probe. In this way the dewar could be scanned in any horizontal plane from the centre to the wall.

The probes were separated by 25.4 mm and the relation between the degree of rotation and the radial position of a thermocouple supported on a 25.4 mm arm was nearly linear. The rotational position could be

determined to better than ±2.5 counts on the dial which corresponded to approximately ±0.1 mm when translated into radial distance. The worm gear suffered from backlash equivalent to 43.5 counts on the dial, but this was reproducible and could easily be allowed for. The vertical positioning gear was more positive and was reproducible to ±0.2 mm.

There was little frictional resistance to rotation of the probe but this was not the case for vertical movement, where the dry "O" ring gas seals (9) offered some resistance. Grease could not be used as it would freeze and cause trouble on trying to operate the tubes. Graphite was used to lubricate the seals and the performance was improved.

The spacing ring (1) was supported on three 4.76 mm O.D., 0.56 mm thick, 600 mm long stainless steel tubes, and pin vices were used to link the tubes to the ring. The same type of pin vice (10) was also used on the end of the probe arms and provided easy mounting facilities and a heat brake to the measuring heads. The spacer ring was designed to maintain the probes a known distance apart and to restrain the probes to move in a vertical line. Only four near point contacts with the wall were possible.

Thermal radiation into the helium was reduced using baffles (11) according to Lynam and Scurlock (1969). The anticipated maximum thermal contraction of the probes as calculated from Scott[3] was 0.2 mm. However, since both probes were identical as far as the pin-vices then this contraction would not be seen relatively between the probes, which is important in the heat transfer measurements. The heat inleak will be discussed in the temperature measurement section.

Flowmetering

In practice, commerical flowmeters proved to be both unreliable and inaccurate. The Parkinson-Cowan wetmeter, generally used for medium to low flow rates, is quoted to be accurate to within 0.25%. However

five out of six proved to be faulty in some respect and could not be totally depended upon. Rotameters are a useful alternative since they can be seen to respond quickly to fluctuations in flow and hence are also a measure of the steadiness of flow. However the manufacturers cannot guarantee the bore of the tube to better than 3% and this, coupled with the non-linear and compact scale makes it difficult to read accurately.

A simple alternative was to use the pressure drop of a gas flowing through a capillary tube. This has the advantage of having no moving parts and of obeying a linear law. Other systems such as the Krondberger and Kalmus ultrasonic meter are attractive but complex and would have needed extensive development. A disadvantage of capillary tubes is that unlike wetmeters or rotameters they create a backpressure, and in order to avoid any possible complications it was decided to use them only as standards, in order to continually check the behaviour of the wetmeter.

Initially the pressure drop was measured across the total length of the capillary tube, but the simple Poiseuille law was not obeyed. It was found that the curves of length of a given bore capillary versus pressure drop for given flow rates extrapolated to "negative lengths" at zero pressure drop, as shown in Figure 8. This anomolous behaviour was due to the excess pressure drop associated with the development of Poiseuille flow in the entrance region of the tube. The "negative lengths" agreed to within 9% with the accepted development lengths as calculated from the 0.057 R_e pipe diameter law, as given in Perry.

It was therefore necessary to measure the pressure drop over the fully developed flow region and hence pressure tappings had to be drilled into the glass capillaries. A steel pin and carborundum paste were used to drill through the glass and care was taken to avoid damage to the capillary itself on breaking through. Three tubes were drilled in this way, having average diameters of 1.62 mm, 1.33 mm and 0.77 mm

FIGURE 8 ENTRANCE EFFECTSIN A CAPILLARY TUBE FOR FIXED FLOW RATES

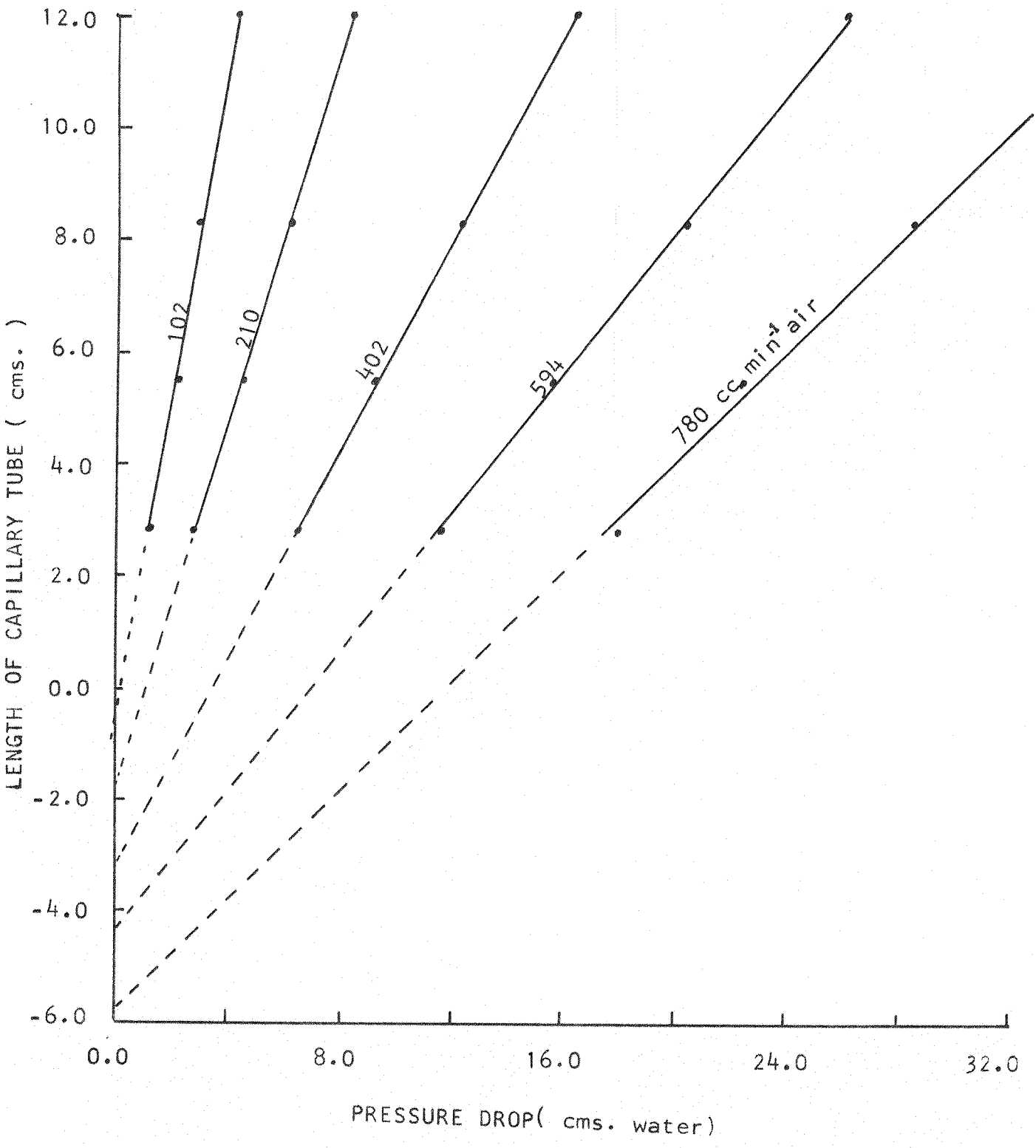

(as measured by a mercury weighing method) to cover the laminar flow range up to 2350 cc nitrogen (2160 cc helium) per minute at N.T.P. A transition to turbulence was anticipated in all three tubes for high flow rates and this occurred at the expected rate in the two larger bore tubes (i.e. for R_e = 2000). The transition was not seen in the smallest bore tube which was calibrated up to 1200 cc/min.

The rotameter, wetmeter and tubes were initially calibrated in series using gaseous nitrogen evaporated at a known rate from liquid nitrogen. The rotameter had also been calibrated at fixed points using a constant head device and a water displacement method, and was a useful cross-check.

The capillary tubes gave results which were within 1% of those predicted by Poiseuille flow, while the wetmeter gave flowrates which were 8% too high.

The cool gas from the dewar was passed through a simple copper coil heat exchanger in a constant temperature water bath before being passed into the flowmeter. The temperature was maintained at 302.6 K using an AEI EA4M relay unit and adjustable contact thermometer. This temperature (approximately 30°C) was chosen to be just in excess of the maximum anticipated room temperature. The wetmeter was the last flowmeter in the line and a mercury thermometer in the well gave the exit temperature of the gas. This was on average 2 K less than the water bath temperature. Selector switches could connect in either a 180 watt dissipation resistor for fast warm up of the water bath, or a 6 watt heater for control purposes. An electrical stirrer in the bath maintained uniform temperature throughout the bath.

Thermometry

The numerous advantages of thermocouples make them the obvious choice of temperature sensor for small scale heat transfer measurements. This

is particularly true for a heated surface where the gas environment at a distance is not constant in temperature but suffers a large vertical temperature gradient requiring point to point measurement. Thermocouples have the advantage that they have a low heat capacity and hence are quick to respond to temperature changes. They are easy to use, are physically small and hence measure very localised temperatures, and are well behaved thermometers being reproducible and moderately sensitive.

In general, thermocouple elements lose sensitivity with decreasing temperature and this has restricted their useful low temperature range. In 1932 Borelius et al showed that the addition of small amounts of a transition metal in gold caused an increase in thermopower at low temperatures. This discovery made it possible to extend the low temperature range of thermocouples. Gold-cobalt alloys were used initially but were superseded by gold-iron alloys which were more sensitive and were also metallurgically more stable.

Berman, Brock and Huntley have reported on various properties of gold-iron alloys prepared by Johnson Matthey & Co. The curves of thermopower versus temperature for different alloys confirm that the low temperature sensitivity is reduced by increased iron content, and the higher temperature sensitivity (approximately greater than 10 K) is increased. They recommend Chromel-P (90% Ni and 10% Cr) as the second thermoelement, since it has a positive thermopower in contrast to the negative thermopower of gold-iron and hence an increased combined sensitivity. It also has a high thermal resistance which minimises heat inleak problems and metallurgically is both stable and insensitive to small variations in composition.

Rosenbaum has investigated the effect on this particular thermocouple combination of alloy inhomogeneities, temperature cycling, aging and annealing. He tested the thermocouple wire in the unannealed state ('as received') and found that the thermoelectric emf varied by $\pm 0.15\%$ from length to length on the same spool of wire. This was most pronounced

in the 25 to 45 K range and corresponded approximately to a variation of ±0.05 K. The original bar of material from which the wire was drawn (manufacturered by S. Cohn USA) varied slightly along the bar and produced spools which were different by a maximum of 0.65%. The room cycling reproducibility was better than 0.01°K between 0.4 K and 85 K and showed no aging over a period of three months. Annealing produced dramatic changes for both low iron content wires (.02 At%, 57 ppm) and higher iron content (.07 At%, 200 ppm) wires, and the low iron content wire was more susceptible to both work hardening (from the unannealed state), and emf variations due to inhomogeneity. The characteristic minimum in the thermopower at about 40 K was attributed to the chromel, since a similar effect was seen in a copper/chromel thermocouple calibration.

Figure 9 compares the published data from these sources and Sparks et al and it can be seen that the agreement between Rosenbaum and Sparks (both using Cohn manufactuered alloys) is close, apart from some unusual kinks in Rosenbaum's results. The results of Berman et al do not agree in magnitudes with these authors, particularly at the low temperature end, and seemingly reflect the difference in manufacturing technique of the two suppliers.

Calibration of Thermocouples

During the course of the heat transfer experiments three spools of gold .03 At% Fe were purchased from Johnson Matthey and a sample from each spool was calibrated against a calibrated Cryocal CR2500L germanium thermometer between 3 K and 100 K. The quoted accuracy is better than .01 K below 20 K, better than .04 K in the range 20 K to 40 K, and 0.1 K in the range 40 to 90 K. The thermocouples were varnished into a hole in a 0.5 kgrm copper block at the low temperature end of a closed cycle refrigerator (Pye Unicam 2000), with the standard germanium in a separate hole and covered in "j" oil to improve contact. A perspex disc provided

FIGURE 9 PUBLISHED THERMOPOWERS OF GOLD/IRON VERSUS CHROMEL THERMOCOUPLES

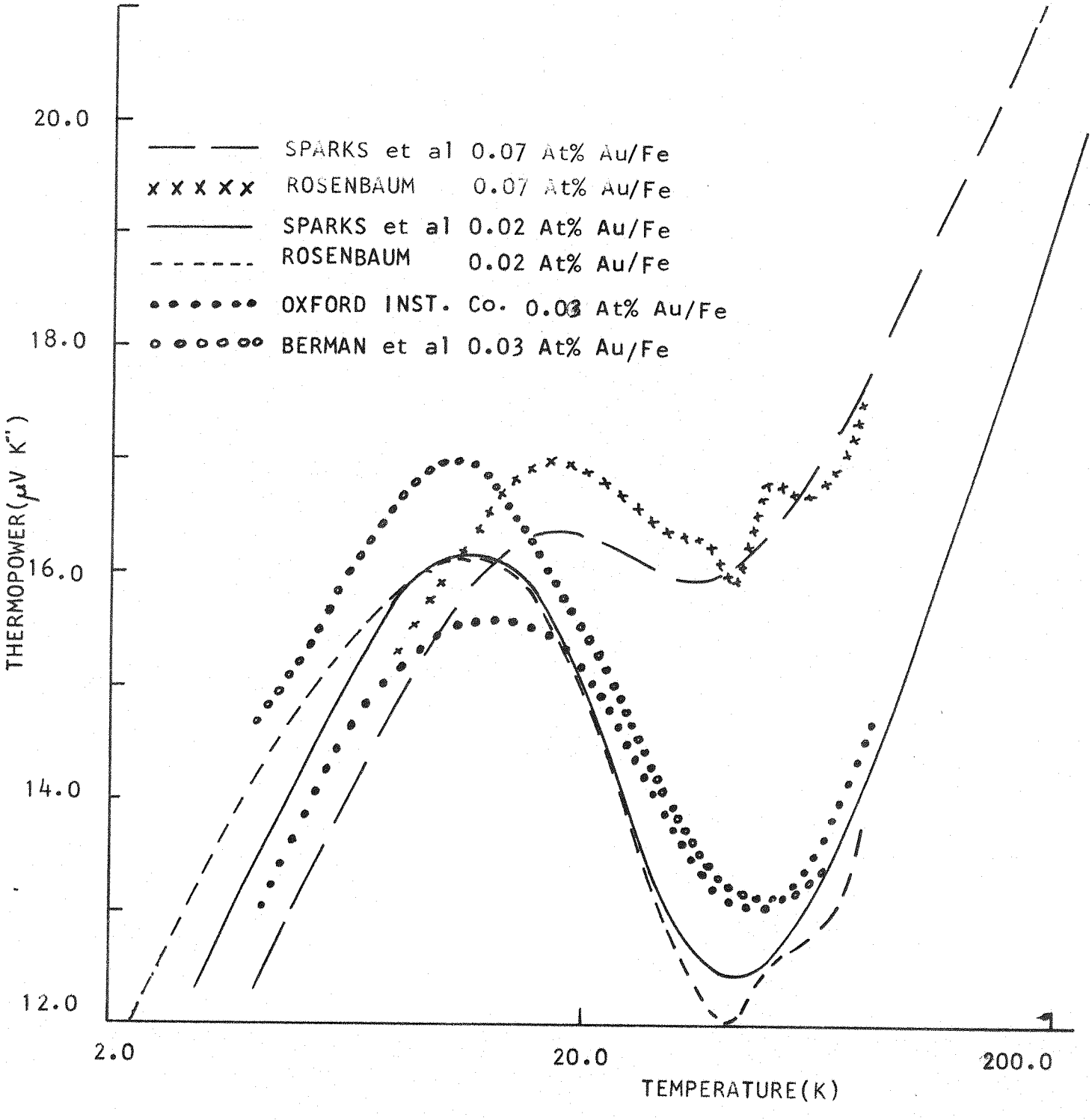

a thermal break between the copper block and the refrigerator and a heater on the block allowed for temperature stabilisation. All wires were thermally anchored at the 15 K point, and were fed out to a potentiometric system similar to the one to be described in this chapter. Calibration runs were performed under cooling down, warming up and "steady" temperature conditions. The drift rates were approximately 5 K per hour and were almost linear during warming up and cooling down, and were less than .060 deg K per hour for "steady temperature" results. The results were taken in a timed sequence, such that the thermocouples and standard germanium thermometer in the switch were swept in a forward and reverse direction. This meant that the results could be averaged and first order time drifts accounted for.

A computer programme then least squares fitted all the data using orthogonal polynomials, which had been generated on the data points (Fortran ICL library routine F4CFORPL). The programme produced the root mean square error after every polynomial had been evaluated so that it was possible to see at which stage the combined polynomial began to fit the data closely. It was important not to increase the order of the polynomials to such an extent that they fitted the data points exactly since at this point and beyond the curve would be oscillating, being of no value for interpolation. That is, the curve would be fitting a data point with its experimental error included. These characteristics of the curves were revealed in the rate of change of R.M.S. value with increased number of polynomials, the smoothness of the first differential, and the random nature of the residuals on the data points. An examination of these features made it possible to choose a suitable approximating curve. Appendix A gives details of these features and choice of polynomial as well as giving the coefficients of the polynomials used.

The thermopower obviously possesses a logarithmic character and hence it might have been better to have fitted the logged data points.

In practice, however, this was not necessary, and a comparison of this method and the method of Splines gave almost idential results,even agreeing in the very sensitive first differential to better than 0.1 $\mu V\ K^{-1}$.

The details of the thermocouple wire calibrated are summarised in the following table.

Spool	Resistivity Ratio	Number of Data Points	RMS Error	Terms	Temperature Range
1	8.556	168	0.51856×10^{-3}	8	3 K to 100 K
2	9.308	252	0.15919×10^{-2}	9	3 K to 100 K
3	7.963	234	0.73120×10^{-3}	8	3 K to 100 K
Published Data	-	53	0.13818×10^{-2}	13	2 K to 300 K

The published data used is that given by the Oxford Instrument Company and the Resistivity ratio is a comparison of resistance of a length of wire between room temperature and helium temperature. The Terms column relates to the number of terms in the series of the polynomial describing the computer fit, when rearranged from the orthogonal set.

These calibrations were checked by deeply immersing the thermocouple junctions in boiling liquid nitrogen. The agreement between the curve at this temperature and the boiling point of nitrogen was better than 90 mK. The thermopowers of the various thermocouples are given in Figure 10.

Finally, an interesting point emerges from this work. The difference in thermal voltage between the calibrated wires and the published data can be closely approximated on a linear deviation versus logarithmic temperature plot by two straight lines crossing at nearly 45 K (Figure 11). This clearly shows the dominance of gold below 45 K and that of chromel above. Spool 2 showed a negative slope below 45 while spools 1 and 3 showed positive slopes. It is thought that because of the high thermopower, the unusual deviation plot and the higher residuals on the data points

FIGURE 10 COMPARISON OF THERMOPOWERS OF FOUR BATCHES OF 0.03 At% IRON IN GOLD VERSUS CHROMEL

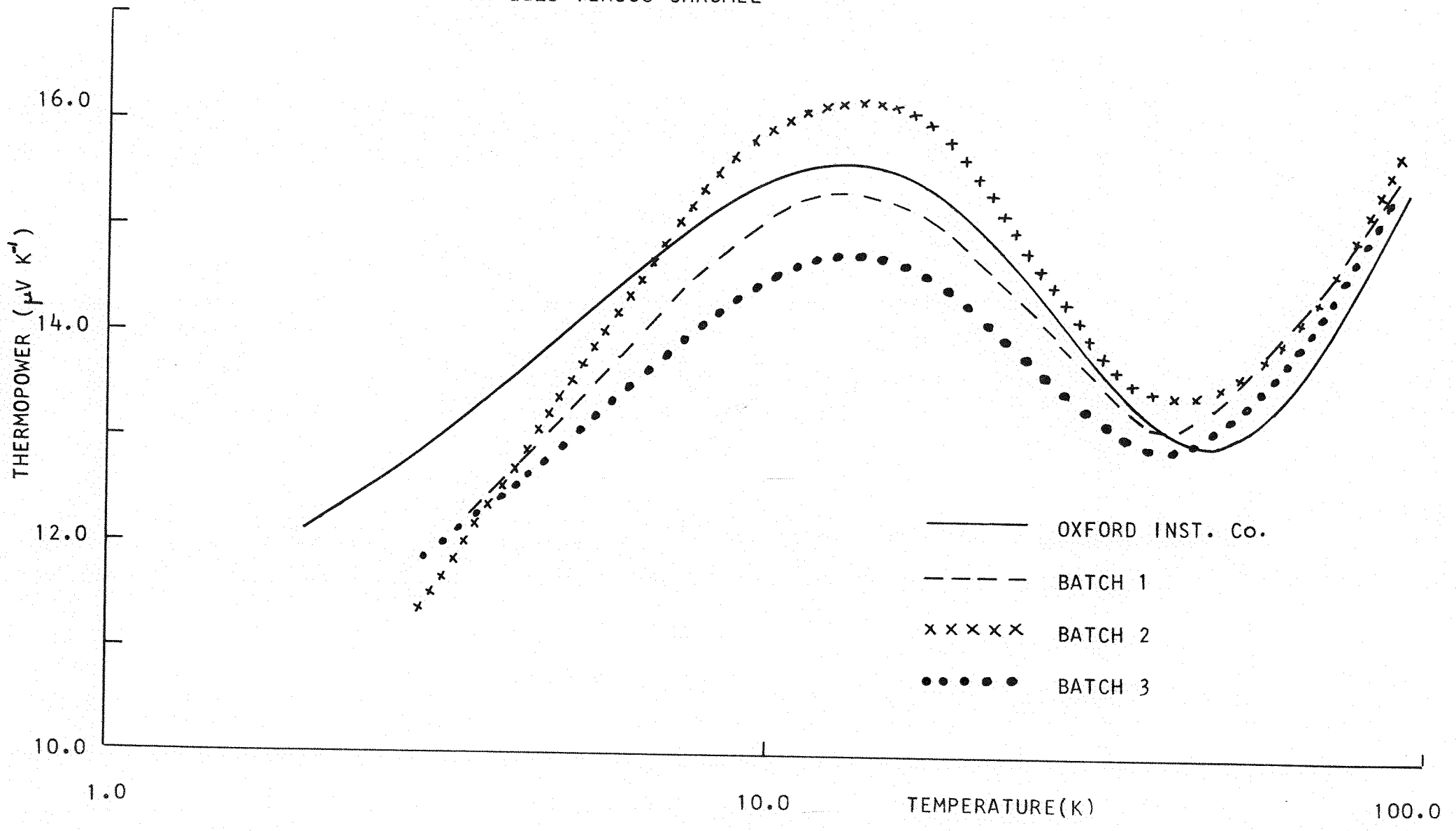

FIGURE 11 DIFFERENCES IN THERMAL E.M.F. BETWEEN BATCHES 1to 3 AND OXFORD Co. DATA

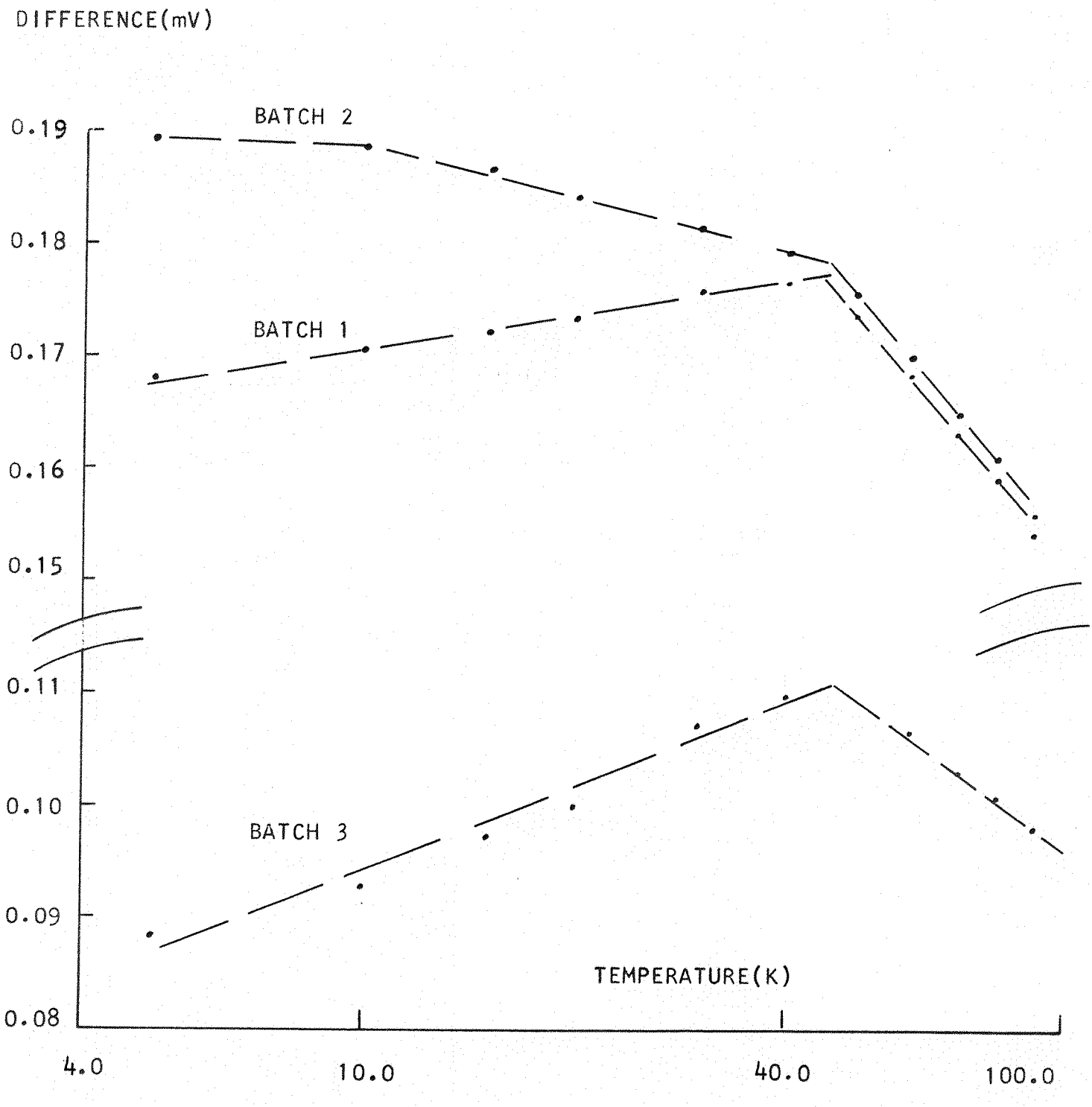

(related to inhomogeneity difficulties in low iron content, well annealed wire) that Spool 2 wire was in a better annealed state when received. This is confirmed by the resistivity ratios of the gold iron wires (between room and helium temperatures), since these have the same order in mangitude as does the thermal emf, with Spool 2 having the highest resistivity ratio and thermal emf.

Measurement of Thermal E.M.F.

In the early experiments a diesselhorst potentiometer was used to measure thermal emf to better than 0.1 μV. For the sake of speed and convenience this was superseded by a Solartron 0.1 μV resolution LM1490 digital voltmeter.

The potentiometric network consisted of a conventional Tinsley 3589R diesselhorst potentiometer, type 5214 photocell galvanometer amplifier and 5214A thermal compensator, and an MS2/45E indicating galvanometer and a type 4092 reversing switch. The amplifier and null circuit components were mounted on earthed aluminium plates in a vibration free stand. The potentiometer was also mounted on an earthed aluminium plate and this reduced the effects of static on the equipment, which at times could be very severe. A full discussion of similar effects appears in Lynam's thesis. A type 5750 current controller was used to maintain the calibrated voltage drop across the potentiometer and hence a linear deflection on the galvanometer. The sensitivity of the system was reduced slightly by the high input resistance of about 400 ohms, due to the long lengths of thermocouple wire used, but this did not affect the ability to easily balance the voltages.

As mentioned this system was superseded by a Solartron LM1490 digital voltmeter which offered numerous advantages. It was necessary to quickly take multiple readings of widely differing voltages and the potentiometer was a severe limitation. A certain loss of accuracy was anticipated

but this proved to be minimal.

The digital voltmeter was a sophisticated piece of equipment and showed outstanding qualities. Its sensitivity of 0.1 μV coupled with automatic calibration, mains voltage synchronization, low pass noise filters and various voltage integration times made it a very easy instrument to use. Under initial test and throughout the experimentation it proved to be both stable and accurate. The quoted accuracy is about $\pm$1.5 μV for a reading of 5 mV, but continual comparisons with the potentiometer never showed it to be more than 0.5 μV different, and most times only 0.2 μV different.

The eighteen thermocouples used in the experiments were lead via either an isothermal box or an ice point cell to two twelve-way Tinsley thermal free switches (type 4092B). These were connected to a Tinsley reversing switch which was wired to be a two-pole two-way switch, presenting one voltage to the potentiometer and one to the digital voltmeter. The isothermal box consisted of two aluminium boxes, the inner mounted on four tufnol feet, and an inner massive aluminium short cylinder on tufnol feet with thirty isolated copper terminals in it, connected to thirty isolated copper terminals on the outside. Foam was used between the boxes to prevent convection heat transfer. This maintained the junctions of the gold-iron and chromel wires at the same temperature. Unfortunately these terminals were insufficient for all the thermocouples and their particular spool common reference junction, and so the Frigistor ice point reference cell (stability better than 0.01 K) was used as a reference and junction point for the remaining thermocouples.

It would have been preferable to have used helium as the reference temperature but this posed difficulties. A wetted contact with helium was desirable and yet this was incompatible with the requirement that nothing be placed in front of the measuring heads in the dewar. An alternative was to make a lead-through seal into the helium reservoir

from the vacuum space, but this arrangement was cumbersome and impracticable.

The ice point cell had a noisy microswitch which was used for controlling the amount of ice in the sealed compartment. The switching caused the galvanometer to leap about periodically, and so the cell was modified to use a triac for control purposes with the microswitch "gating" the triac. This reduced the effect of spurious voltages to a tolerable level.

Thermocouple Arrangement

Six thermocouples were lead via a lead-through seal to the dewar vacuum space. These thermocouples were mounted on the side of the stainless steel helium tube at 0.11 m, 0.25 m, 0.39 m, 0.53 m, 0.66 m and 0.85 m below the top plate (the latter one being on the copper helium reservoir). Each wire was wound around the tube twice and varnished to it, before the junction was varnished into position on a piece of thin nylon stocking. This ensured electrical isolation and that the heat leak to the junction was minimised according to the recommendations of Scott[4] for measurements in vacuum. Unfortunately the top thermocouple was broken by the nitrogen shield collar after some early experiments and could not be repaired.

Twelve thermocouples were fed through the seals at the top of two of the stainless steel spacer support tubes (C on Figure 7). Six each were used for the measurement of localised gas temperature profiles and for the heater temperature profile, both constituting the heat transfer measuring assemblies. There were some difficulties in arranging for independent movement of the spacer (1 on Figure 7) and measuring assemblies while being joined via the thermocouple and heater wires. Some 0.50 m lengths of the wires were wound around the spacer and a gentle helical loop was formed with the wires. This was held away from the measuring heads by a 0.1 m long nicroalloy wire spring. The Hooke's constant was very small and no appreciable change was noted when the spring was immersed in liquid nitrogen. The thermocouple junctions were made by

carefully removing the varnish at the tip of the wires, twisting gently together and soldering them together with indium and a non-corrosive flux.

Two carriages were built to support the local gas profile thermocouples. Figure 12A shows the first design schematically. The 3.05 mm O.D., 40 mm long stainless steel rod with a milled out 6.3 mm diameter disc at one end supported three 24 swg (0.55 mm) 50 mm long stainless steel hypodermic tubes. These were spaced with milled out stainless steel discs which supported horizontally 20 mm lengths of the hypodermic tube. This carriage was constructed in a jig, and finally rotated in a lathe to ensure good symmetry properties. The thermocouples were lead down the carriage and out horizontally. They overhung the horizontal arms by 5.4 mm having passed through another piece of hypodermic placed at the tip and varnished (GE7031 varnish).

After scanning horizontal planes in the dewar neck and finding no variation in temperature across the neck (cf Lynam and Scurlock (1968)) it was decided to eliminate possible doubt about the carriage interfering with the measurements. An even lighter structure was designed and this is shown schematically in Figure 12B. It was simply a length of 24 swg hypodermic tube bent into the form of a squared off bow, with an 82 mm length of 0.08 mm chromel thermocouple wire as the bow string. The thermocouple wires were fixed horizontally across the carriage and stuck with GE varnish on both the hypodermic tube and the chromel wire. The overhang in this case was 13.4 mm while the total horizontal length of 25.4 mm remained the same.

Temperature Measurement

Questions in the past have been raised about the problem of measuring temperatures in low velocity gas streams at low temperatures. In experiments of the type to be discussed temperature errors can arise

THERMOCOUPLE CARRIAGES

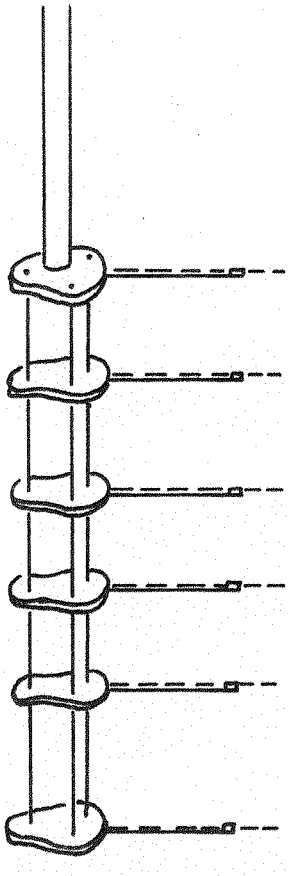

FIGURE 12a

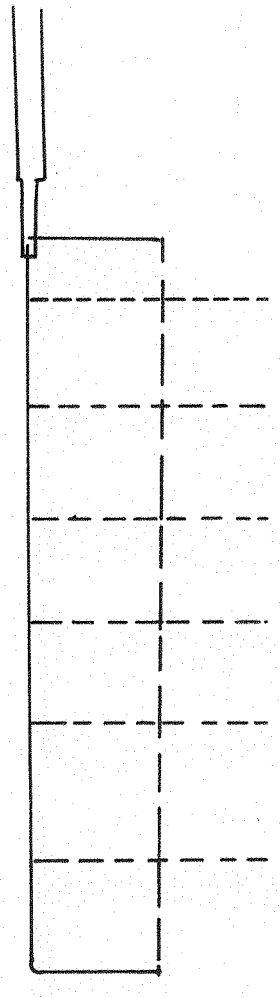

FIGURE 12b

from conduction or radiation of heat to the thermocouple. It was found difficult to investigate these complex effects theoretically since they are dependent on heat transfer to vertical and horizontal wires, and also on radiation from a non-constant temperature wall to a point, with the associated problem of temperature dependent emissivities.

An experiment was carried out to determine whether or not these effects were appreciable. A differential thermocouple was mounted in a similar manner to the actual thermocouples on the heat transfer probes. Several small copper foils were soldered in turn onto one junction while the other was at the same horizontal level and close by. The probe was then lowered into the cold dewar to see if the copper foils were increasing the heat transfer, thereby lowering the excess temperature that had been caused by the heat conduction. Even with foils of 2 mm x 5 mm and varying lengths of probe in the gas column no effects were observed.

Finally the distinction must be made between the requirement for the determination of absolute temperatures and that for temperature differences. Heat transfer primarily requires temperature differences to be known accurately; while the absolute temperature, used to evaluate the properties of the gas, need be known less accurately. Therefore in experiments using heated surfaces with small temperature excesses, the conduction effects will cancel, when the temperatures before heating and after are subtracted.

Heat Transfer Surfaces

In the design of a vertically heated surface for convective heat transfer measurements it was necessary to incorporate four features. It was required to be able to measure the temperature anywhere along the surface, to have a smooth low thermal conducting surface, to have an even distribution of heat flux across a known area, and to minimise non-vertical surfaces and edge effects. Although the cylindrical symmetry of the

dewar neck would suggest the use of cylindrical heaters, plate-like heaters were built for ease of construction and the avoidance of surface curvature problems (Sparrow and Gregg (1956(ii))).

A heat transfer surface was made by folding a rectangular piece of .025 mm thick stainless steel foil which had been cut with 2 mm by 2 mm flaps or windows in it. A piece of woven constantan-terylene mat half the size of the foil was covered with nylon stocking and soaked in GE7031 varnish. The mat was placed between the faces of the bent foil and the assembly was placed between aluminium plates and clamped tightly. The ends of the constantan wire had been teezed from the mat and previously varnished. These had been lead outside the heater assembly. After two days the heater was removed from the clamps and tested to see if its resistance was unchanged, and to see if the heater was electrically isolated from the stainless steel. If the heater was satisfactory, the flaps were folded back, the thermocouples were indium soldered onto the inner surface of the heater and then the flap was varnished and put back into place. The completed heater had clean smooth surfaces and was less than 1 mm thick. A piece of hypodermic needle not less than 40 mm long was soldered to the top of the foil and to a piece of stainless steel rod which fitted into the pin-vice at the end of the probe. The heater wires were connected and the heater was adjusted to a position where its own thermocouples were opposite those of the gas profile thermocouples.

Heater Voltage Supply

An emitter follower circuit using a ten turn 5 K ohm helipot and a 2N696 transistor was used to provide a linear adjustable voltage from 0 to 30 V across the heater resistor. An APT power supply stable to 1 in 10^3 provided the rail voltage for the transistor. The output could be connected either to a decade box acting as the dummy heater

or to the heater. This dummy resistor enabled power levels to be preset and switched into the heater quickly, and also maintained the transistor at the same power dissipation level, thereby avoiding voltage drifts.

Two similar circuits were built, one used to drive the heat transfer heater and another used to drive a heater varnished to the bottom of the helium reservoir. The voltage and current in either heater was read on a Solartron LM1420.2 (2 μV resolution) digital voltmeter.

Visual Experiments

Glass System

Flow visualisation experiments on the vapour column above cryogenic liquids and also on isolated heaters placed in the gas column were undertaken using a 1 m long 76.2 mm bore unsilvered glass dewar. A second larger bore 0.60 m long unsilvered dewar was used as a liquid nitrogen shield and a neoprene cover on top of this dewar prevented excessive cooling and misting of the remaining portion of the 76.2 mm dewar which was used as the "visual" section. Photographs were taken using a reflex Canon camera mounted on a stand; an Omega stop watch and a ruler were placed in the field of vision for reference purposes. The dewar was pumped continuously to a vacuum better than 4×10^{-5} torr.

Some temperature measurements were taken and a similar thermocouple carriage to the one described previously and drawn schematically in Figure 12B was used. This particular one was .216 m long and had eleven 40 swg copper constantan thermocouples spaced along it. A Tinsley two-pole twelve-way switch selected the thermocouple voltages and presented them to the LM1490 digital voltmeter. The constantan wires were commoned inside the switch and enabled a single reference junction to be used. A Frigistor ice point cell was used to maintain the reference temperature.

The thermocouples were calibrated by checking their voltages at

liquid nitrogen temperatures and room temperatures with published data (Cryogenics). The agreement was within 27 μV and it is not anticipated that errors arising from this method would lead to inaccuracies in temperature measurement greater than 1 K.

A variac supplied power to a resistor placed at the bottom of the dewar and by this means the nitrogen evaporation rate could be artifically increased.

CHAPTER 3

A merry road,a mazy road, and such as we did tread
The night we went to Birmingham by way of Beachy Head.

The Rolling English Road
G.K.Chesterton

HEAT TRANSFER IN VAPOUR COLUMNS

This chapter describes four series of experiments both non-visual and visual, designed to investigate the heat transfer characteristics within the vapour column above boiling liquid nitrogen and helium in a 76 mm diameter stainless steel dewar. The first section details three of the experimental arrangements and methods, and presents the corresponding results, while the second section analyses and discusses these results. The third section presents visual evidence of the fluid flow behaviour around extended and small heaters in vapour columns.

I - Experimental Arrangements and Methods

(a) Dewar Equilibrium

The equilibrium evaporation rate of liquid helium in the dewar was measured for various heat inputs via the heater attached to the helium reservoir. In this way it was possible to look at the variation of heat fluxes into the dewar with increased mass flow rates. The results are shown in Figure 13. The time taken to reach equilibrium conditions was in excess of eight hours. It was also hoped to present the wall temperature profiles for each mass flow rate but unfortunately the wall thermocouples suffered some damage before these results could be taken.

(b) Temperature Development

In the first set of experiments using a 12 mm x 12 mm heater and an array of six thermocouples the temperature response of the vapour to a sudden heat flux from the heater was measured. The physical arrangement is shown schematically in Figure 14, with the thermocouples placed symmetrically above and below the heater at a horizontal distance of 18 mm and vertical distances of 10 mm.

In order to measure the response times two stop watches were used, and the out-of-balance voltage from the potentiometric system was monitored on the galvanometer with a sensitivity of 13 mm deflection per microvolt. The supply voltage was preset to dissipate 19.5 mW in the heater, and both stop watches were started simultaneous to switching on the voltage to the heater. As soon as the galvanometer was seen to move the Omega watch was stopped and the time noted and the time taken for the galvanometer spot to reach a given deflection was noted using the second Smith stop watch. This procedure was repeated for the six thermocouples in turn, having waited for the temperature levels to return to their equilibrium values between each run. The wall thermocouple opposite thermocouple number 12 was also monitored. The whole experiment was performed in both helium

DEWAR EVAPORATION RATE VERSUS HEAT INPUT

FIGURE 13

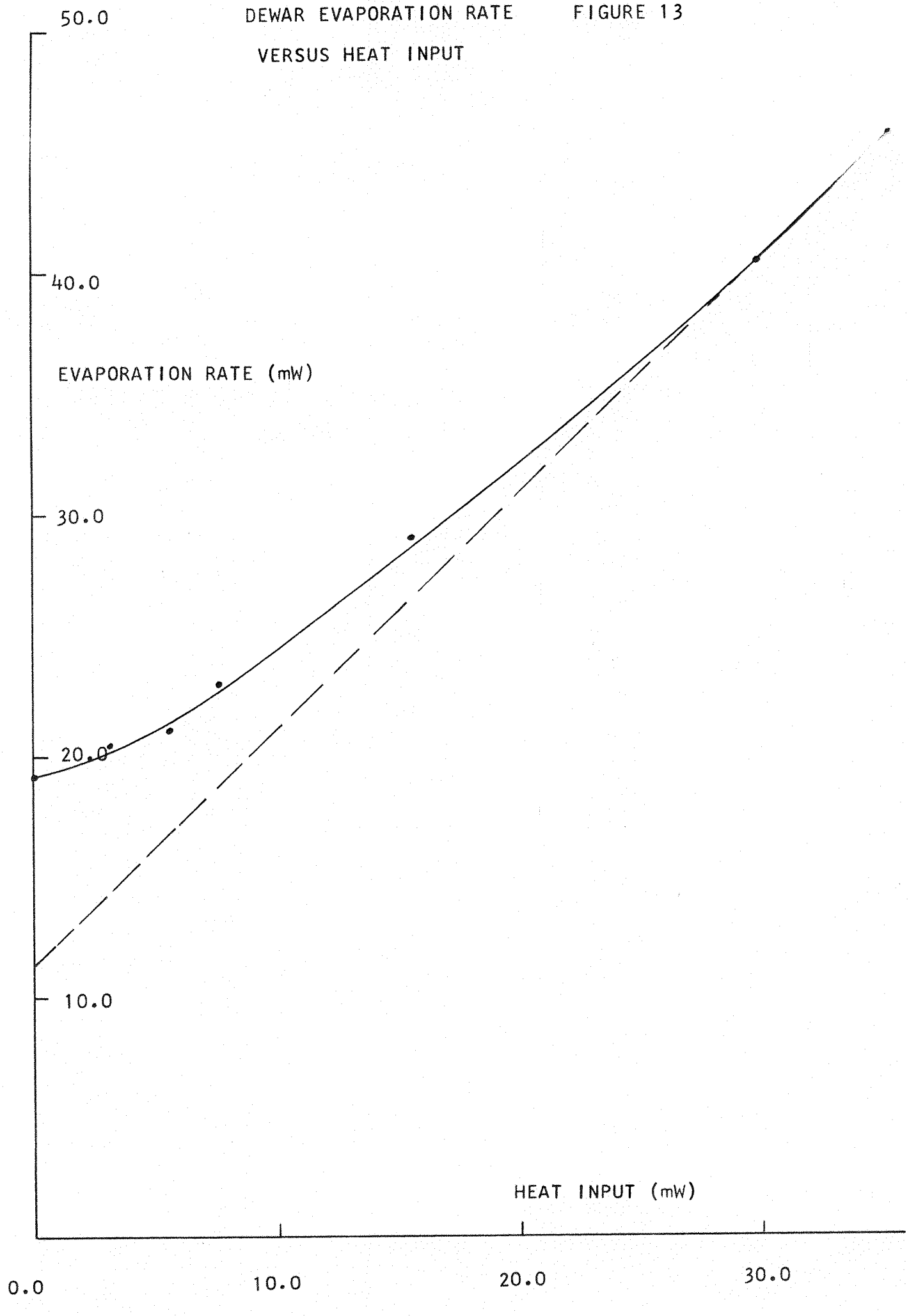

FIGURE 14 SCHEMATIC VIEW OF 1.2cm x 1.2cm HEATER WITH GAS PROFILE AND DEWAR WALL THERMOCOUPLES

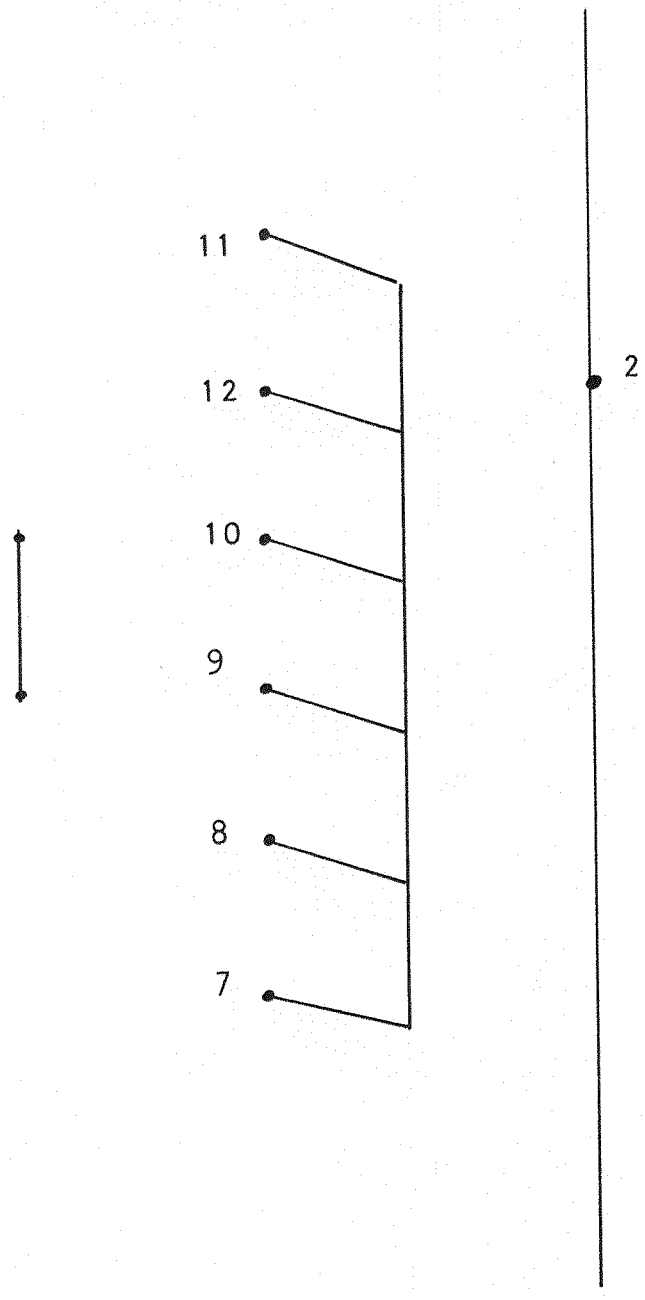

and nitrogen vapour, and the results are presented in Figure 15 and 16. Also the response of a thermocouple on theheater (number 5) and a thermocouple situated horizontally opposite number 10 was monitored with time after switching the heater on and then off. Figure 17 shows the results of two such runs.

(c) Heat Transfer

Because of the highly stable nature of the temperature difference between a point on the heater and a point horizontally opposite in the vapour, it was possible to define an effective heat transfer coefficient as

$$h_e = \frac{Q}{A_r(T_s - T_o)}$$

Q = heat dissipation

A_r = total vertical area of heater

Several experiments using both 12 mm by 12 mm and 52 mm high by 21 mm wide heaters were performed for increasing heat fluxes (temperature differences) in both nitrogen and helium vapour.

It was important to take both absolute and differential voltages and hence the sequence of taking results was complicated. The equilibrium absolute thermovoltages were first taken on all thermocouples, and then differences via the switches on certain pairs of thermocouples were read. A known power, which had been preset on a dummy resistor, was switched to the heater and the steady increased differential voltage between the pairs of thermocouples was noted. The absolute thermoelectric voltages (referred to ice) were read by sweeping the thermocouples on the switches in a forward and reverse direction in strict time sequence. The time averaged values could then be determined, and so drifts in temperature eliminated. The absolute temperatures, the differences via absolute temperature and the differential voltage readings could then be determined and compared. The disagreement was at worst 3% in the differential

FIGURE 15 RESPONSE OF THERMOCOUPLES AFTER SWITCHING ON HEATER -- HELIUM VAPOUR

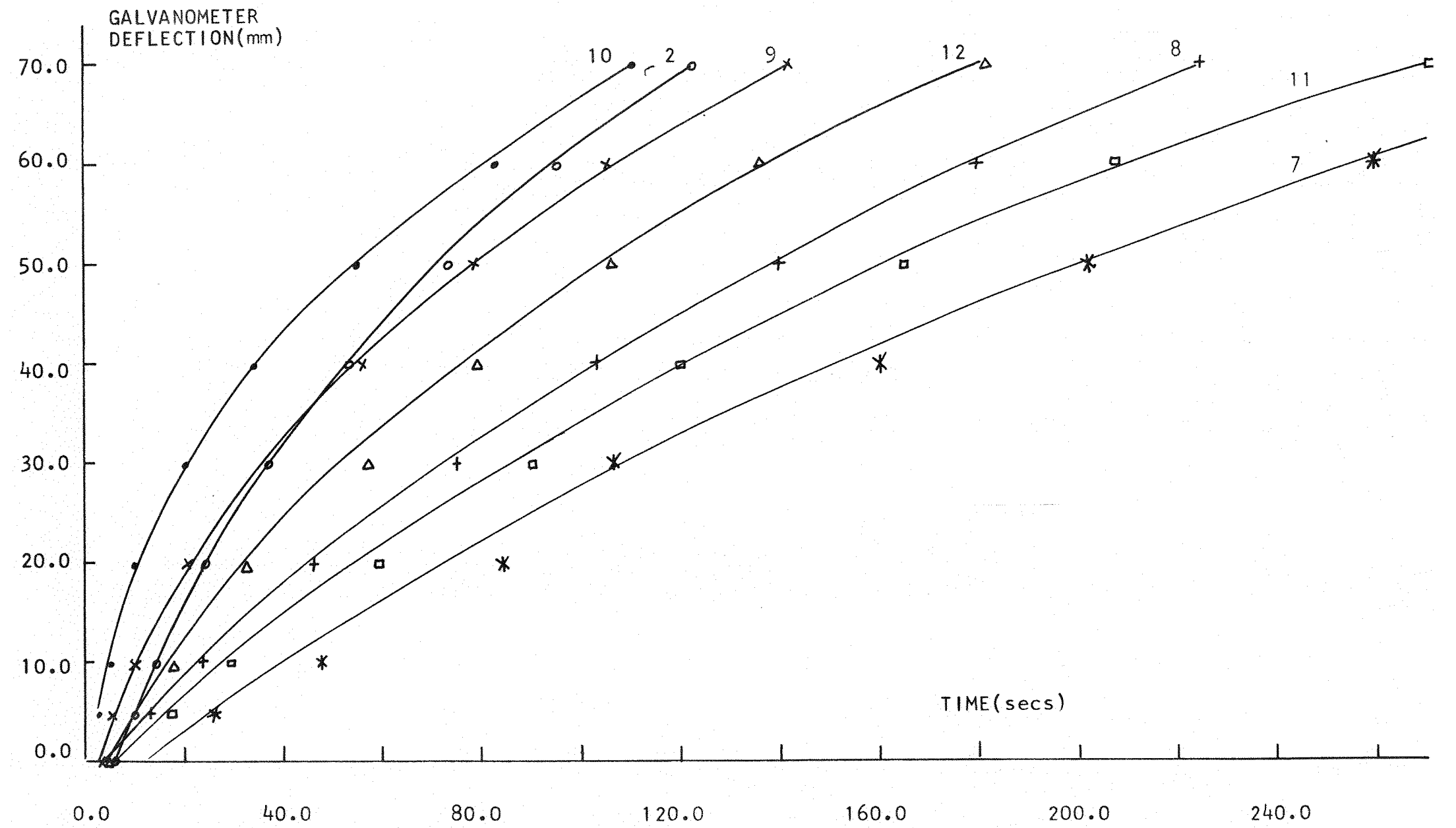

FIGURE 16 RESPONSE OF THERMOCOUPLES AFTER SWITCHING ON HEATER --- NITROGEN VAPOUR

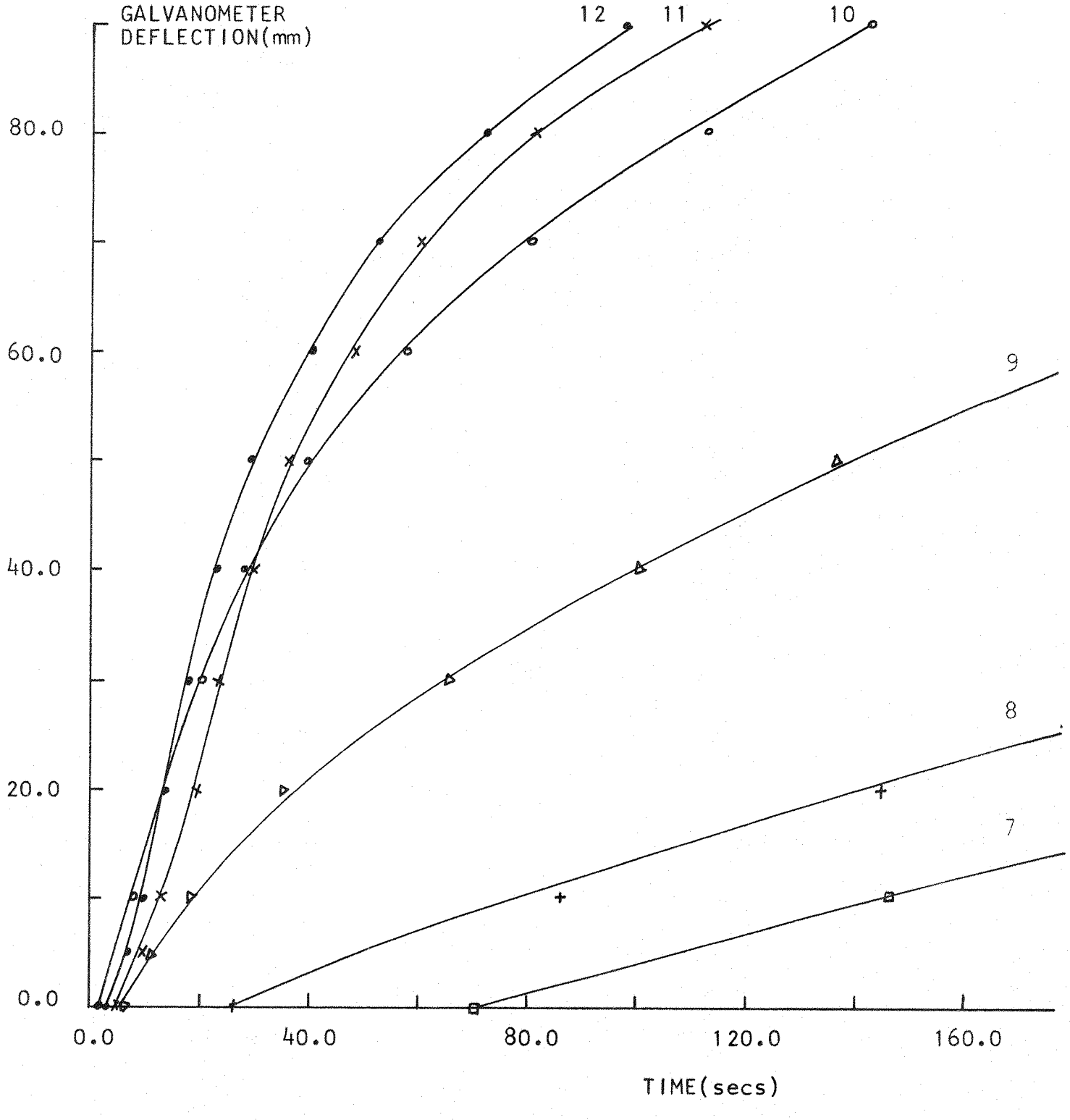

FIGURE 17 RESPONSE OF THERMOCOUPLES ON HEATER AND IN GAS AFTER SWITCHING ON HEATER

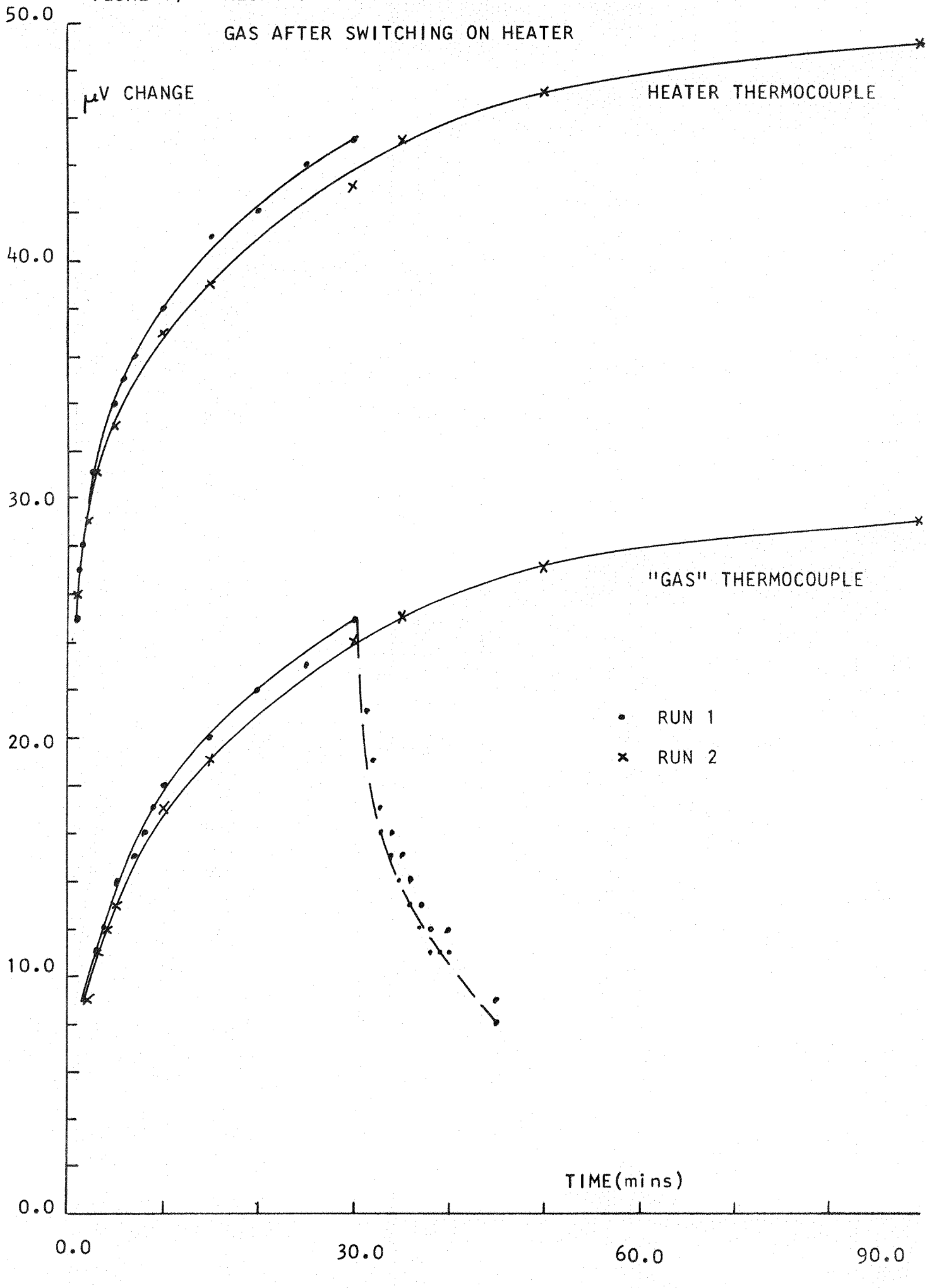

voltage readings. The effective heat transfer is plotted against heat flux for the 12 mm x 12 mm heater in helium and nitrogen vapour respectively in Figures 18 and 19.

It was necessary to reduce the possible adverse influence of edge effects and as mentioned the heat transfer experiments were repeated with a 52 mm x 21 mm heater. The influence of the edge effects and of this heater itself on the local temperature distribution within the vapour column can be seen by reference to Figure 20 where the numbering corresponds to the thermocouple numbering. This temperature distribution is drawn for the case of the maximum heat flux used in these particular experiments. Also presented in Figures 21 and 22 are the local effective heat transfer coefficients for the points 10 mm and 30 mm from the leading edge and on the centre line of the heater, in helium and nitrogen vapours respectively.

FIGURE 18 HEAT TRANSFER FROM 1.2cm x 1.2cm HEATER IN HELIUM VAPOUR

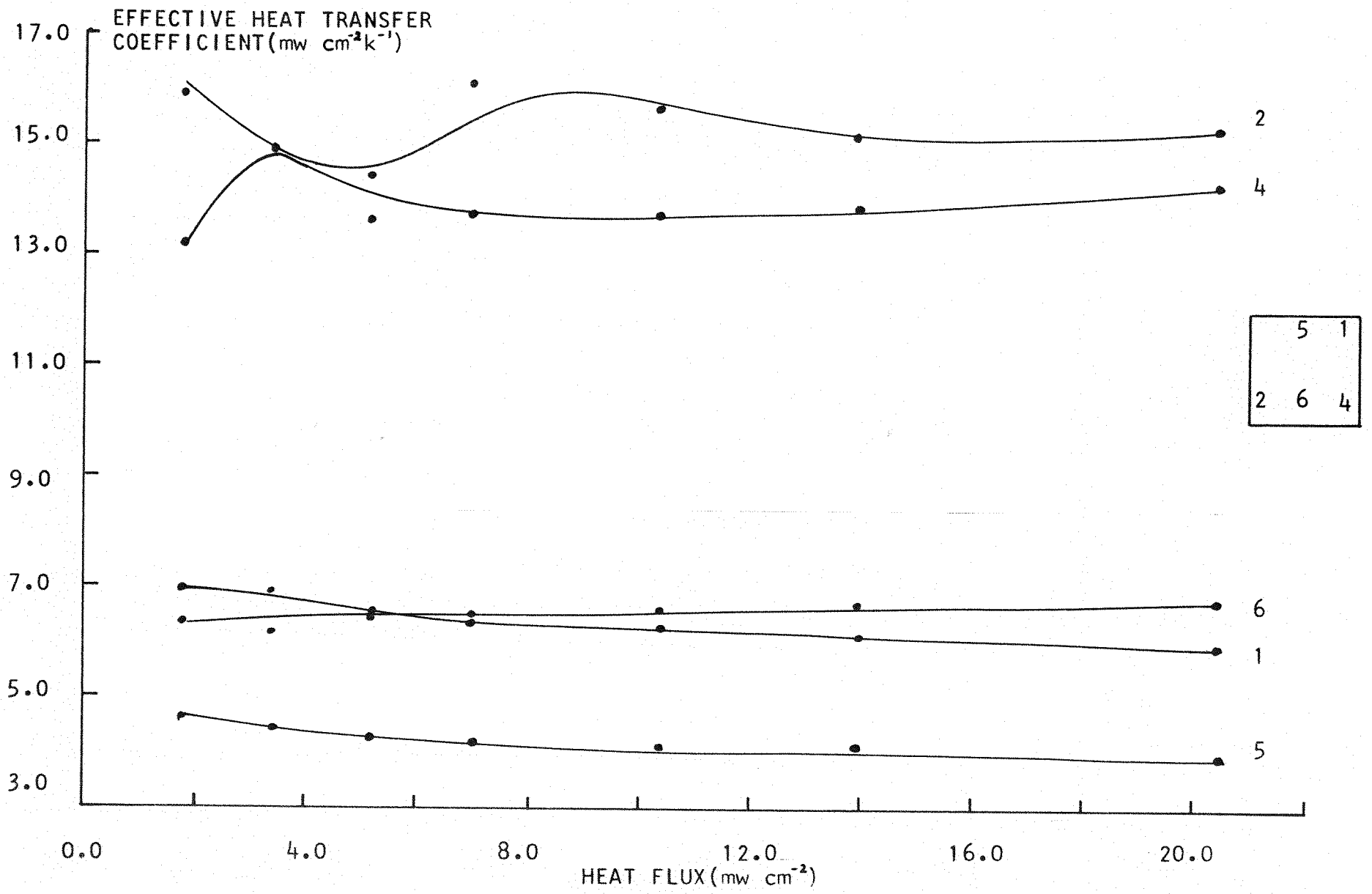

FIGURE 19 HEAT TRANSFER FROM 1.2cm x 1.2cm HEATER IN NITROGEN VAPOUR

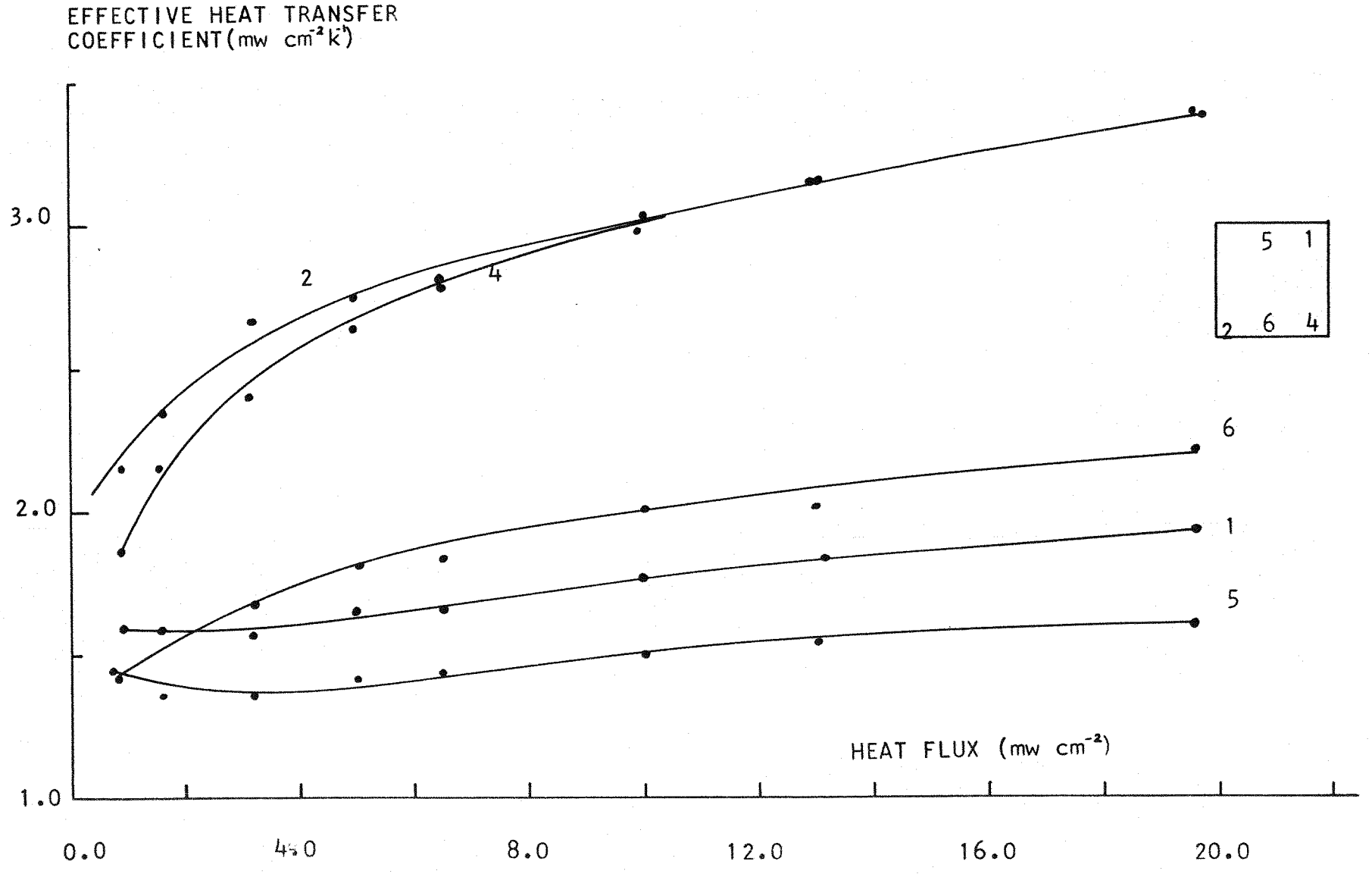

FIGURE 20 MAXIMUM DISTORTION EFFECTS ON 5.2cm x 2.1cm HEATER

(11.192 mw cm^{-2})

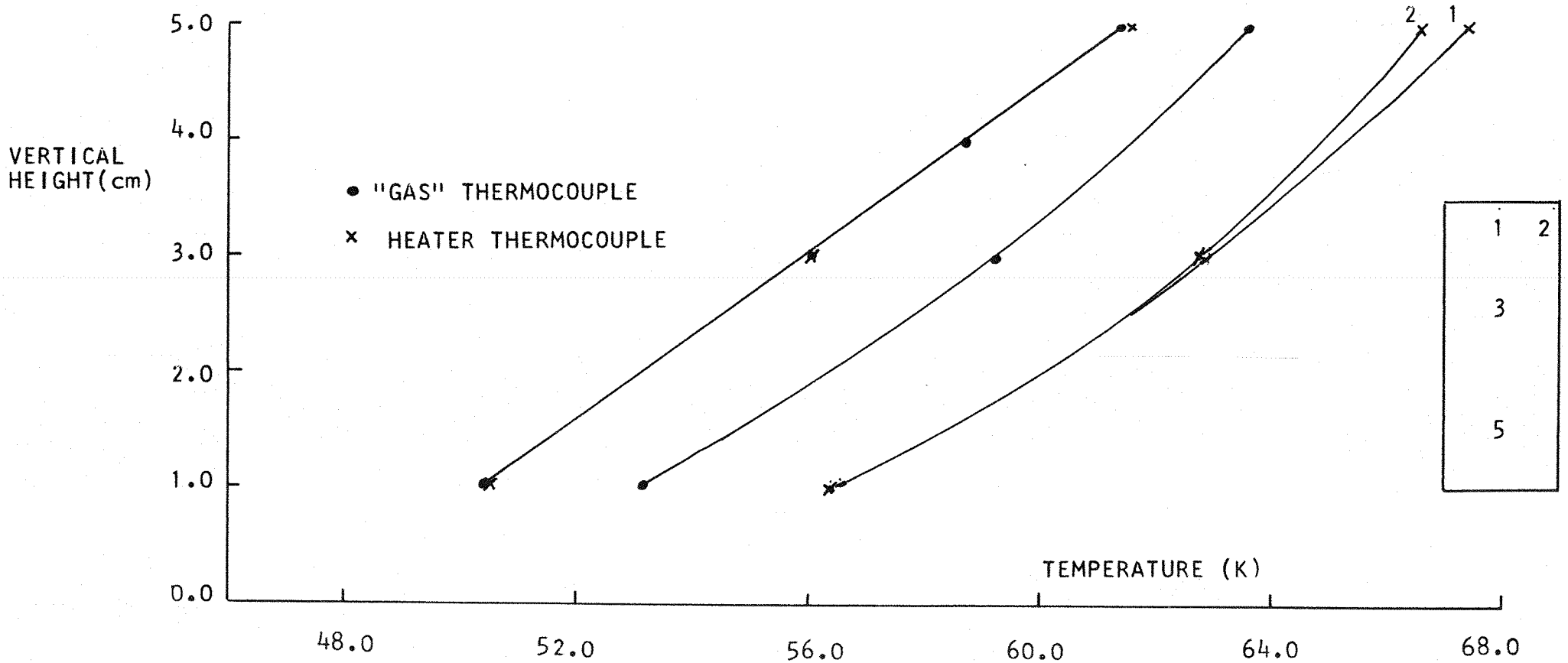

FIGURE 21 HEAT TRANSFER FROM 5.2cm x 2.1cm HEATER IN HELIUM VAPOUR

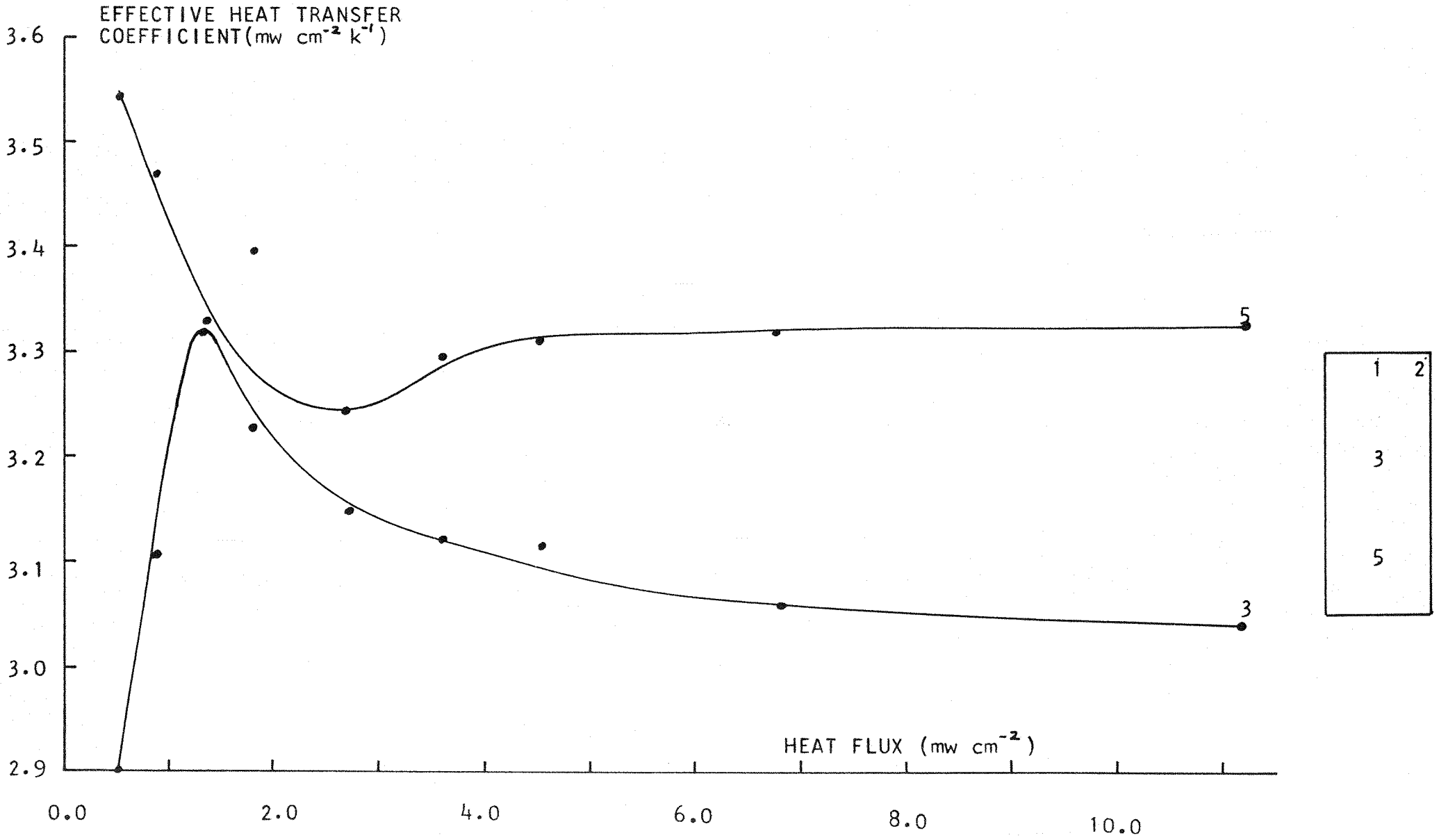

FIGURE 22

HEAT TRANSFER FROM 5.2cm x 2.1cm HEATER IN NITROGEN VAPOUR

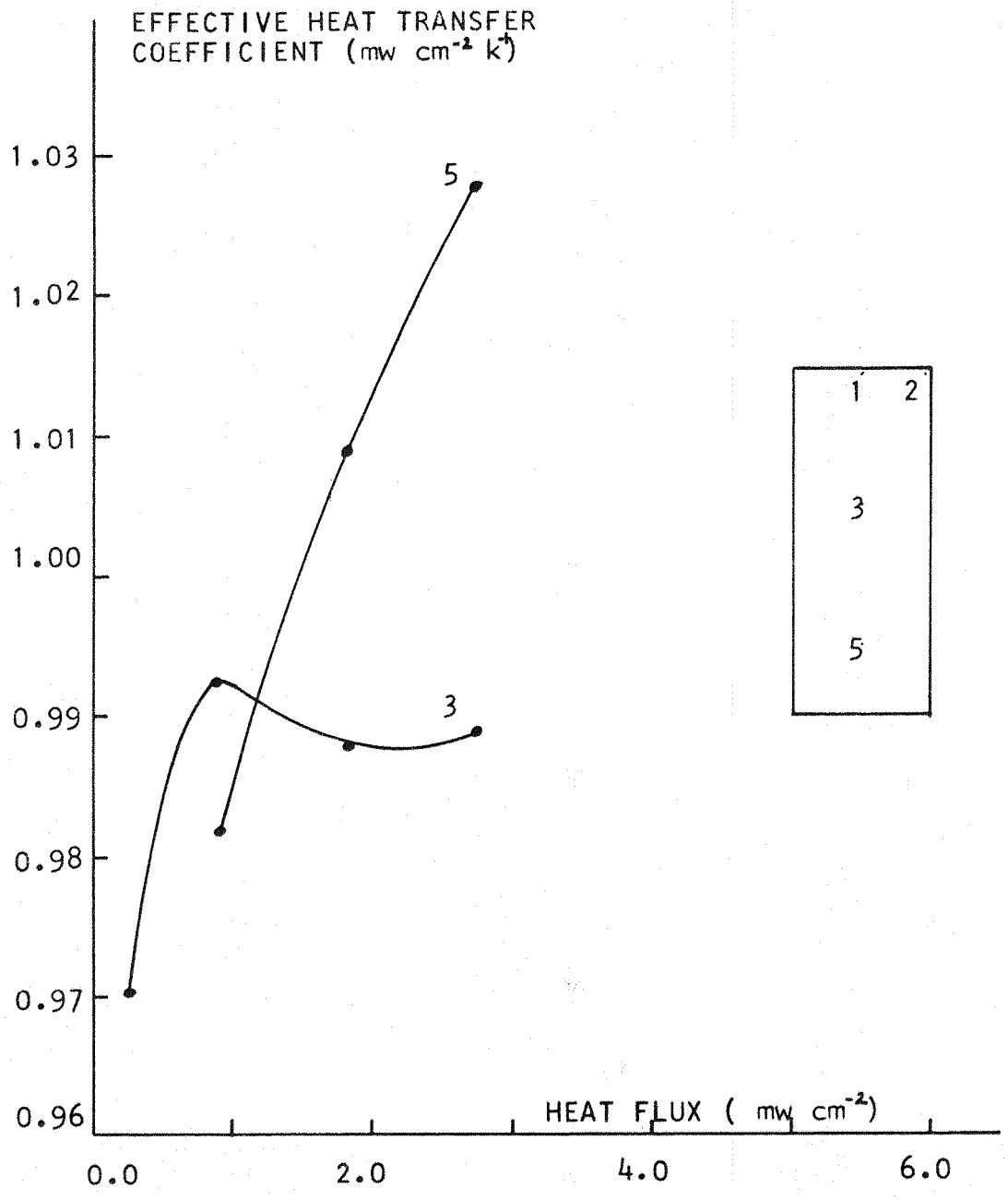

II - Analysis

(a) Dewar Equilibrium

Because of the lack of information on the temperature profiles with increasing helium mass flux, it is not possible to present a complete analysis. From earlier indications it appears that the gradient, as would be expected, is determined largely by the connection to the nitrogen shield. The influence of the mass flow rate will therefore be reduced by this fixed temperature point, which can either absorb or supply heat from the nitrogen shield as temperature levels demand. In fact the nitrogen shield boil off was seen to reduce as the mass flow rate of helium was increased. In practice, the contact resistance between the nitrogen shield collar and the stainless steel dewar neck could add a further complicating factor.

The normal evaporation rate of the nitrogen shield was 240 cc liquid hr^{-1} and the helium evaporation rate was 19 cc liquid hr^{-1}. From the radiation heat flux tables presented in Scott[5], and noting that the emissivity value is linearly related to the heat flux for a fixed area ratio, the average emissivity of the radiation surfaces 300 K to 77 K is 0.07 and correspondingly 0.08 for the 77 K to 4.2 K surfaces. These represent average, not too well polished, surfaces (Carslaw and Jaeger[1]).

Finally Figure 23 presents the residual heat contribution for various induced mass flow rates (the abscissa is the actual heater input corresponding to Figure 13). This residual heat input is determined by subtraction of the heater input and the radiation contribution from the total evaporation rate. The radiation contribution is assumed to be the intercept of the straight line portion of the boil off curve on the ordinate axis. This is in accordance with an analysis by Lynam and Scurlock (1968) and Figure 23 shows in more detail the variation of this residual heat input with increasing mass flow rates.

FIGURE 23 RESIDUAL HEAT CONTRIBUTION

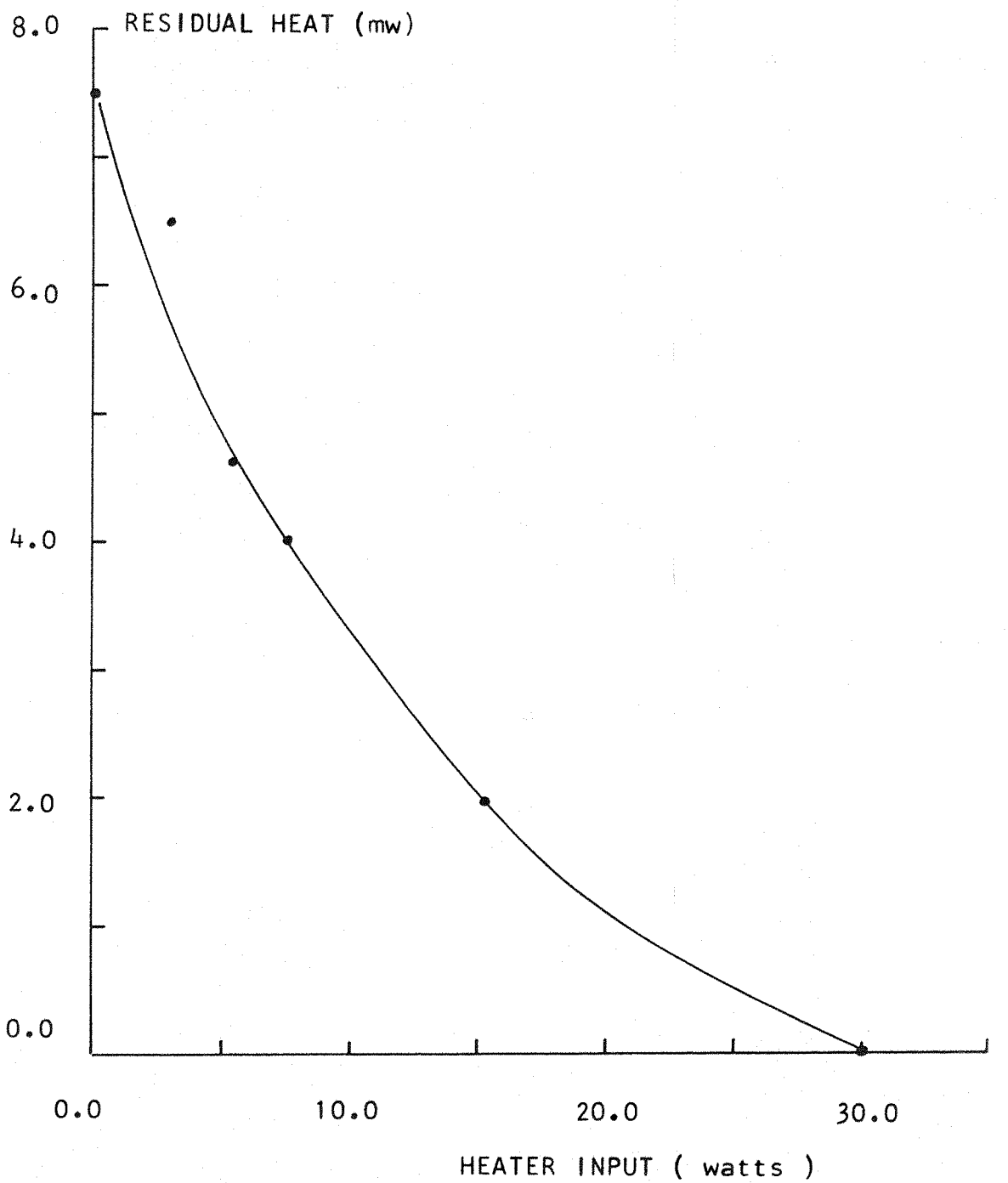

(b) Temperature Development

The Figures 15 and 16 provide information about the manner and extent of the interaction of the heater and the vapour. It has become quite obvious that the heater cannot be considered, in heat transer terms, to be isolated.

In the case of helium (Figure 15) the thermocouples respond within approximately the first five seconds. It is then noticeable that in order of increasing speed of response we have: 7, 11, 8, 12, 9, 10. This particular ordering of thermocouples would immediately suggest that angular distance from the source of heat is of primary importance, and hence one is led to believe from the rate of warming that the heat flux is being distributed non-uniformly, the greatest concentration being horizontally opposite and diminishing with increased positive or negative angle from the horizontal. Also because the responses are similar whether they are above or below the heater suggests that conduction is the determining parameter. However there is some difference, and since the thermocouples above the heater show slightly increased response times over those below, this difference can be attributed to convection. Further a thermocouple attached to the outside surface of the stainless steel dewar neck surrounding the vapour and heater and at the same level as the No 12 thermocouple (Figure 14) responds just as quickly as No 12 at first, and then begins to respond faster, in a manner more like No 10. The wall is therefore responding to the heat transferred in the horizontal plane corresponding to the top of the heater.

These considerations are reinforced when a comparison is made with a similar experimental arrangement in a nitrogen environment (Figure 16). The response curves show a marked difference. Thermocouples 7 and 8 have a large time lag before a response can be seen while Nos 10, 11, 12 respond within approximately the first five seconds. The initial

order in speed of response now becomes 7, 8, 9, 11, 12, 10 changing to 7, 8, 9, 10, 11, 12 after the first thirty seconds. This grouping and time delay distribution (the upper thermocouples showing a faster response than lower thermocouples) shows that the convection mechanism is stronger than the conduction mechanism.

It must be stressed, here, that because the heater is influencing the temperature levels over such a wide area the problem of flux distribution becomes extremely complex. It is not difficult to determine the flux distribution when the heater can be considered as isolated, behaving as a free convective surface. The symmetry problems however become extremely acute when there is this degree of interaction, not only for the case of a flat plate in a cylinder with a temperature gradient, but also for a plate which terminates within the cylinder. Even if a mathematic model were solved then, apart from the justification of the inherent assumptions that would have to be made, the amount of information to be gained would not be very general giving a solution which would be peculiar to this situation. An alternative approach to the problem will be discussed in the heat transfer section.

The Grashof number based upon the radius of the neck of the dewar is 1.26×10^5 for the helium case discussed, and 1.07×10^7 for the nitrogen case. Obviously the degree of convection will be proportional to these numbers. Again the next section will discuss this more fully.

Finally Figure 17 shows the extended response time curves for the No 5 heater thermocouple and No 10 "vapour" thermocouple. This demonstrates the rapid establishment of a fixed temperature difference between the heater and vapour (in this case in helium) and the immediate drop in temperature difference with switching off power, showing little heat capacity in the heater. Figure 24 is a logarithmic plot of these curves and an interesting feature emerges. The initial slope is proportional to the square root of the time.

FIGURE 24 RESPONSE OF THERMOCOUPLES ON HEATER AND IN GAS AFTER SWITCHING ON HEATER

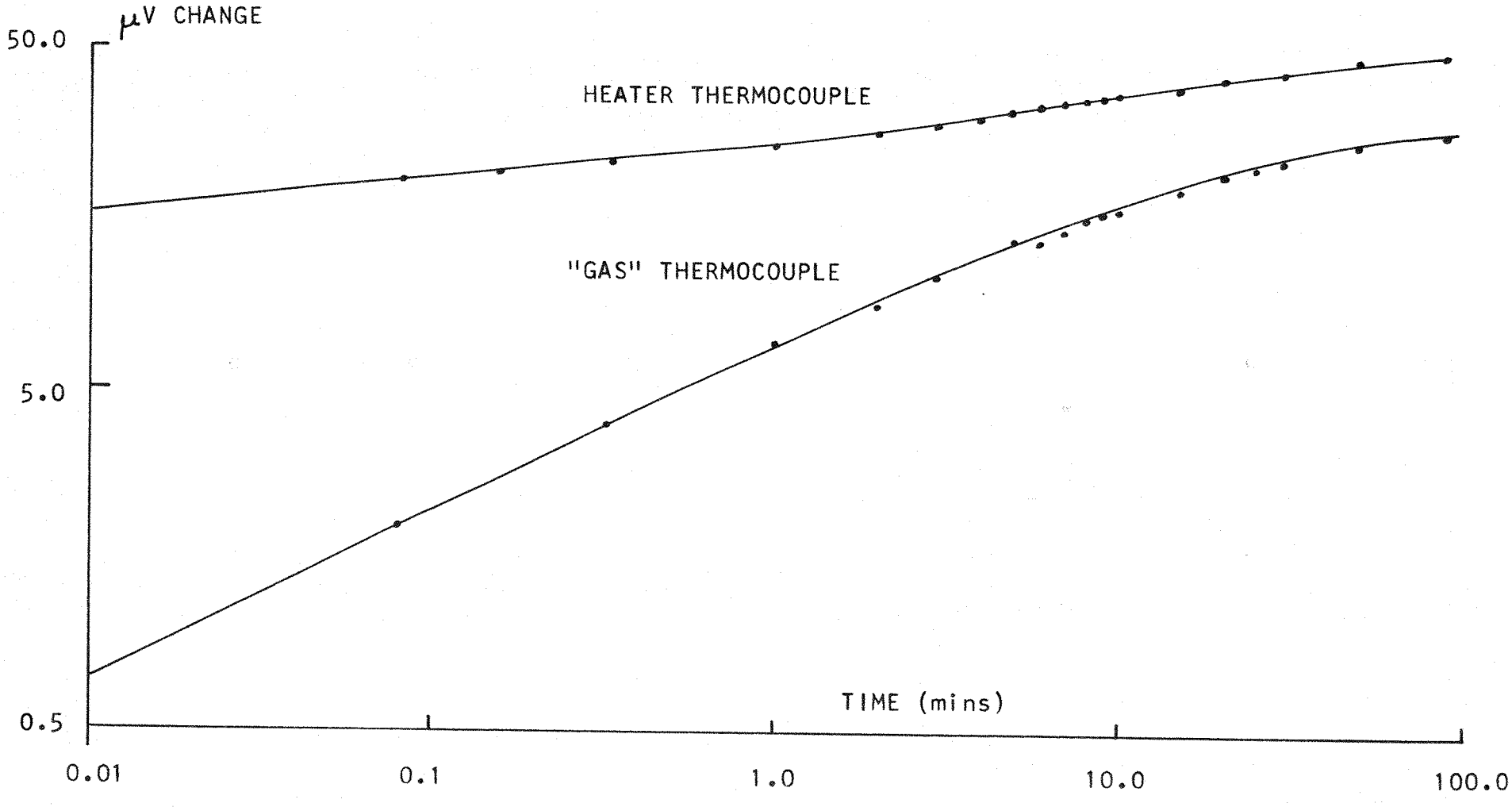

In the Laplace solution of the constant flux boundary condition in a semi-infinite conducting medium the rate at which the surface temperature rises can be shown to be proportional to $\tau^{\frac{1}{2}}$.

We have

$$q = -k\frac{dT}{dx}$$

$$\frac{\partial^2 q}{\partial x^2} = \frac{\partial q}{\partial \tau} \qquad x > 0 \quad \tau > 0$$

$$q = q_o \qquad x = 0 \quad \tau > 0$$

which has the solution (Carslaw and Jaegar[2])

$$q = q_o \operatorname{erfc} \frac{x}{2\sqrt{\alpha\tau}}$$

leading to

$$T = \frac{q_o}{k} \int_x^\infty \operatorname{erfc} \frac{x}{2\sqrt{\alpha\tau}}\, dx$$

$$T = \frac{2q_o\sqrt{\alpha\tau}}{k} \operatorname{ierfc} \frac{x}{2\sqrt{\alpha\tau}}$$

for $x = 0$ this gives

$$T = \frac{2q_o}{k}\left(\frac{\alpha\tau}{\pi}\right)^{\frac{1}{2}}$$

In order that this solution be applicable in our case one would have to assume that the heat transfer is conduction dominated and that a horizontal plane through the heater behaves as a constant flux source. It has been shown that conduction is the determining parameter and also that the wall response is closely linked with the response of the gas at the same horizontal level.

It is not possible, however, at present to show an exact numerical agreement because of the uncertainty of aportioning the flux as previously mentioned.

(c) Heat Transfer

The heat transfer measurements were made for low heat fluxes, (low temperature differences) and for relatively small surface areas in

order to make measurements under near equilibrium conditions within the dewar. The edge effects in the case of the 12 mm x 12 mm heater are quite large, while in the 52 mm x 21 mm heater the temperature differences across the heater are not very severe. Also in the larger heater the gradient up the heater is hardly changed. The local effective heat transfer has been given for the positions 10 mm and 30 mm up this plate. In order that these be of general use it is necessary to try and correlate this work with previous similar work.

Jakob[2] considers the case of free convection between parallel plates which incorporates combined conduction and convection heat transfer. An overall heat transfer is defined

$$q = \frac{k_c}{w}(T_1 - T_2)$$

where q = heat flux

w = distance between plates

$(T_1 - T_2)$ = temperature difference between plates

k_c = equivalent thermal conductivity - including the effects of conduction and convection.

For plates at a large distance from each other we find the free convection analysis applies

i.e. $$(T_1 - T_m) = (T_m - T_2)$$

$$q = h(T_1 - T_m) = h(T_m - T_2)$$

$$q = \tfrac{1}{2}h(T_1 - T_2)$$

hence

$$k_c = \frac{h}{2} \cdot w$$

However as the plates are brought closer there is a greater degree of interaction. Jakob quotes semi-empirical formulas based on the work of Mull and Reiher for the effective Nusselt number and Grashof number, both numbers being based on the distance between the plates. These are

$$\frac{k_c}{k} = 0.18\, G_{r_w}^{\frac{1}{4}} \left(\frac{H}{w}\right)^{-1/9} \qquad 2 \times 10^4 < G_{r_w} < 2 \times 10^5$$

$$\frac{k_c}{k} = 0.065\, G_{r_w}^{1/3} \left(\frac{H}{w}\right)^{-1/9} \qquad 2 \times 10^5 < G_{r_w} < 11 \times 10^6$$

H = height of plate.

Since these equations relate to normal fluxes between the plates (or concentric cylinders) they cannot be applied directly to the present situation. Also we have the problem of the magnitude of the flux. It is necessary to choose to analyse these results in an indirect and approximate way. If we assume that the theory does apply and that the adjustment in the flux in order to allow for side effects is considered to be a factor f, and we also assume that this side heat q_s is proportional to the temperature excess, then we have:

$$q_s = Z \cdot \Delta T$$

where Z depends on geometric, conductive and convective factors and and

$$\frac{1}{f}\left(\frac{qw}{(T_1 - T_2)k}\right) = \frac{1}{f} \cdot \left(\frac{k_c}{k}\right) = F(G_{r_w})$$ (where F is the theoretical functional relationship) with

$$q/f = q - q_s$$

as the relation of the side heat

hence

$$q_s = q(1 - 1/f)$$

hence

$$Z \cdot T = q(1 - 1/f)$$

This relationship results from the assumptions made and Figure 25 shows this relationship as obtained from the data for both helium (the upper line) and nitrogen (the lower line). The approximation of the data to the same straight line for the two thermocouples in the cases of both helium and nitrogen is extremely close. Also both lines go through the origin. If the geometric factors remain the same in both cases, and one were to consider the constant Z to be the thermal conductivity, then the ratio of the slopes of the curve should be equal to

FIGURE 25 SIDE HEAT EFFECTS ON 5.2cm x 2.1cm HEATER

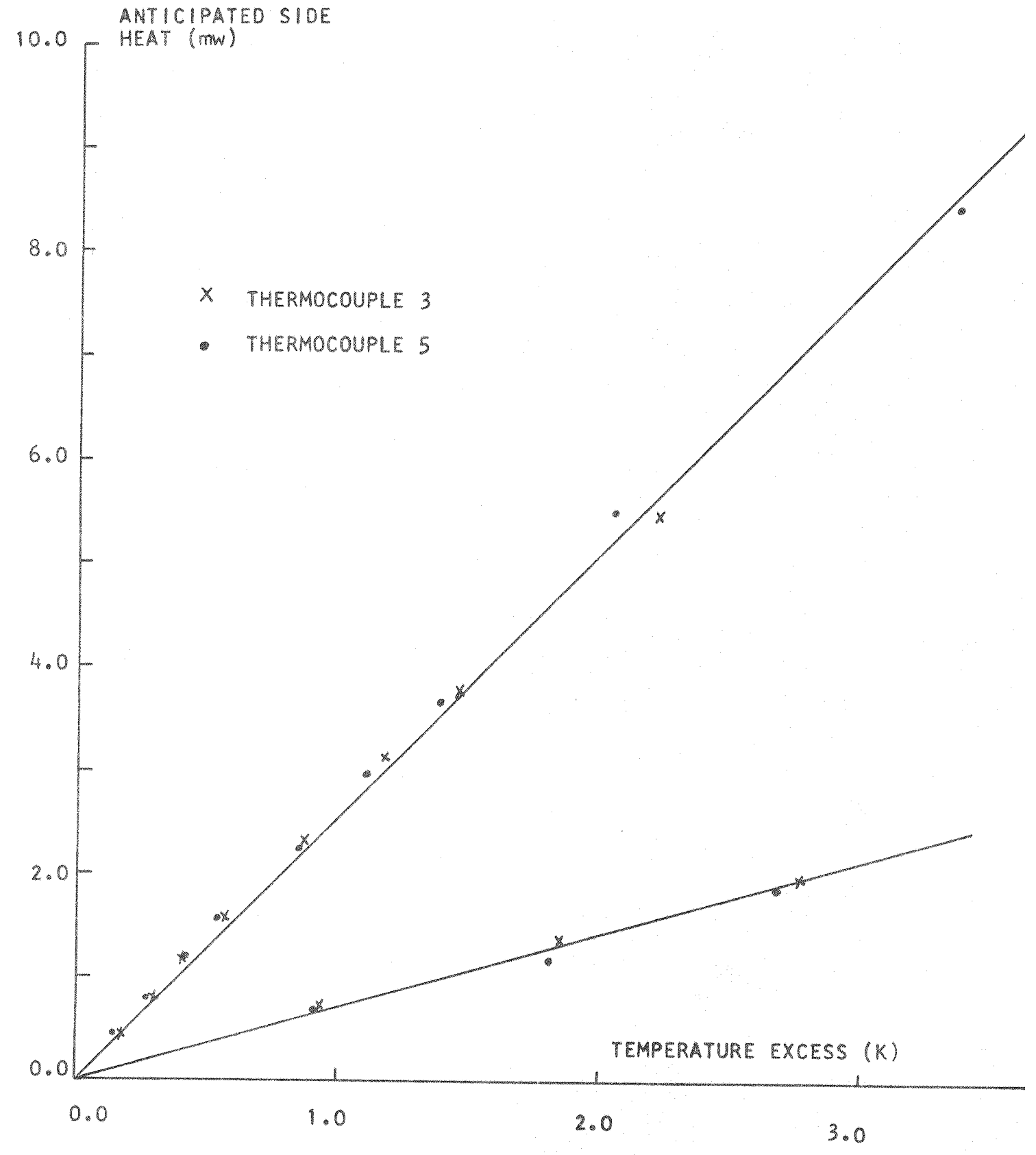

the ratio of the thermal conductivities of the gases. The ratios are 3.6 (results) and 5.8 (theory). The method cannot be considered to produce conclusive evidence of the heat transfer process but there is, nevertheless, a very strong indication that the assumptions are correct, and that the theory does apply.

III - Flow Visualisation Experiments

Some qualitative visualisation studies have been started in order to examine the fluid flow behaviour around extended and non-extended heaters in cryogenic vapour columns. This section describes the methods and experiments, and presents the photographic results.

Method

Two types of heater were used. The first was a wire wound vitreous enamel resistor which was 15.3 mm long and 7.7 mm in diameter. The second was a .450 m long closely wound nicralloy spring with an overall diameter of 2 mm. In these experiments it was necessary to have high dissipation type heaters because of the nature of the tracing element, which required large temperature differences.

In order to display the flow the heating element was first immersed in either water or trichloroethylene and then immediately in liquid nitrogen, thereby freezing the tracing element onto the surface. The heater was then suspended by its current wires in the vapour column above boiling liquid nitrogen inside a 76 mm diameter glass dewar. The voltage across the heater was increased until the tracing element was ejected from the surface, and the fluid flow lines displayed. Using this method the flow patterns could be easily seen without interference from unrequired tracer.

Other tracing elements were tried but as yet they have not been successful. Nitrous oxide with a freezing point of 182.4 K, and argon with a freezing point of 84.0 K would appear to provide a more sensitive tracer, requiring less temperature excesses. However, as mentioned, the techniques of depositing them on the surface have yet to be developed.

The photographs were taken using a Canon reflex camera with normal incident lighting. The same method was used in later experiments and

a fuller description will be left to the next chapter.

Results and Discussion

The first series of photographs show the experiments on the non-extended heater. The first photograph (A) is taken at an angle slightly above the horizontal in order to show the pattern which occurs in the horizontal plane. The vapour can be seen to rise along the vertical sides of the heater overshooting the end of the heater and finally turning over. It then drops to a new level and moves outwards in a wave-like manner.

The next three photographs (B, C, D) were taken normal to the heater and dewar axes, and show the development of the flow sequentially. Again in B we have the formation of the overshoot, the reverse flow, and the horizontal motion. The vapour in the next photograph has moved slowly downwards and also towards the heater. Vapour is also being entrained in a boundary layer flow close to the dewar wall. This particular feature will be explained in the next chapter. The third and last photograph (D) of the development shows the completion of the recirculation of the vapour. Towards the lower edge it is possible to see in the fine detail a U-shaped streamline which extends into the overshoot. The power dissipation of the heater at this point is 4.32 watts. The time scale is approximately 25 seconds, 50 seconds and 90 seconds for the sequential photographs. The overshoot plume and the recirculation move upwards with increasing power and a more turbulent picture is produced. The next photograph (E) is one such example which is taken for a power dissipation of 30.31 watts.

The last two photographs (F, G) are examples of flow patterns using the extended heater. The boundary layer is initially laminar and can be seen to slowly develop turbulent waves. These grow and finally involve regions at a distance from the wire in turbulent motion. The first photograph was taken at a power dissipation of 8.6 watts and the

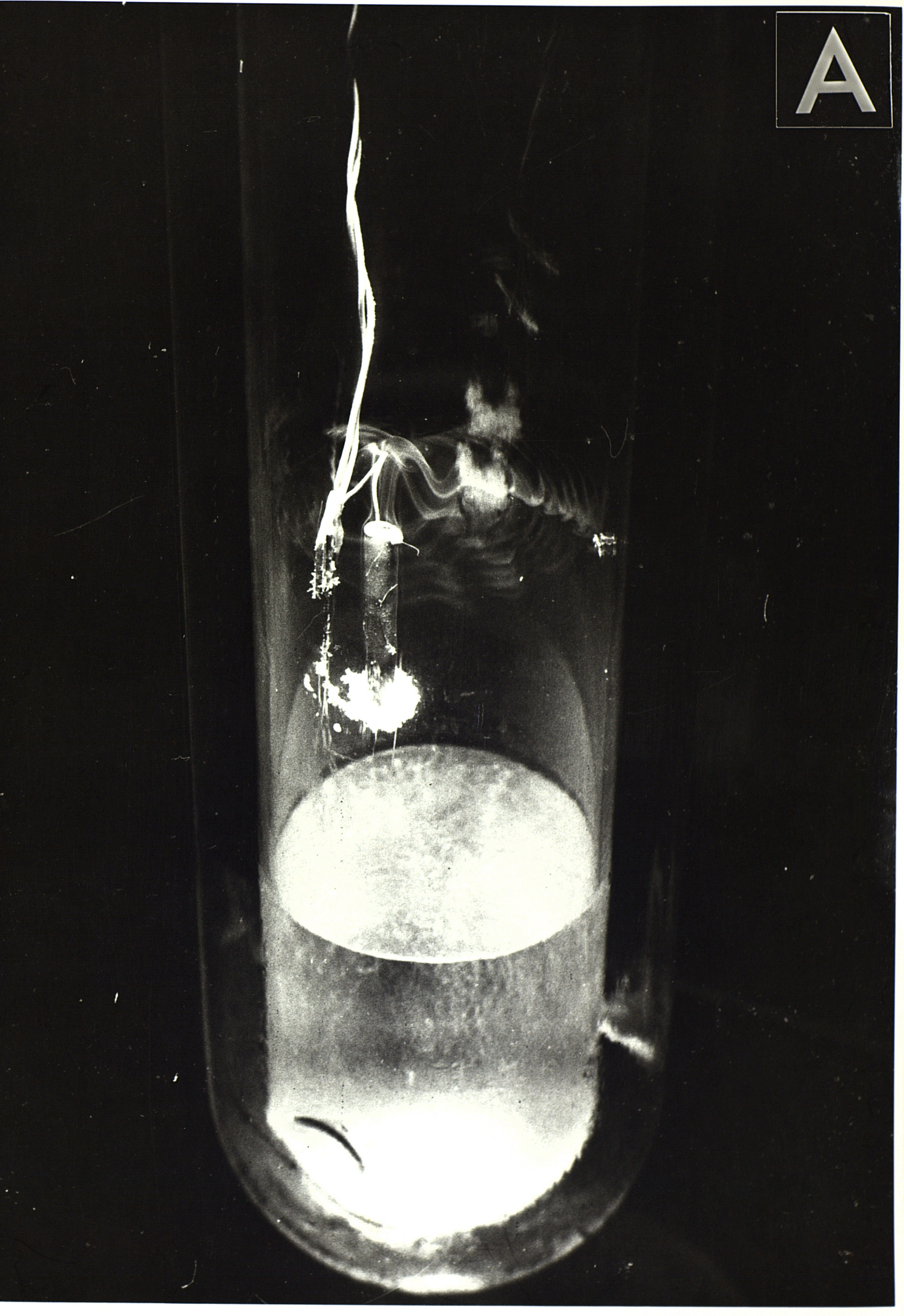
A


B

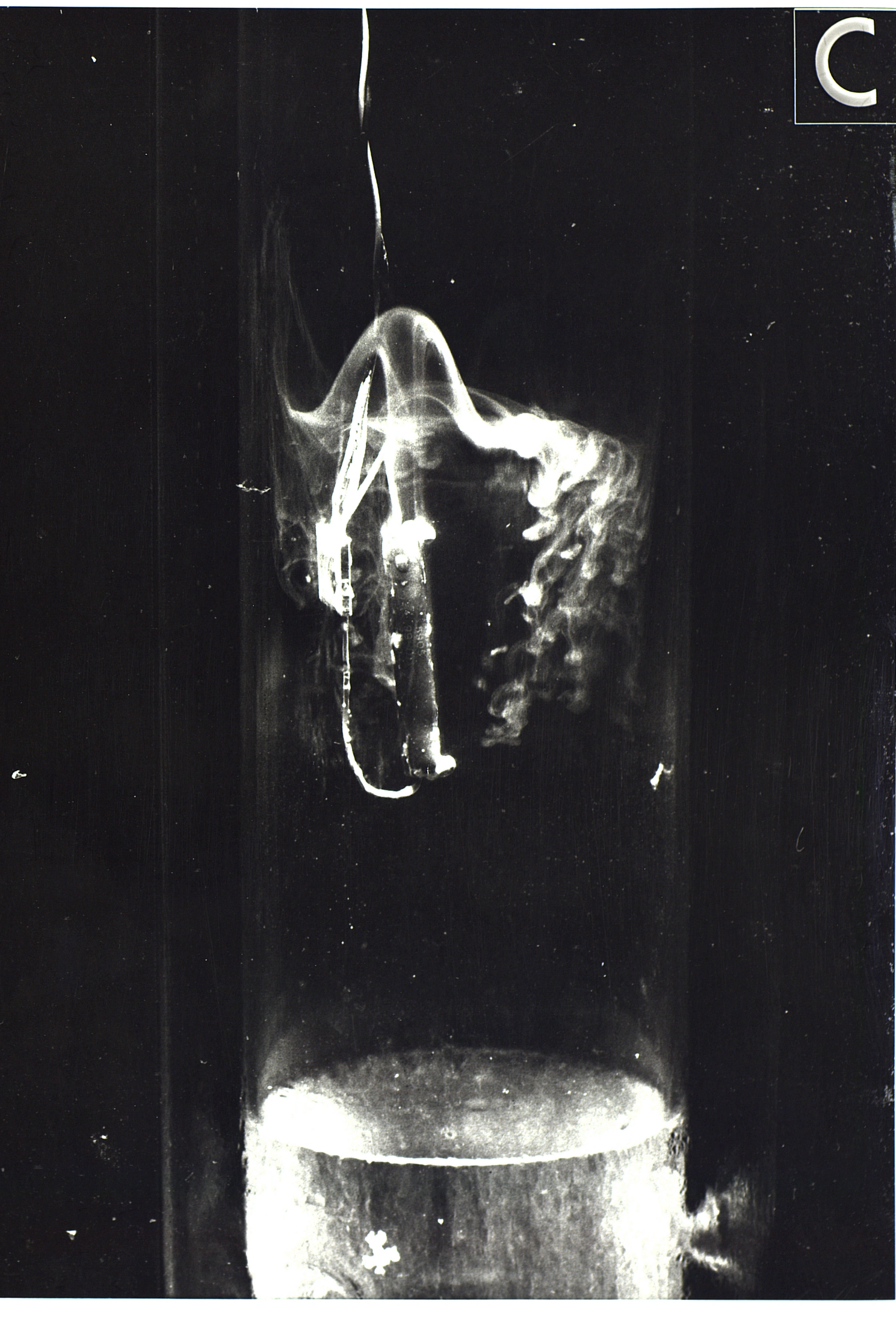
C

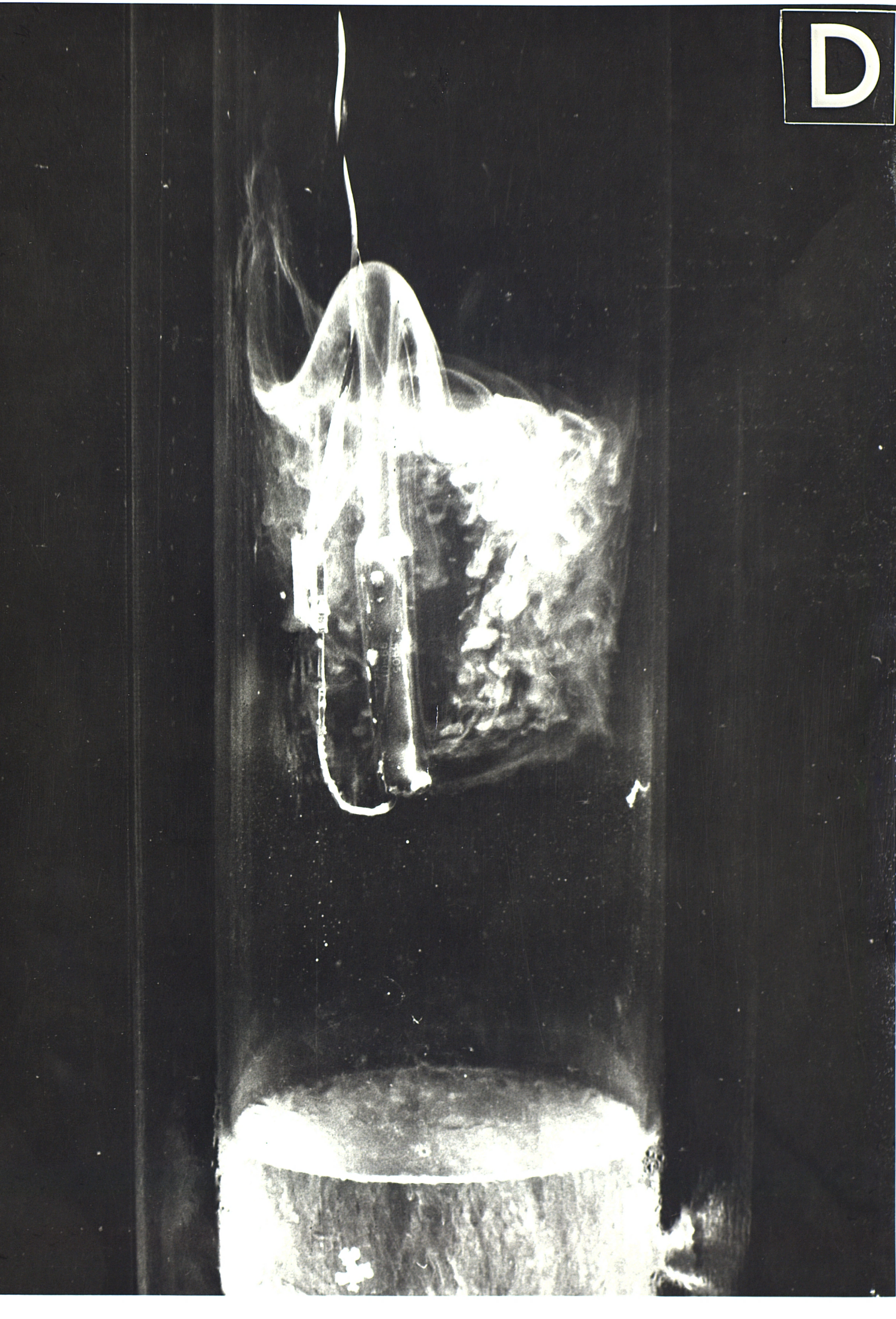
D


E


F

G

second at 17.1 watts.

In the case of the extended heater the formation of a boundary layer is predictable. Its transition to turbulent flow is similarly predictable in a general sense. The question of the effect of stratification and the possible reduction of the boundary layer growth must remain open but no indications of a peeling off of vapour have been seen. This would occur in some highly stratified fluids.

The flow behaviour around the non-extended heater is however more unusual. After leaving the heated surface the momentum of the plume is eventually lost by reduced buoyancy either because of heat exchange or change of temperature level in the stratified environment. The direction of motion is reversed for a brief time with a small horizontal velocity, and then in finding its equilibrium level begins to move horizontally with an apparent damped simple harmonic motion. Fluid then begins to drop slowly downwards and also with a transverse velocity towards the heater. Eventually the boundary layer suction draws the fluid into the boundary layer and the whole motion is repeated.

Accuracy

In order to determine the accuracy of the results from the measurements which have wide ranging values it is necessary to apply the limits given below for each case.

(1) Current ± 0.01 mA

(2) Voltage ± 0.01 V

(3) Flowmeter $< 2\%$

(4) Omega stop watch ± 0.1 secs

Smith stop watch ± 0.2 secs

(5) Thermocouple voltages $\pm 0.1\ \mu V$

(6) Absolute temperature (including calibration) < 90 mK

Difference Temperatures (a) via differential $< .02$ K

(b) via absolute $< .04$ K

(7) Heater dimensions ± 0.5 mm

CHAPTER 4

fluid dynamics....

"Observations no one can explain , and explanations no one can observe."

Anon.

CONVECTIONS IN STRATIFIED FLUIDS

This chapter describes visualisation experiments and results on the fluid flow characteristics of the vapour column above boiling liquid nitrogen. A corroborative example is also presented using liquid heluim. The first section outlines the methods and techniques used in displaying the flow patterns at low temperatures. The second section presents the results and qualitative interpretation of the visual effects, while the third presents an extension of this work with the determination of velocities and "boundary layer" thickness. The final section compares these results with existing theories in related fields.

I - Display Methods

Various methods were tried in order to make the flow pattern in the neck of a glass dewar visible, including Schlieren diffraction and dust particles used as streamline tracing elements. Unfortunately in the former method problems arose not only because of the geometry of the dewar but also because of the extremely poor optical quality of the glass. Again dust particles (e.g. lycopodium) were not found to be of any use since they were far too dense for the low gas velocities encountered. Finally a cloud of condensed water vapour was used. This simply involved breathing through a tube placed in the dewar, and filling the space above the liquid with water vapour and traces of carbon dioxide. A white cloud was formed, and streamlines could be inferred from the way in which this cloud was removed. There were originally some misgivings above the violent way the vapour was introduced and also about the fact that it was initially at room temperature. Temperature profiles were checked during and after the process, and apart from the initial disturbance, lasting approximately 10 seconds, they were not found to be severely affected. However, it was noticed that vapour was being drawn from the dewar mouth into the central core of the dewar neck, and it was thought preferable to introduce the tracing element at this point. In this way the temperature and turbulence effects would be minimised, the tracer being drawn in "naturally". Tobacco smoke was found to be suitable as a tracer and using this method it was possible to watch the development of the total flow pattern. Apart from reinforcing the first method it was possible to measure velocities and to watch the individual streamlines in a much clearer way.

Photographs were taken of the various effects, both from above and from the side of the dewar. The majority of the photographs however were taken from the side, normal to the axis of the dewar. Various

lighting configurations, including flash and flood lights, and camera settings were tried and by far the most successful proved to be an overhead flood light with a camera setting of f5.6. This form of lighting made it possible to distinguish fine detail which flash and flood lights from the side could not pick out owing to spurious light reflections. The flood light was connected to a variac, and was mounted on top of a piece of heat resistant glass which acted as a cover plate to the dewar. All the light was therefore fed into the dewar. Using the variac it was possible to observe the vapour clouds at a very low intensity light, and only momentarily increase it to full intensity for photographic purposes. This avoided disturbing the normal equilibrium conditions of the dewar. The outer glass wall of the dewar was treated with teepol in order to resist the formation of mists and droplets on the cold surface, near the liquid nitrogen shield outlet, and was successful in maintaining the dewar transparent.

II - Visual Effects

Numerous series of photographs were taken as the flow patterns developed, using the two methods already described, for various mass flow rates of evaporating liquid nitrogen. As can be seen from photographs H and I complementary patterns are produced using these two methods, the one being the "negative" of the other. That is in the first method water vapour is removed in the convection streams while it remains in the stagnant parts; whereas in the second method cigarette smoke follows and "fills in" the convection streams leaving the stagnant parts clear. This provided a useful cross check on possible spurious effects caused by a tracing element, and in fact no such effects could be seen on comparing the two methods.

Examples of photographs taken with water vapour as the tracing element are shown in the contact print J. The series run from bottom to top and from left to right, and are numbered in this order in the table below. The table also gives the time in seconds after the introduction of the water vapour and the mass flow rate of evaporating nitrogen.

Number	1	2	3	4	5	6	7	8	9	10	11	12	13	14	15	16
Time (secs)	12	30	60	20	30	30	-	15	50	15	45	55	40	8	20	60
M.F.R. grms s^{-1}	.032			.039			0.078						.133	.271		

The last photograph was taken within the first 8 seconds and at a mass flow of 0.032 grm sec^{-1}.

The second contact print K shows two series of photographs using tobacco smoke. The mass flow rate is 0.039 grm s^{-1}, and the time sequence in a similar order to that above is:

Number	1	2	3	4	5	6	7	8	9	10	11	12
Secs	11.8	15.3	19.6	24.4	29.8	36.8	44.1	50.5	58.3	66.1	75.8	85.4

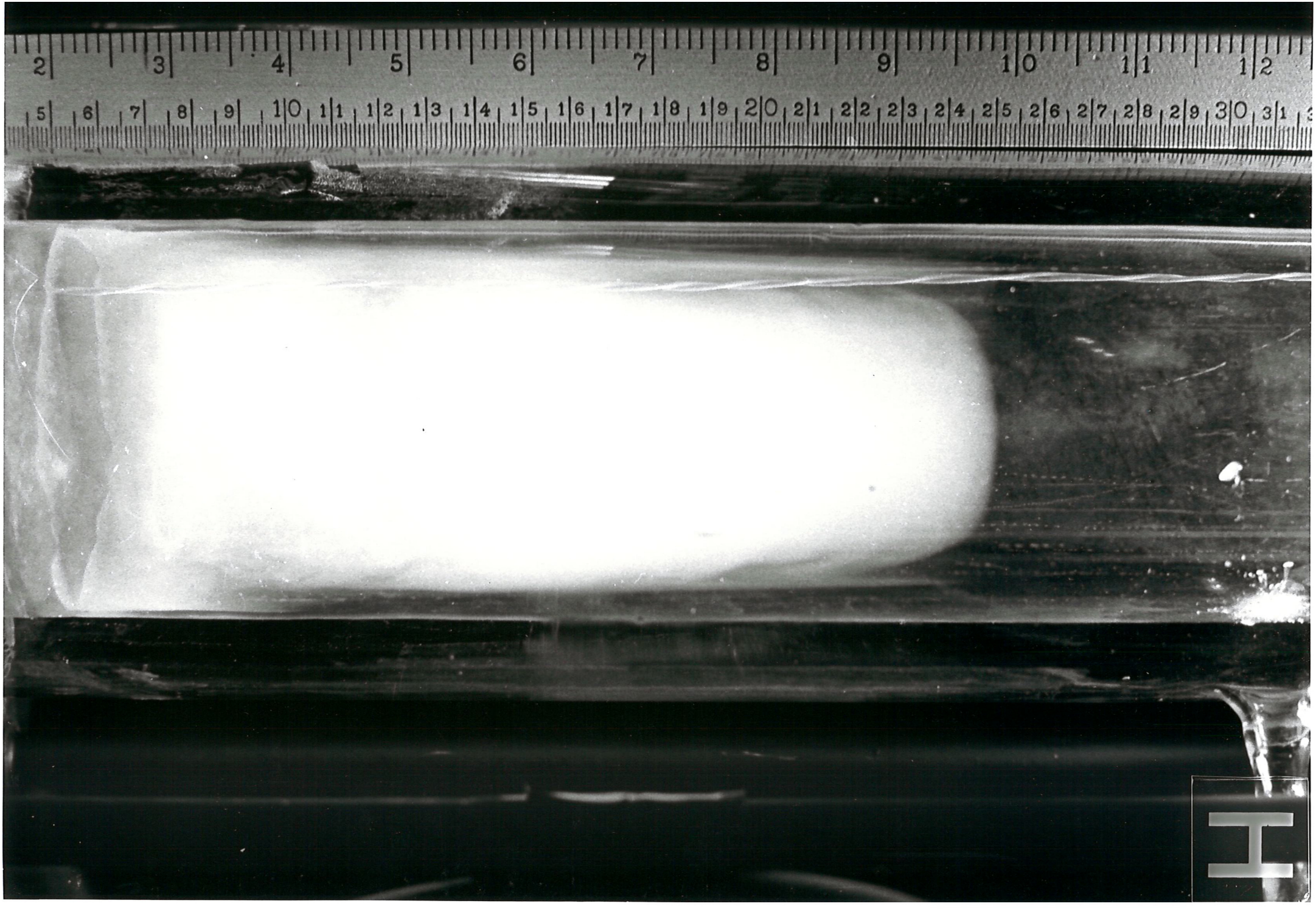

OMEGA


3
3A
4
4A
5
5A
7
7A
8
8A
15
15A
16
17A
18
20
20A
33
33A
34A
35
35A
36
36A
4
4A


ILFORD FP4
1 1A 2 2A 3 3A 4 4A 5 5A
6A 7 7A 8 8A 9 9A 10 10A 11 11A 12
18 20 20A 21 21A 22 23 23A 24
25 25A 26 26A 27 27A 28 28A 29 29A 30

Number	13	14	15	16	17	18	19	20	21	22
Secs	16.4	21.8	27.3	33.7	39.9	69.9	80.6	85.8	95.2	105.8

The general features of the series of photographs using the water cloud are exemplified in photograph H and may be summarised as follows.

(a) The upper region of the dewar clears of water vapour by a downward movement of the cloud, leaving the lower section with an almost stagnant vapour cloud.

(b) A "boundary layer" is seen to form at the walls leaving an annular, clear ring around the white central core and next to the glass wall. Some of the condensed water cloud in this region is initially removed by a rising convection stream. Also some of the water cloud is occassionally seen to rise in the boundary layer.

(c) A region just above the boiling nitrogen is seen to be in turbulent motion and quickly clears of water cloud.

(d) An annular "V" shaped notch just outside the boundary layer and at the top of the remaining cloud is seen to form, as water vapour is removed from the central region. The water cloud in this area is seen to move downwards and towards the boundary layer, eventually undergoing a sharp turn in velocity as it becomes entrained into the boundary layer and moves upwards. The top of the cloud also becomes rounded in shape.

(e) With increased mass flow rates the turbulent region described in (c) increases in height and the clear portion at the top of the dewar diminishes in length. Further increased mass flows produce turbulent waves approximately 5 cm in wave-length, which travel up the edge of the boundary layer and eventually with high mass flow rates (circa 0.4 grm sec^{-1}) the turbulence extends to fill the whole dewar. At these high mass flow rates the dewar is

usually cleared of any water cloud in a few seconds.

(f) During a change in evaporation rate the whole pattern moves upwards in a uniform and stable manner with the whole medium behaving very "elastically".

The features observed using tobacco smoke are exemplified in photograph I and may be summarised as follows:

(g) The tobacco smoke formed itself into pear shaped droplets, and enabled identification of particular parts of the smoke. Velocities could then be determined. An explanation of this feature is offered in Appendix B.

(h) The smoke initially moves downwards in the central portion of the dewar with a vertical velocity of about 3 mm s^{-1} and a radial velocity of about 0.3 mm s^{-1}. After some short distance into the dewar an annular portion of the cloud, just outside the boundary layer, continues to drift downwards leaving the core in this region clear.

(i) Smoke is entrained into the "boundary layer" as the annular sheath moves downwards, and "V" shaped flowlines are produced.

(j) As the downward velocity is lost the smoke turns inwards just above the turbulent region described previously in (c).

From these observations it is possible to construct a picture of the streamlines of the convections in the neck of the 76 mm I.D. dewar investigated. Figure 26 shows schematically the resulting flowlines. The complete flow pattern can be divided into four regions. The first region (a) is annular shaped and is in contact with the wall. The fluid has a vertical upward velocity and resembles a boundary layer. The region (b) extends over much of the diameter, and the downward velocity is distributed non-uniformly across the diameter. The maximum velocity is developed close to the boundary layer. The region (c) has little velocity associated with it. Finally the region (d) is in turbulent motion and in contact

FIGURE 26 FLOW PATTERN IN A 76mm DIAMETER GLASS DEWAR OVER BOILING LIQUID NITROGEN

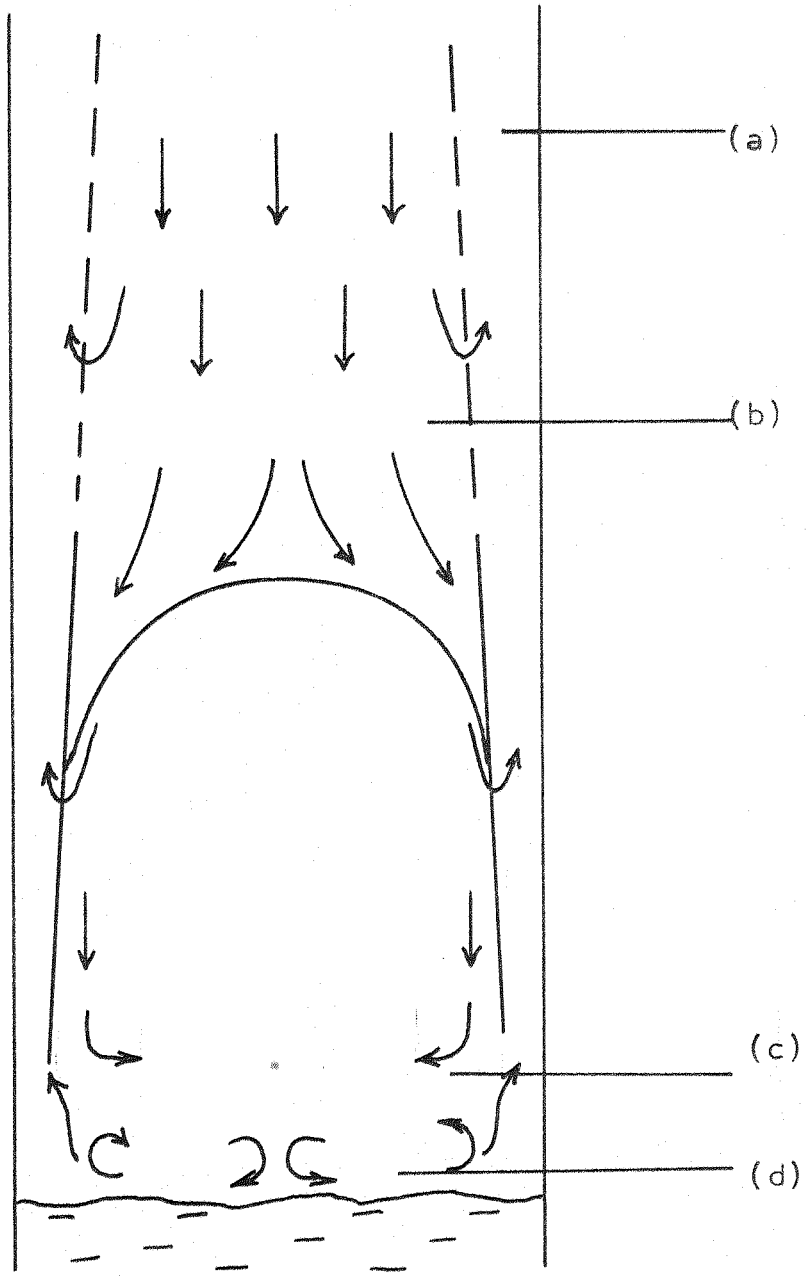

with the liquid.

In general, it is not difficult to explain the causes of this particular type of flow since the mass throughput is low and the natural convection forces are high. There is therefore a very strong tendency towards containing the upward flow close to the walls where the heat influx is the driving force. The negative central flow arises as a consequence of boundary layer flow and the requirement for mass continuity. The turbulent region just above the surface of the liquid is no doubt generated by the disturbances of vapour bubbles breaking through the liquid surface.

This simple picture however is complicated by non-uniform heat fluxes at the wall, which in this case are transferred to the inner wall of the dewar by radiation, and also complicated by the presence of large vertical temperature gradients, with the associated rapidly changing fluid properties.

Helium Vapour Column

Flow visualisation of a helium vapour column was tried in order to widen the scope of the experimentation. Some difficulties were encountered in obtaining clear photographs of the behaviour of the vapour column and it must be left to subsequent work to develop these techniques. However, moist helium gas was injected into the vapour space of a glass helium dewar and the results photographed. It was possible to see the formation of a boundary layer at the wall in much the same form as for the case of nitrogen. The fine detail could not be observed, but one significant point was noticeable. The vapour column showed large eddies and took a long time to settle down after the initial disturbance. One assumes that this is due to the low density of helium coupled with its low viscosity.

III - Temperature, Velocity and Boundary Layer Measurements

(a) Temperature

Using the probe described in the previous chapter the lower half of the vertical temperature profiles in the dewar for various mass flow rates of liquid nitrogen were taken, and are shown in Figure 27. The low mass flow temperature profiles show a marked non-linearity whereas those above 0.078 grm s^{-1} are almost linear, even up to mass flow rates of 0.47 grm s^{-1}. The 77.3 K point in the dewar is also seen to rise with increased mass flow rate and an isothermal region above the liquid in created, and is in general agreement with previously published results, both in glass and metal systems (Lynam and Scurlock 1968, Crooks). Superimposed on the graph and joined by a dotted line are the lowest positions of the water cloud in the dewar for each mass flow rate, i.e. the ordinate gives the distance between the bottom of the water vapour cloud and the liquid surface, and is a measure of the extent of the turbulent region. The points are seen to fall on the 82 K isotherm.

(b) Velocity and Boundary Layer

In order to quantify the effects, measurements of velocity and "boundary layer" thickness were taken from the photographs. The negatives were projected onto a screen and the image magnified by approximately four and a half times life size. In this way it was possible to trace the magnified image and to take measurements from this. The positions of particular features at the most advanced part of the tobacco smoke were noted with time and hence maximum velocities could be determined.

Certain precautions were taken since distortions of the photographic image could arise in numerous ways. The dewar is cylindrical and hence it could behave as a lens, the photograph negatives could shrink in being developed and the projection of the image could produce a non-square, distorted picture owing to lens aberrations and non-normal projection.

FIGURE 27 TEMPERATURE PROFILES OVER BOILING LIQUID NITROGEN IN 76mm DIAMETER GLASS DEWAR FOR SEVERAL MASS FLOW RATES

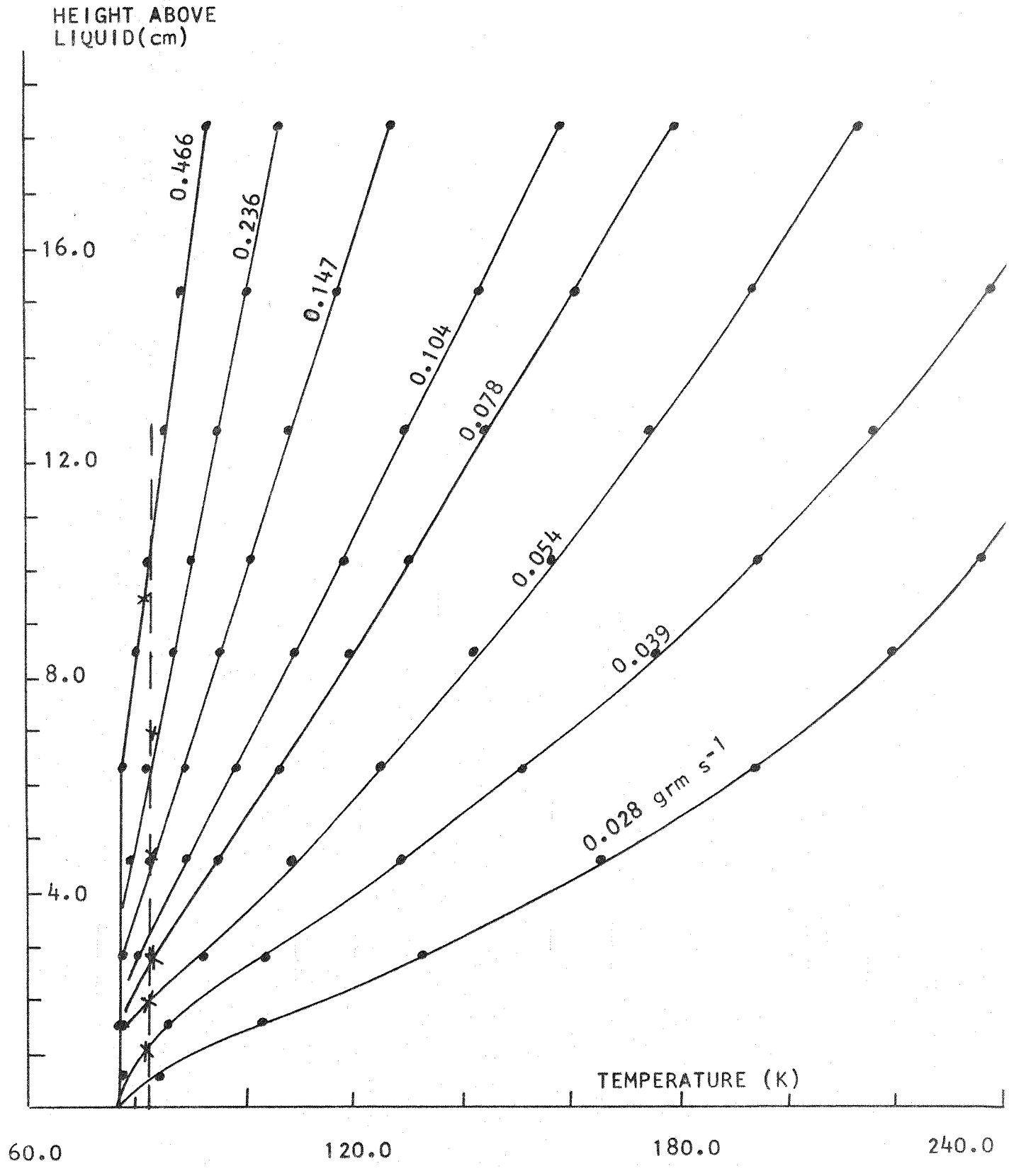

Checks were made on the degree of distortion of a ruler placed radially across the inside of the dewar and photographed and no effects could be appreciated on analysis of the photographs. A ruler was placed vertically alongside the glass dewar and was included in the photographs so that linear measurements could be directly compared. It also simplified setting up procedures for projection where the linear scale was a useful distortion check. A stop watch was also included in some of the photographs and hence time intervals could be accurately determined.

The results of the "boundary layer" thickness measurements are presented in Figures 28 to 32. Because of the downward velocity next to the boundary and the sudden sharp upward motion of the tracing element as it became entrained into the upward moving stream it was possible to define a boundary. However it was difficult in practice to decide at which point in time to take the photograph since the removal of the tracing element is a continuous non-uniform process, and eventually a pattern remains which reflects the stagnant parts. That is, with both negative and positive regions void of tracer, and not just the upward moving stream, as was desirable. Photographs were taken at different intervals and the results are presented at selected times, for various mass flow rates (liquid nitrogen evaporation rates).

The most striking feature of all these curves is the rate at which the boundary layer grows. It can be seen from the results that to a close first approximation the variation of "boundary layer" thickness is linear with distance above the liquid surface. This should be compared with a 1/5th power of distance growth rate which is the accepted room temperature variation of a constant flux, natural convection boundary layer.

Figures 33 and 34 present a plot of distance versus time of particular features of the advanced part of the tracing cloud as it entered the dewar. The curves were normalised, owing to zero time differences,

FIGURE 28 "BOUNDARY LAYER" GROWTH (0.078 grm s^{-1} N_2)

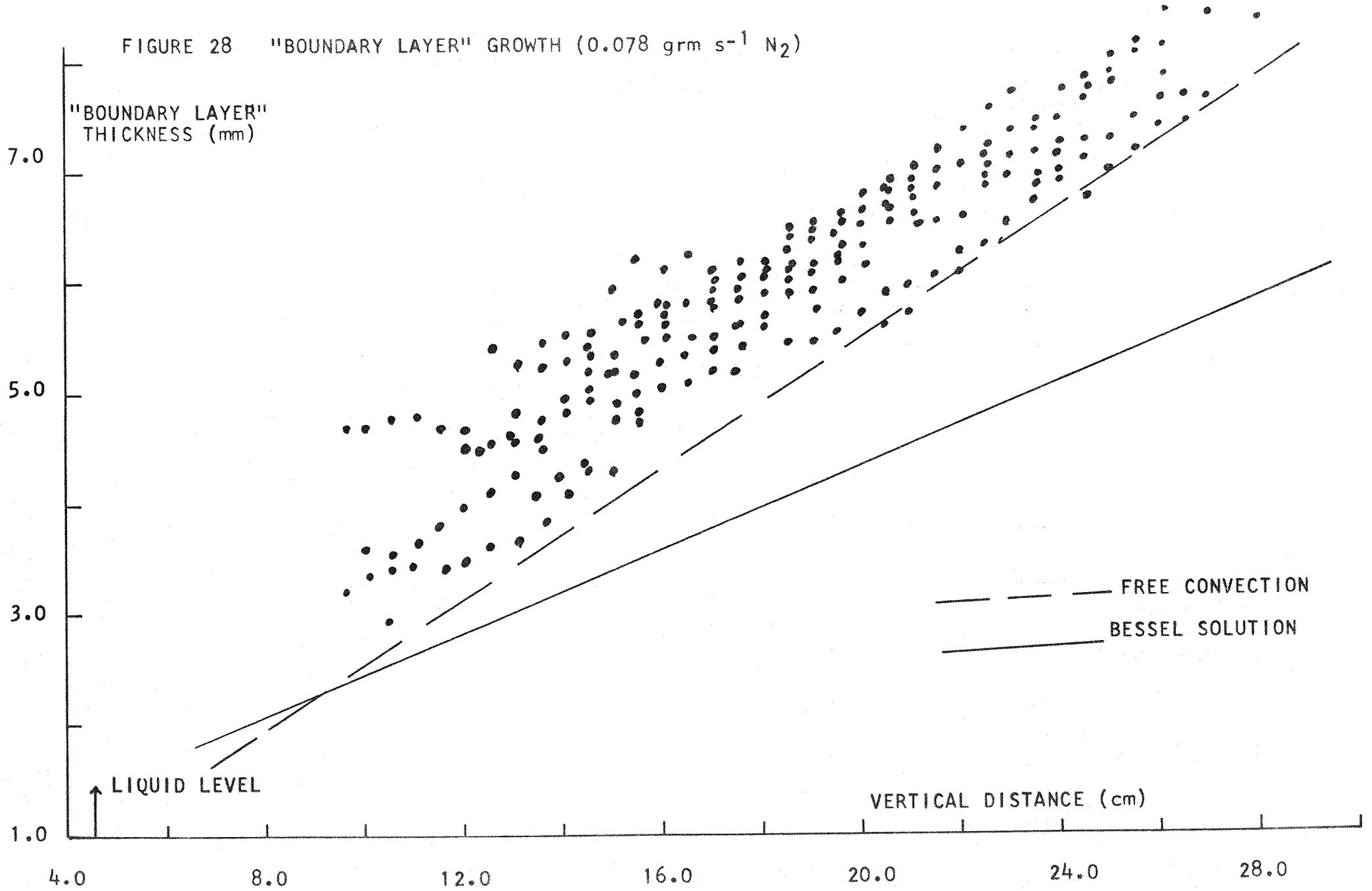

FIGURE 29 "BOUNDARY LAYER" GROWTH (0.054 grm s^{-1} N_2)

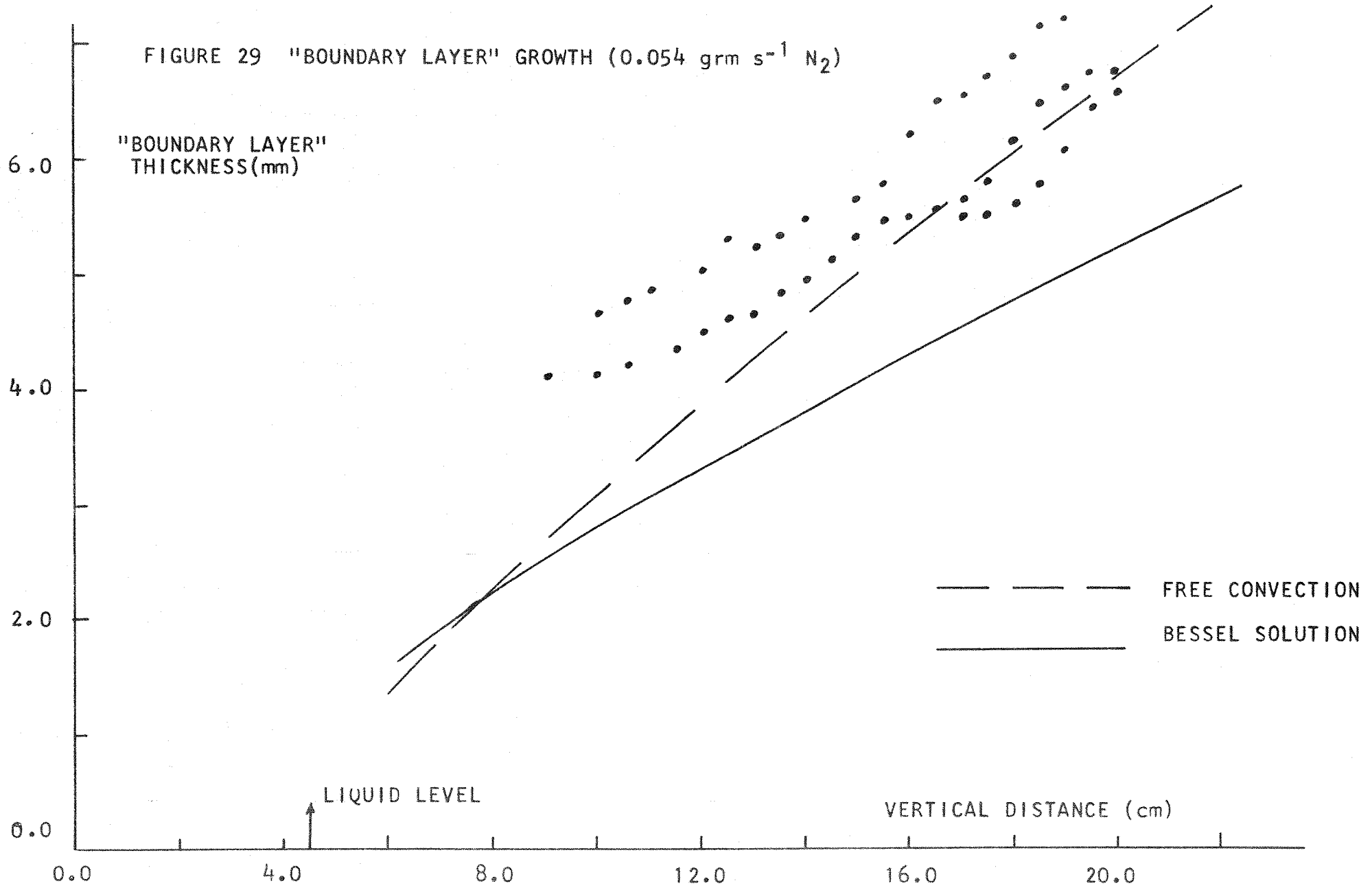

FIGURE 30 "BOUNDARY LAYER" GROWTH (0.039 grm s^{-1} N_2)

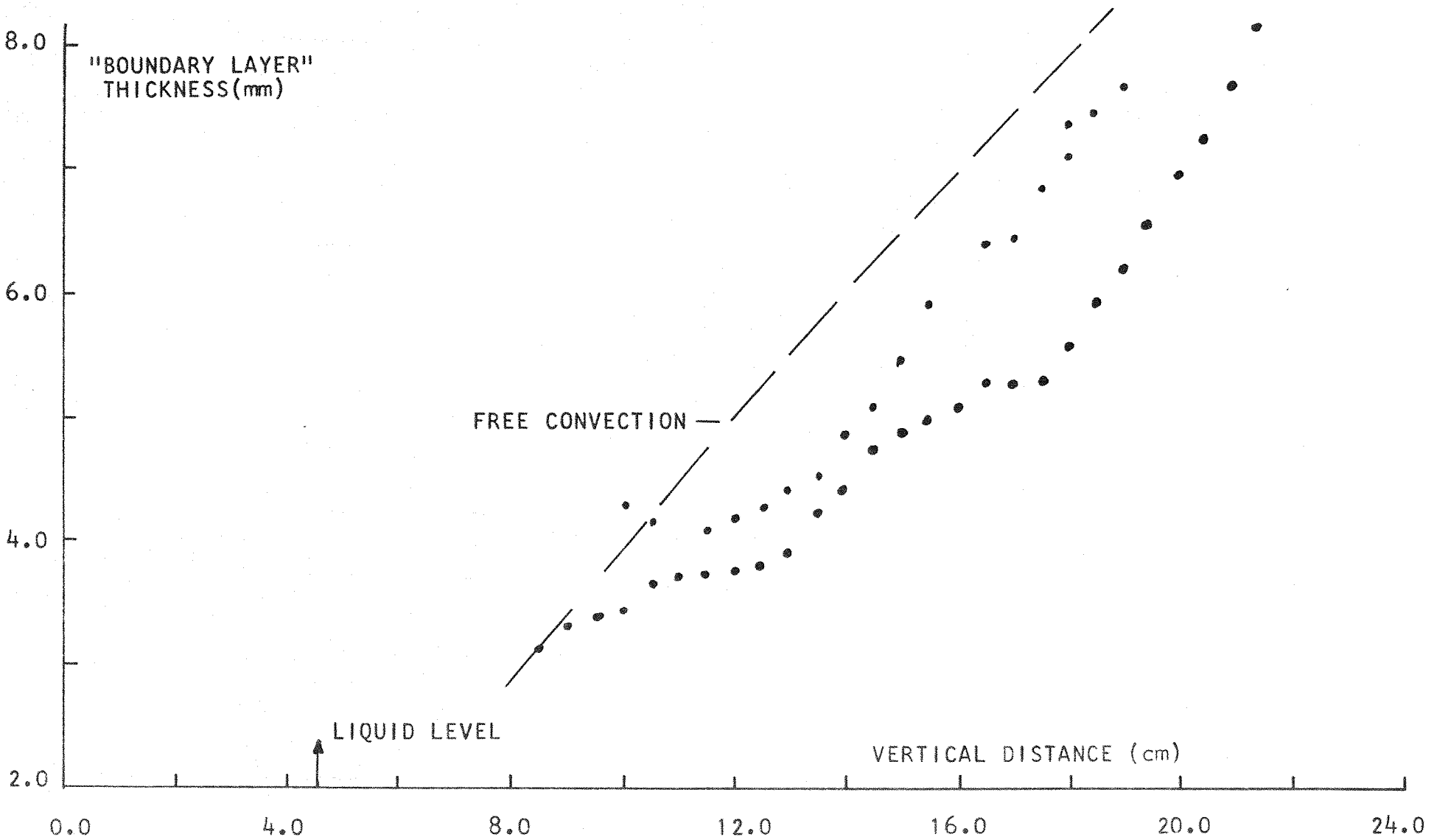

FIGURE 31 "BOUNDARY LAYER" GROWTH (0.028 grm s^{-1} N_2)

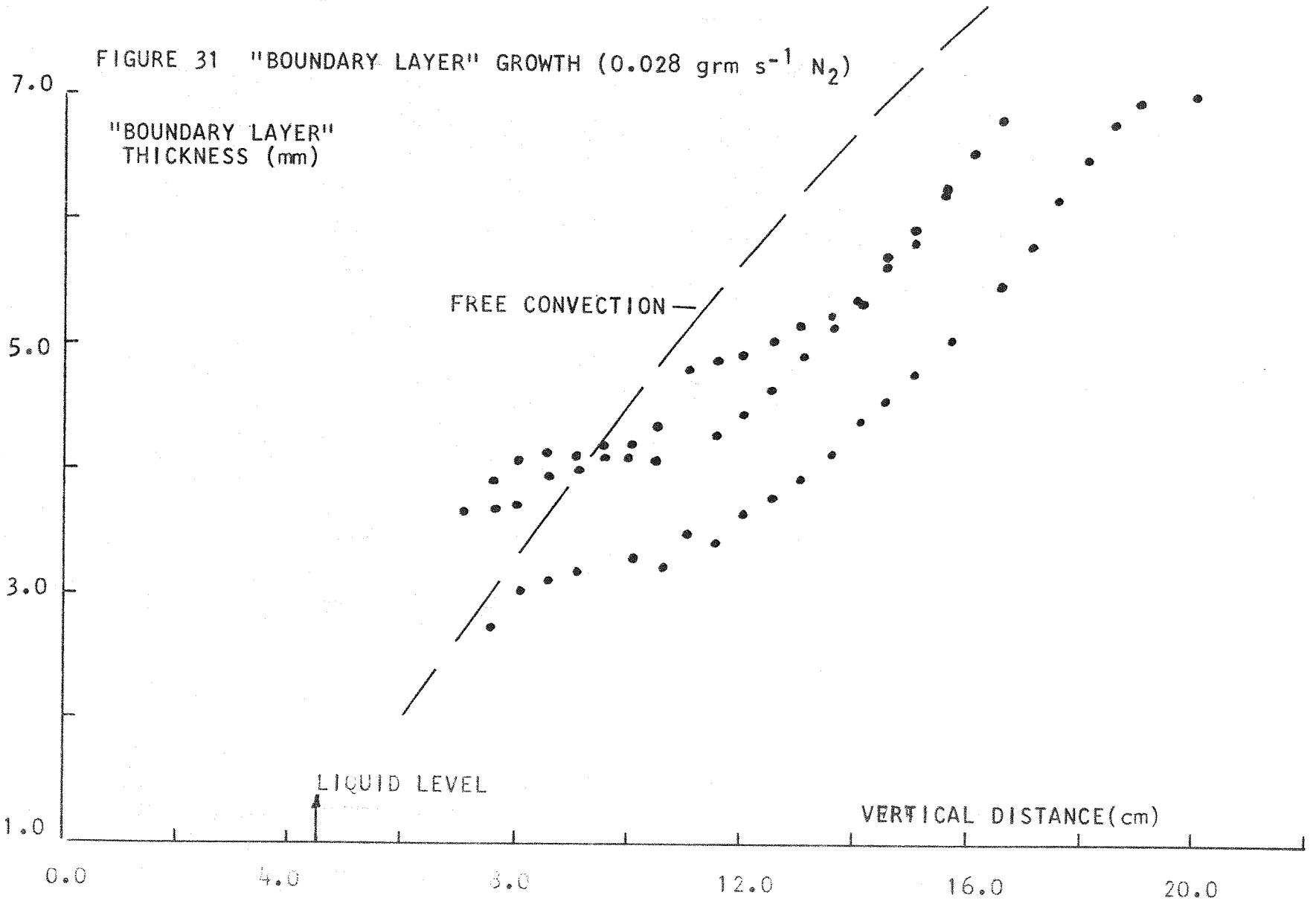

FIGURE 32 "BOUNDARY LAYER" GROWTH(0.104 grm s^{-1} N_2)

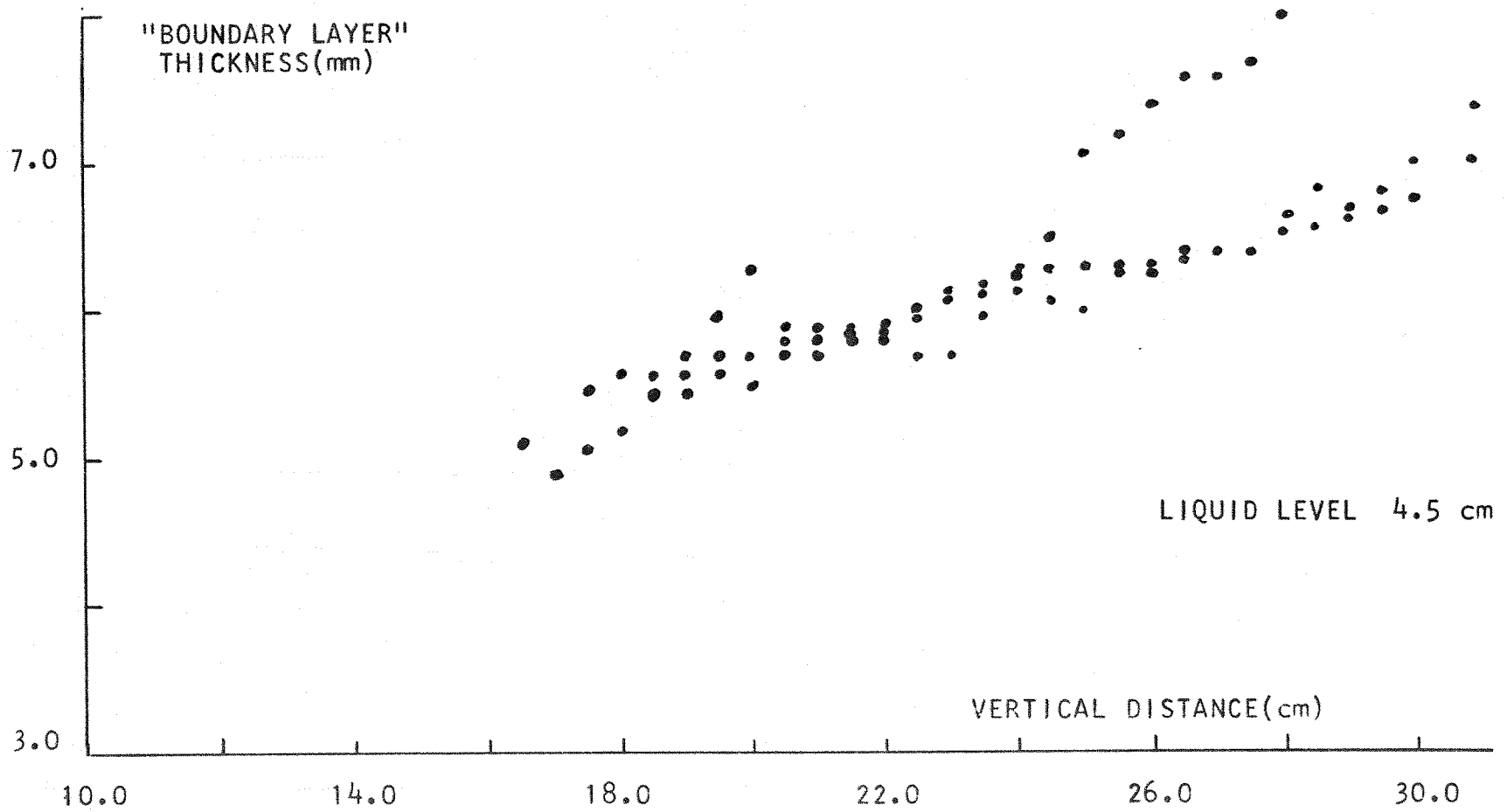

FIGURE 33 VERTICAL POSITION OF TRACING CLOUD WITH TIME

(0.078 grm s^{-1} N_2)

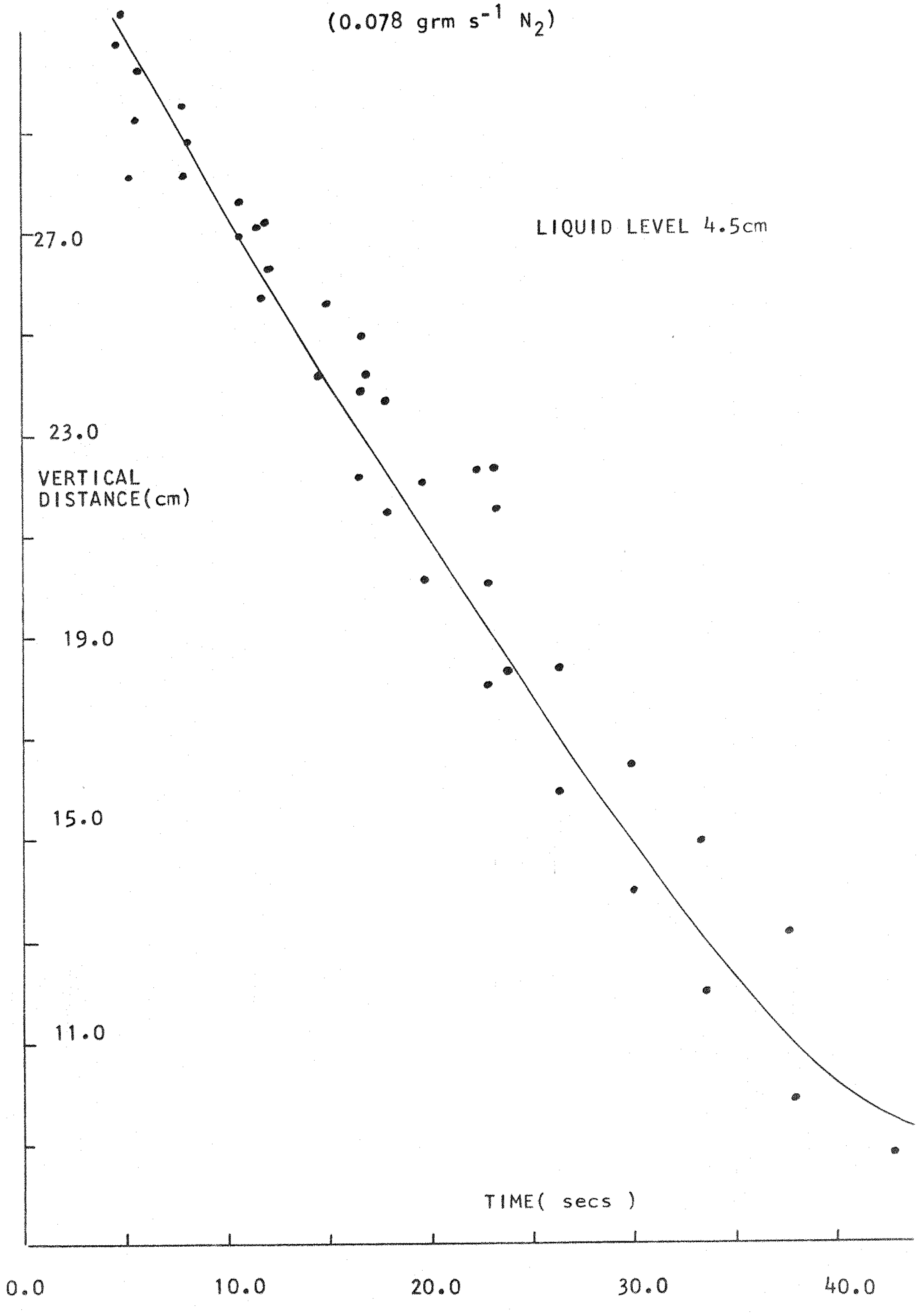

FIGURE 34 VERTICAL POSITION OF TRACING CLOUD WITH TIME

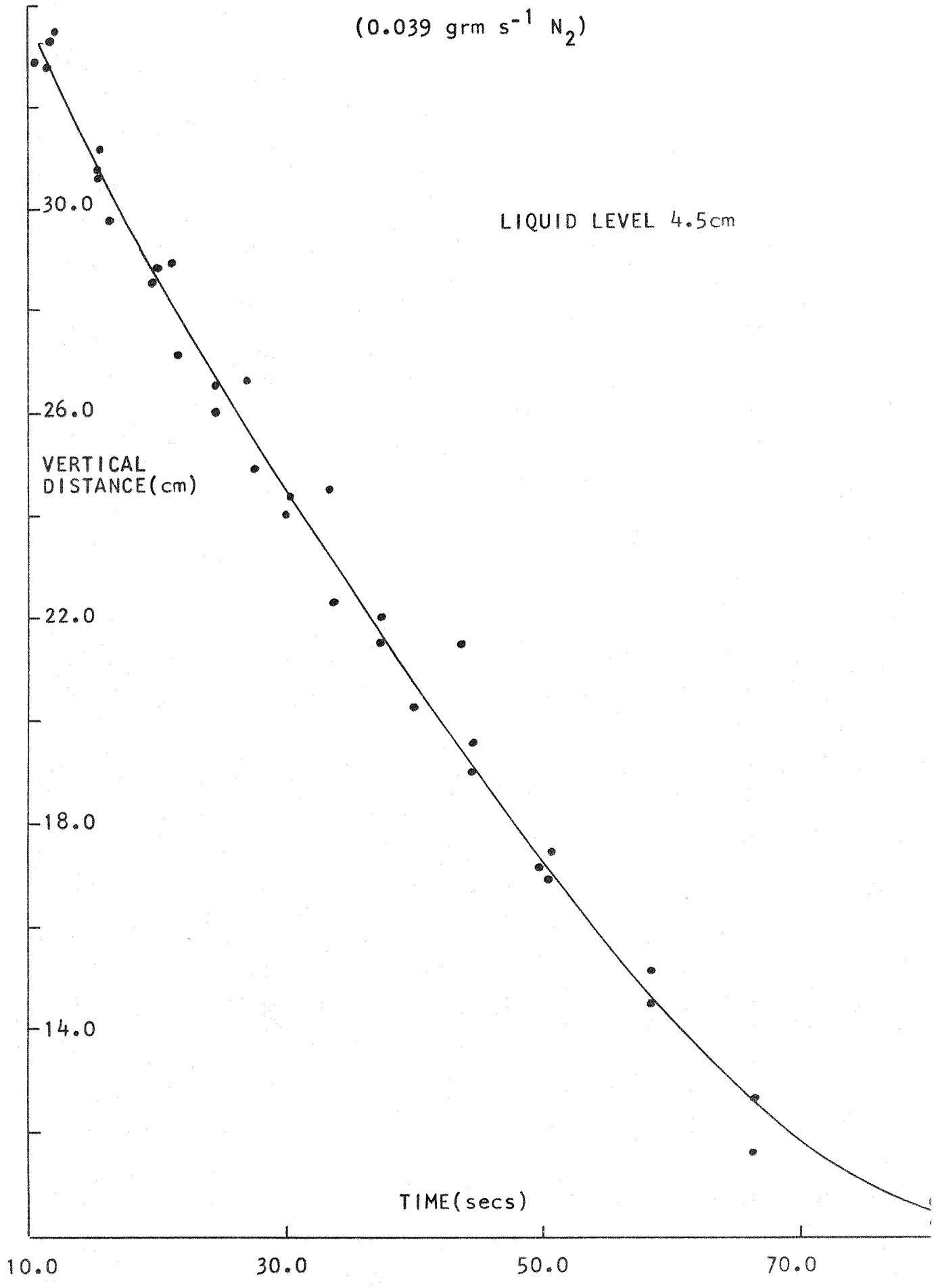

by making one point on the curves coincident. The time ordinate is to be treated as a scale of time and not an absolute value. Thus the maximum negative velocity of the downward moving convection streams can be seen to be almost uniform, decreasing only very slightly at first and then abruptly slowing down close to the liquid surface.

With an evaporation rate of 0.078 grm s^{-1} the velocity varies from about 6.6 mm s^{-1} to 5.5 mm s^{-1} over the more linear portion, and for an evaporation rate of .039 grm s^{-1} the corresponding velocities are 4.4 mm s^{-1} and 2.9 mm s^{-1}.

Figures 35 and 36 present similar graphs to the previous ones for the radial position of a feature of the cloud at a given time. The velocities are approximately 0.36 mm s^{-1} there being a slight but not significant difference between the two curves.

FIGURE 35 RADIAL POSITION OF TRACING CLOUD WITH TIME

(0.078 grm s^{-1} N_2)

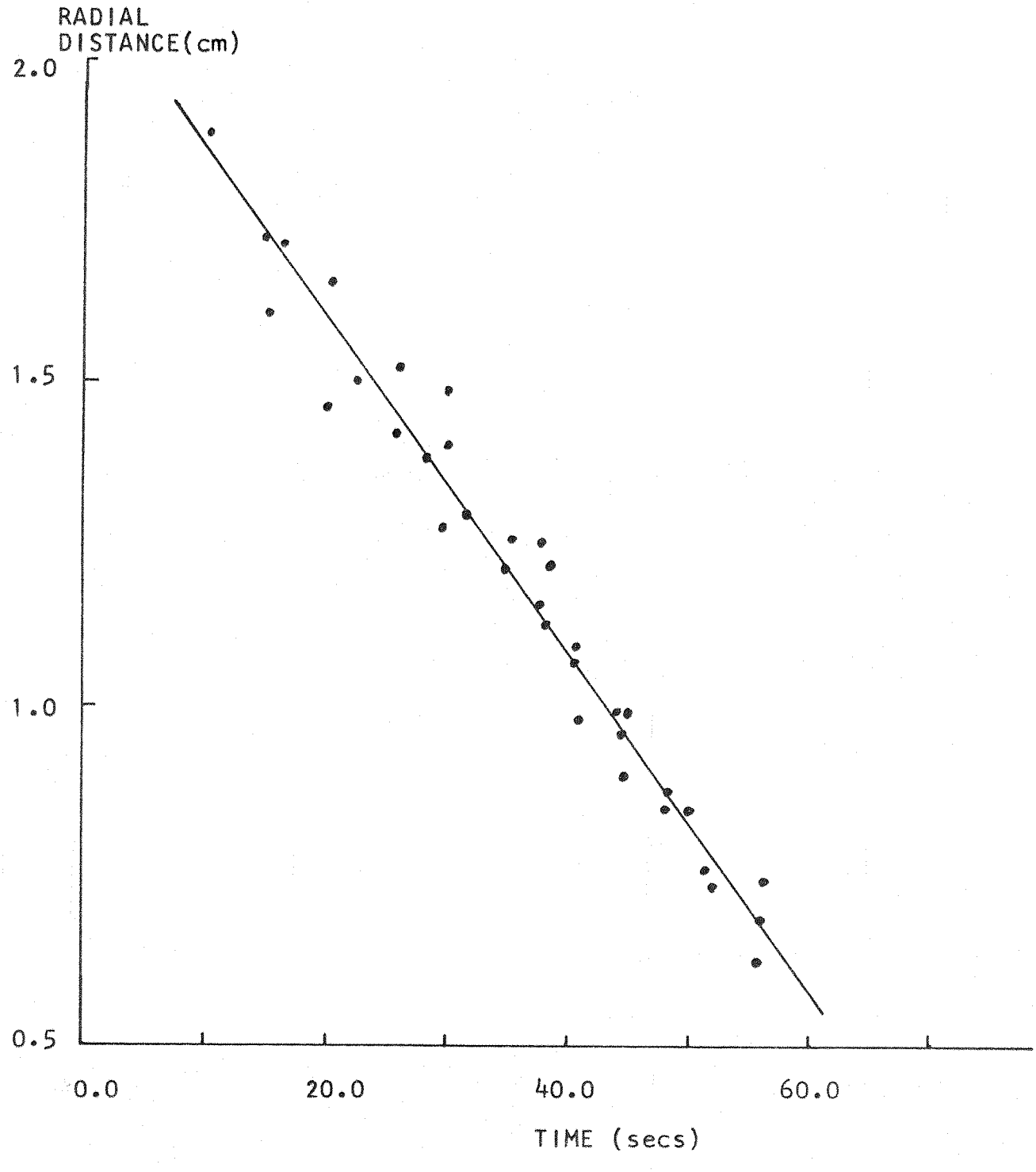

FIGURE 36 RADIAL POSITION OF TRACING CLOUD WITH TIME

(0.039 grm s^{-1} N_2)

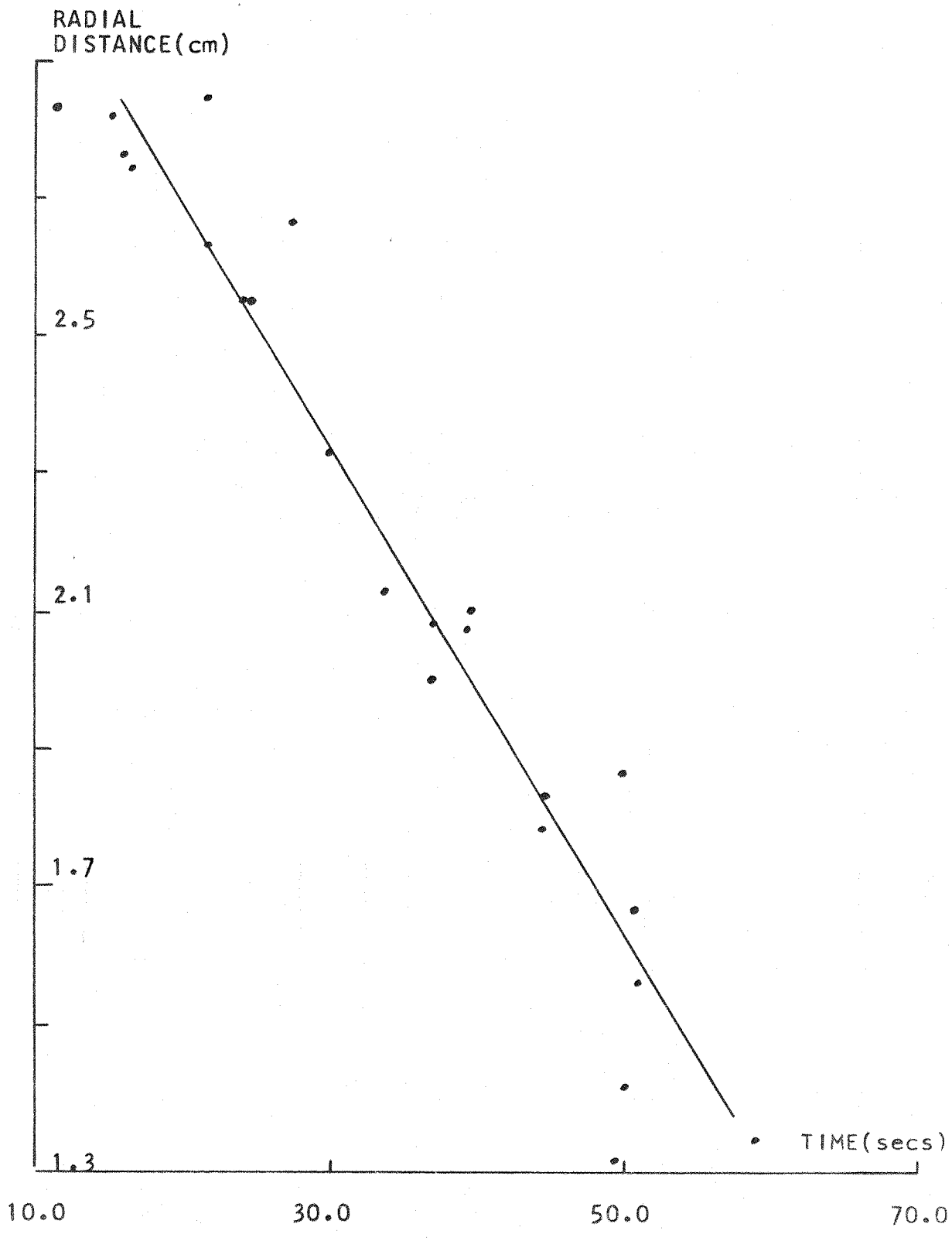

IV - Theoretical Comparisons

Vertical Temperature Profiles

In order to attempt to generate the vertical temperature profiles for given mass flow rates of nitrogen vapour it is necessary to know the heat flux at the wall. Unfortunately this is non-uniform, and the distribution was not measured in any way in the experiment.

However one can safely assume that the equilibrium temperature of the inner wall was maintained by radiation from the outer room temperature wall of the glass dewar, across the vacuum space. Some idea of the vertical distribution of heat flux can be gained by plotting the normalised radiation (where the radiation from 300 K to 77 K is considered to be unity) between 300 K and a given wall temperature against absolute temperature. This variation can be seen in Figure 37 as curve A. It is to be expected that contributions to the heat flux are small below 100 K, and this is clearly shown in the nearly horizontal portion of the curve. The remainder of the curve looks parabolic in behaviour and so a heat flux distribution with temperature of the form

$$q_r = q_o \left(1 - \left(\frac{T - 77}{300 - 77}\right)^2\right)$$

(where q_r is the flux with an inner wall temperature T and q_o is the flux with an inner wall temperature of 77 K) suggests itself. This variation is seen in curve B and compares favourably with curve A. If as a first approximation the wall temperature is considered to be linear with vertical position this may be written

$$q_x = q_o \left(1 - \left(\frac{x}{L}\right)\right)^2$$

where the length L is defined by the boundary condition

$$T = 300 \qquad x = L$$

The other boundary condition $q_x = q_o$ at $x = 0$ is in this case taken from experiment. The heat flux into the dewar from evaporation experiments of liquid nitrogen was seen to be 25×10^{-3} watts cm^{-2}. Using this value

FIGURE 37 PARABOLIC APPROXIMATION TO RADIATION FLUX

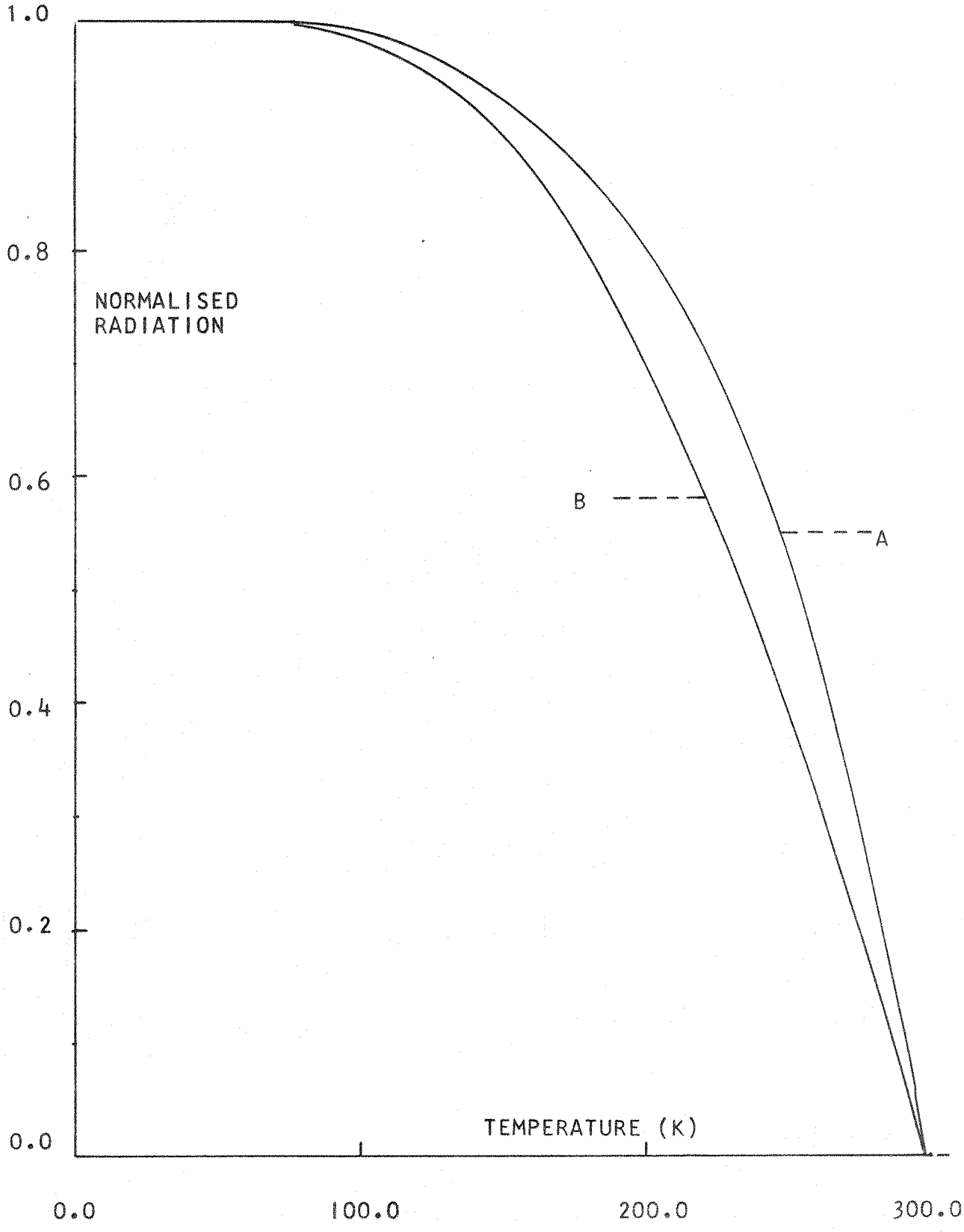

and assuming the heat balance relationship:

$$\dot{m} C_p \Delta T = \pi D q_x dx$$

we can plot the inverse of the initial experimental gradients (where $q_x = q_o$) against total heat input. This is given in Figure 38 along with the theoretical relationship. The assumption can be seen to be justified, and so we can now substitute for q_x and obtain after integration

$$(T - 77) = \frac{\pi D q_o}{\dot{m} C_p} \left(x - \frac{x^3}{3L^2}\right)$$

A plot of the generated vertical temperature profiles from this equation for three selected mass flow rates is compared with observed temperature profiles in Figure 39. The theoretical curves have been adjusted to allow for the isothermal region where the 77.3 K points have been made coincident. The agreement between theory and observation is significant despite the assumptions made. It must however be left to more detailed experimental work to decide whether the sharp decrease in gradient represents solely a different flux distribution or thermosyphoning effects as have been seen in the dewar column.

Boundary Layer Thickness

(a) Free Convection

Because of the observed upward flow close to the wall and the low downward velocities of the central portion, the high Grashof numbers involved, and the manner in which the flow became turbulent (see note (e) in description of visual effects) an analysis based on a free convection boundary layer was tried. This is a similar flow model to that used by Drake et al where the natural convection effects are assumed to be dominant. Thus the dewar flow is divided into a free boundary layer section and a central slow moving core. Also it was assumed that the conventional theory could be applied locally, inferring that vertical variations in temperature are of secondary importance. This is suggested

FIGURE 38 INVERSE OF INITIAL TEMPERATURE GRADIENT VERSUS LIQUID NITROGEN EVAPORATION RATE

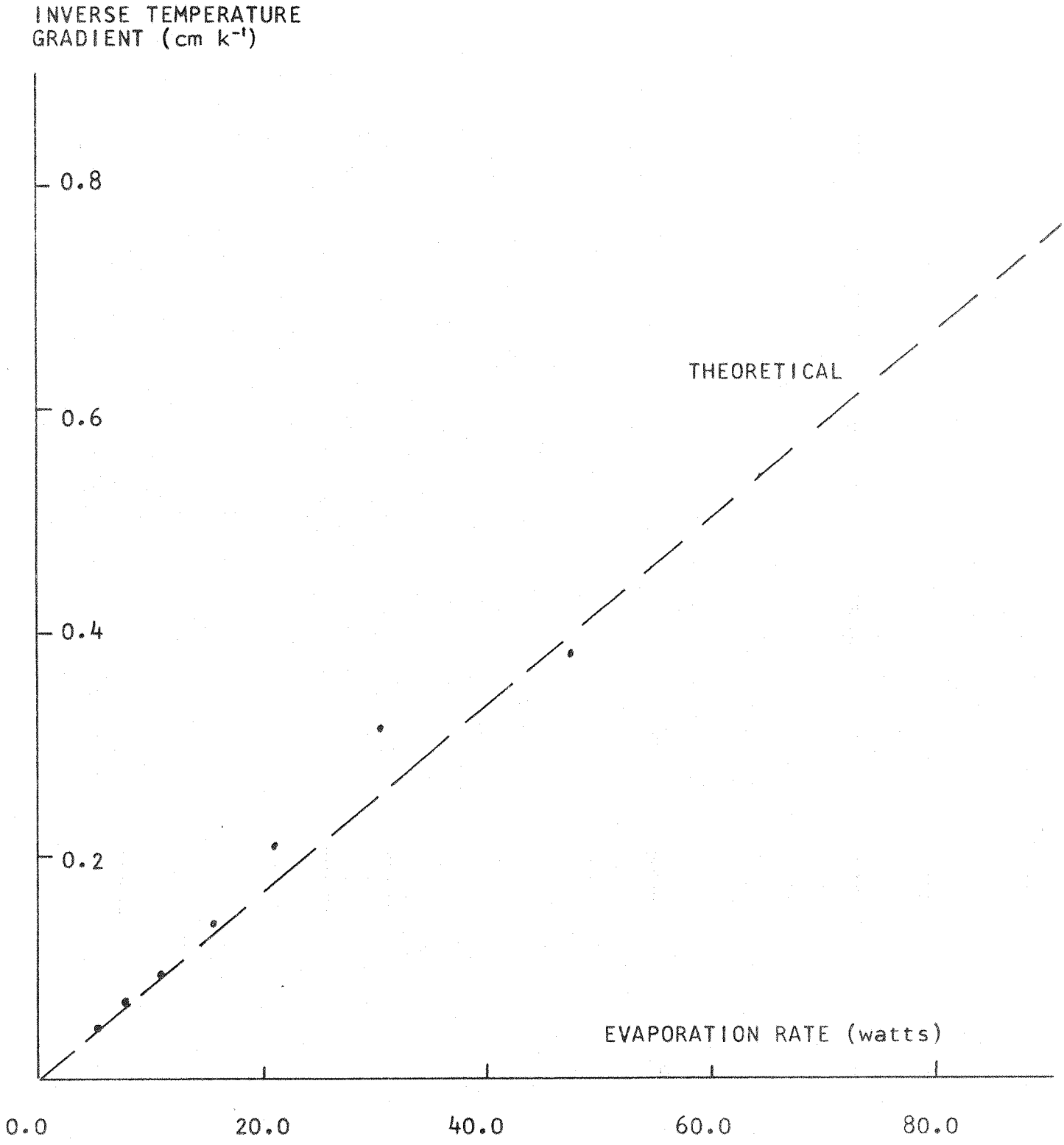

FIGURE 39 COMPARISON OF THEORETICAL AND OBSERVED VERTICAL TEMPERATURE PROFILES

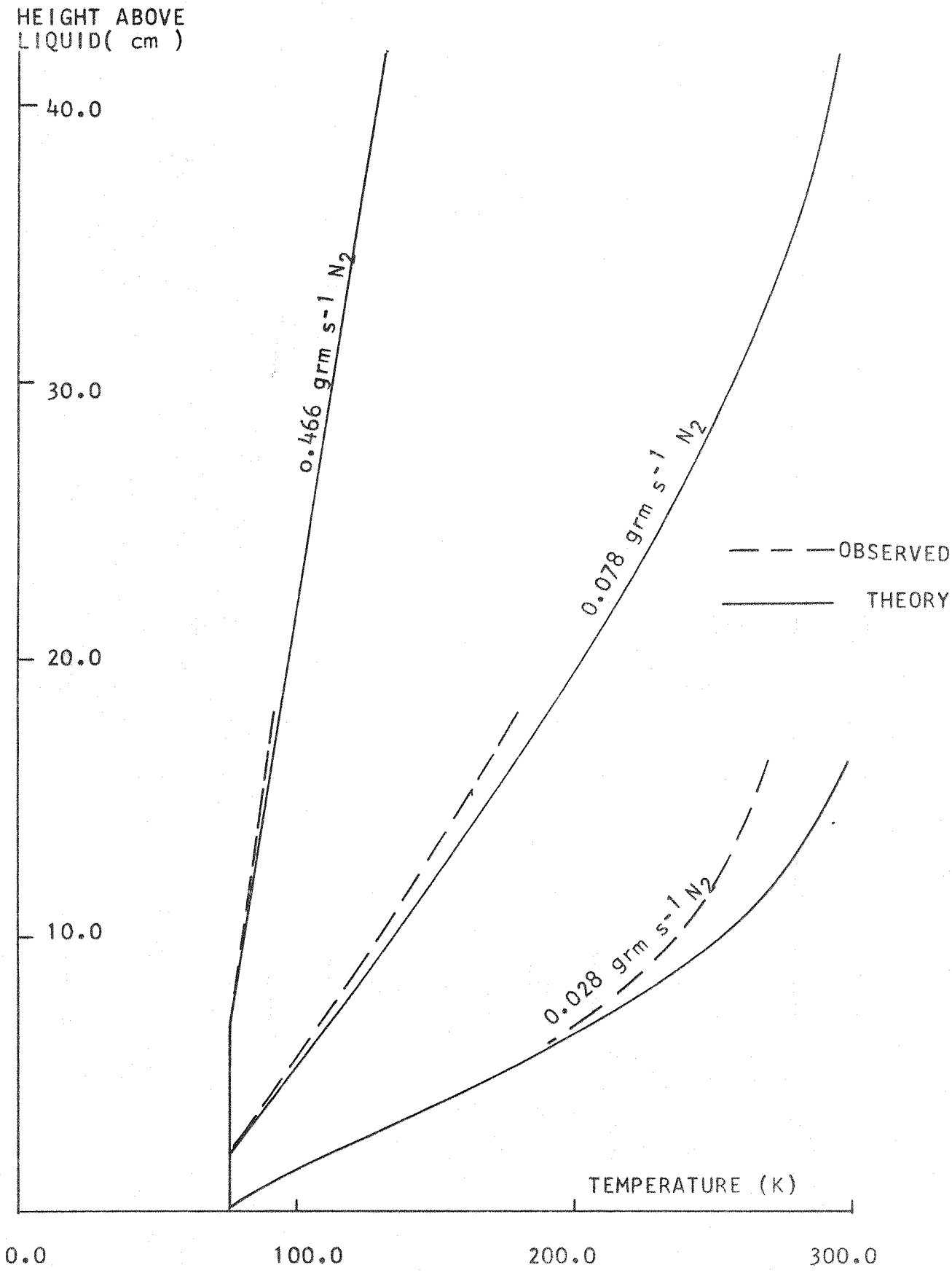

by Sparrow's work and by others mentioned previously on the secondary downstream effects of upstream temperature and flux variations. Hallman has also applied this latter assumption of evaluating the properties at the temperature level under consideration without reference to upstream variations, with some success.

From Drake's analysis the boundary layer thinning due to temperature gradients in the gas can be shown to be small, hence we can take as a first approximation the zero gradient case where the boundary layer thickness can be written

$$\delta = \frac{C_E^{2/3}}{C_M^{2/3}} \left(\frac{g \beta q}{k \nu^2} \right)^{-1/5} x^{1/5}$$

and we can group the terms of the equation into a temperature variable C(T) and a linear distance x

$$\delta = C(T)\, x^{1/5}$$

A plot of the variable C(T) against temperature is shown in Figure 40 and the dependence is very closely linear. Also the rate of growth of $x^{1/5}$ is very small with increasing x and so the temperature effects are seen to be the major contribution with the high gradients experienced in these experiemnts. The anticipated boundary layer thickness as calculated using the experimental temperatures profiles for given mass flow rates are shown in Figure 41. They are also superimposed onto the appropriate experimental boundary layer curves. There is close agreement between the theory and experimental results at the higher laminar flow rates. However the agreement becomes a little worse as the flow rate decreases, while nevertheless the curves remaining parallel particularly in the more well defined higher parts. This reflects the temperature dependence of the results with the rapidly changing properties and Grashof number.

FIGURE 40

TEMPERATURE DEPENDENT TERM(FREE CONVECTION)

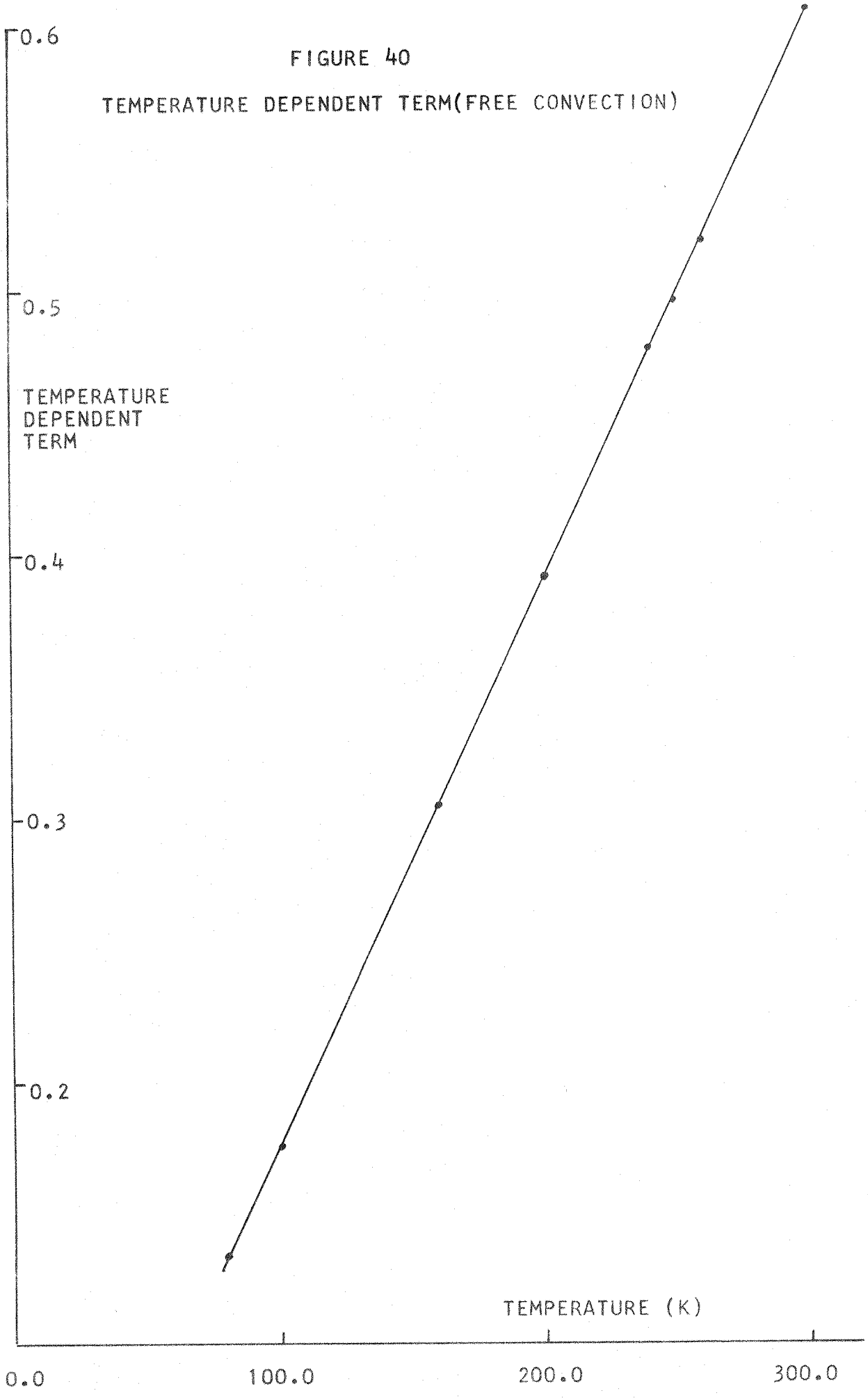

FIGURE 41 BOUNDARY LAYER THICKNESS(FREE CONVECTION)

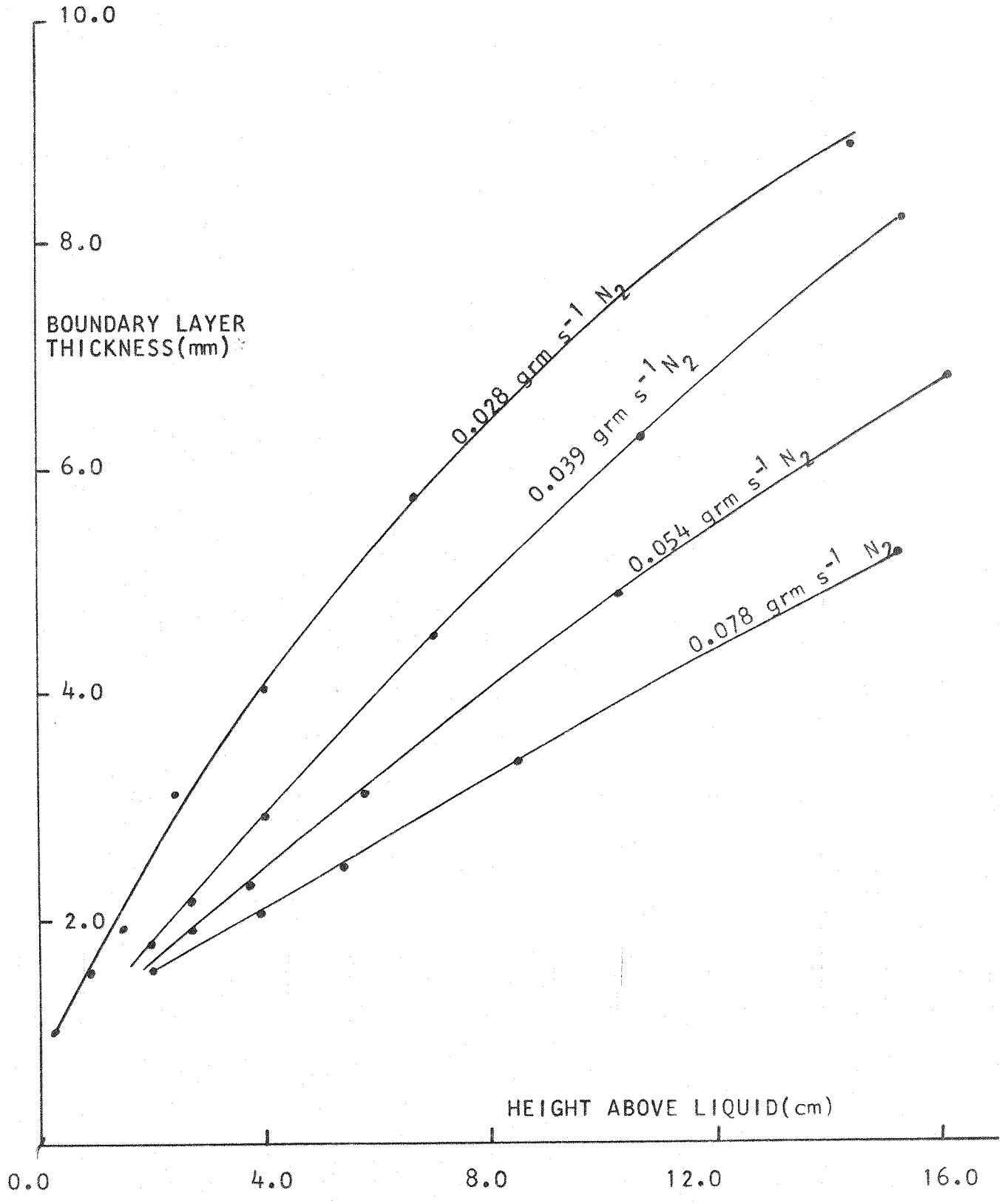

(b) "Mixed" Convection

An alternative form of analysis which may be used is a Bessel solution of the equations and is exemplified by the work of Hallman, Hanratty and others, and also that of Prandtl. Although natural convection effects will be seen to play a major role in the shaping of the velocity profiles the analysis unlike the previous one is based on flows which are contained and have associated pressure drops. Also this analysis will be seen to show a detail of the velocity profile which other analyses of similar situations do not exhibit.

It is necessary to extend this Bessel solution in order to investigate the influence of these large natural convection effects.

The solution of the dimensionless velocity profile is given previously ($R_a^{\frac{1}{4}} = l$) as

$$U_d = \left(\frac{l}{2}\right)\left(\frac{\text{bei}(l)\ \text{ber}(l\,R) - \text{ber}(l)\ \text{bei}(l\,R)}{\text{ber}'(l)\ \text{ber}(l) + \text{bei}'(l)\ \text{bei}(l)}\right)$$

Using the alternative modulus and phase form of the Kelvin functions we can rewrite the numerator of the velocity function as

$$N = M_o(l\,R)\cos\theta_o(l\,R)\,M_o(l)\sin\theta_o(l) - M_o(l\,R)\sin\theta_o(l\,R)\,M_o(l\,R)\cos\theta_o(l)$$

and denominator

$$D = M_o(l)\cos\theta_o(l)\,M_1(l)\cos(\theta_1(l)-\pi/4) + M_o(l)\sin\theta_o(l)\,M_1(l)\sin(\theta_1(l)-\pi/4)$$

where

$$\text{ber}_o x = M_o(x)\cos\theta_o(x) \qquad \text{ber}_o' x = M_1(x)\cos(\theta_1(x)-\pi/4)$$

$$\text{bei}_o x = M_o(x)\sin\theta_o(x) \qquad \text{bei}_o' x = M_1(x)\sin(\theta_1(x)-\pi/4)$$

And these can be rewritten

$$N = M_o(l\,R)\,M_o(l)\sin(\theta_o(l) - \theta_1(l\,R))$$

$$D = M_o(l)\,M_1(l)\cos(\theta_1(l) - \pi/4 - \theta_o(l))$$

thus the velocity becomes

$$U_d = \frac{U}{U_m} = \frac{l}{2}\left(\frac{M_o(l\,R)\sin(\theta_o(l) - \theta_o(l\,R))}{M_1(l)\cos(\theta_1(l) - \theta_o(l) - \pi/4}\right)$$

The zeros of this function are given by

$$\sin(\theta_o(l) - \theta_o(l\,R)) = 0$$

$$\theta_o(l) - \theta_o(l\,R) = n\pi$$

the phase is tabulated (Abramowitz and Segun) for large argument in terms of $(\theta_o(x) - (x/\sqrt{2}))$ and if we denote this by $C_o(x)$ we can write for the zeros of the function

$$(C_o(l) - C_o(l\,R)) = (R - 1)\cdot\frac{l}{2} - n\pi$$

$C_o(x)$ is a very slow moving function and so for values of R away from zero we may write

$$(R - 1)\frac{l}{2} = n\pi$$

$$R = 1 + \frac{n\pi\sqrt{2}}{l}$$

For the maxima and minima values between these zeros we need to differentiate the function. We can see that for zero order Kelvin functions

$$\frac{dU_d}{dR} \propto \text{ber}'(l\,R)\,\text{bei}(l) - \text{bei}'(l\,R)\,\text{ber}(l)$$

which has zeros given by

$$M_1(l\,R)\cos(\theta_1(l\,R) - \pi/4)\,M_o(l)\sin\theta_o(l)$$

$$-M_1(l\,R)\sin(\theta_1(l\,R) - \pi/4)\,M_o(l)\cos\theta_o(l) = 0$$

i.e. $$M_1(l\,R)\,M_o(l)\sin(\theta_1(l\,R) - \theta_o(l) - \pi/4) = 0$$

hence

$$\theta_1(l\,R) - \theta_o(l) - \pi/4 = n\pi$$

As before this can be written with respect to tabulated values

$$\frac{l(R - 1)}{\sqrt{2}} + (C_1(l\,R) - C_o(l)) = (n + \tfrac{1}{4})\pi$$

This gives us the turning points and with the magnitude of the dimensionless velocity at these points we are able to sketch the velocity profile.

The magnitudes are given by

$$U_d = \frac{l}{2}\left(\frac{M_o(lR)\,M_o(l)\,\sin(\theta_o(l) - \theta_o(l))}{M_o(l)\,M_1(l)\,\cos(\theta_1(l) - \pi/4 - \theta_o(l))}\right)$$

In a similar manner to that used previously the tabulated value, say $A_o(x)$, equals $x^{\frac{1}{4}}\, e^{-x/2}\, M_o$. Hence we write

$$U_d = \frac{l}{2}\,\frac{\exp\left(\frac{l(R-1)}{(2)^{\frac{1}{2}}}\right)}{(l)^{\frac{1}{2}}}\,\frac{A_o(lR)}{A_1(l)}\,\frac{\sin\left(B_o(l) - B_o(lR) - \frac{(R-1).l}{(2)^{\frac{1}{2}}}\right)}{\cos(B_1(l) - B_o(l) - \pi/4)}$$

Using these equations the velocity profile for $l = 10$ has been generated and this agrees with that shown in Hallman, and hence the approximations used are valid, even as low as this value. Using these three equations it is possible to sketch the velocity profile for large Rayleigh numbers (l^4).

A comparison is made in Figure 42 between the reported curves up to $l = 10$, and the extended analysis of $l = 50$. It can easily be seen from the curves that the effect of increasing the natural convection influence is to suppress the central flow and to move the maximum velocity radially outwards towards the wall. At sufficiently high Rayleigh numbers the velocity maximum is close to the wall, and there is a reversal of flow near the centre line. Both the maximum and the minimum increase and move closer to the wall at still higher Reynolds numbers. This behaviour is due to the oscillatory nature of the Kelvin functions coupled with an exponentially damping term. The degree and form of the damping with increasing Rayleigh number can be seen by reference to Figure 43. The flow is increasingly limited to regions close to the wall, and any oscillations outside this region are damped to an insignificant level. This damping behaviour also applies to the temperature profiles.

This containment of the flow is understandable and could be anticipated since a non-limited, mixed convection theory must behave in a free convective manner in the asymptotic limit. Thus a 'boundary layer' is seen to form as the Rayleigh number is increased and indicates the almost complete dominance of natural convection forces. There is, however, one feature

FIGURE 42 VELOCITY PROFILES(BESSEL SOLUTION)

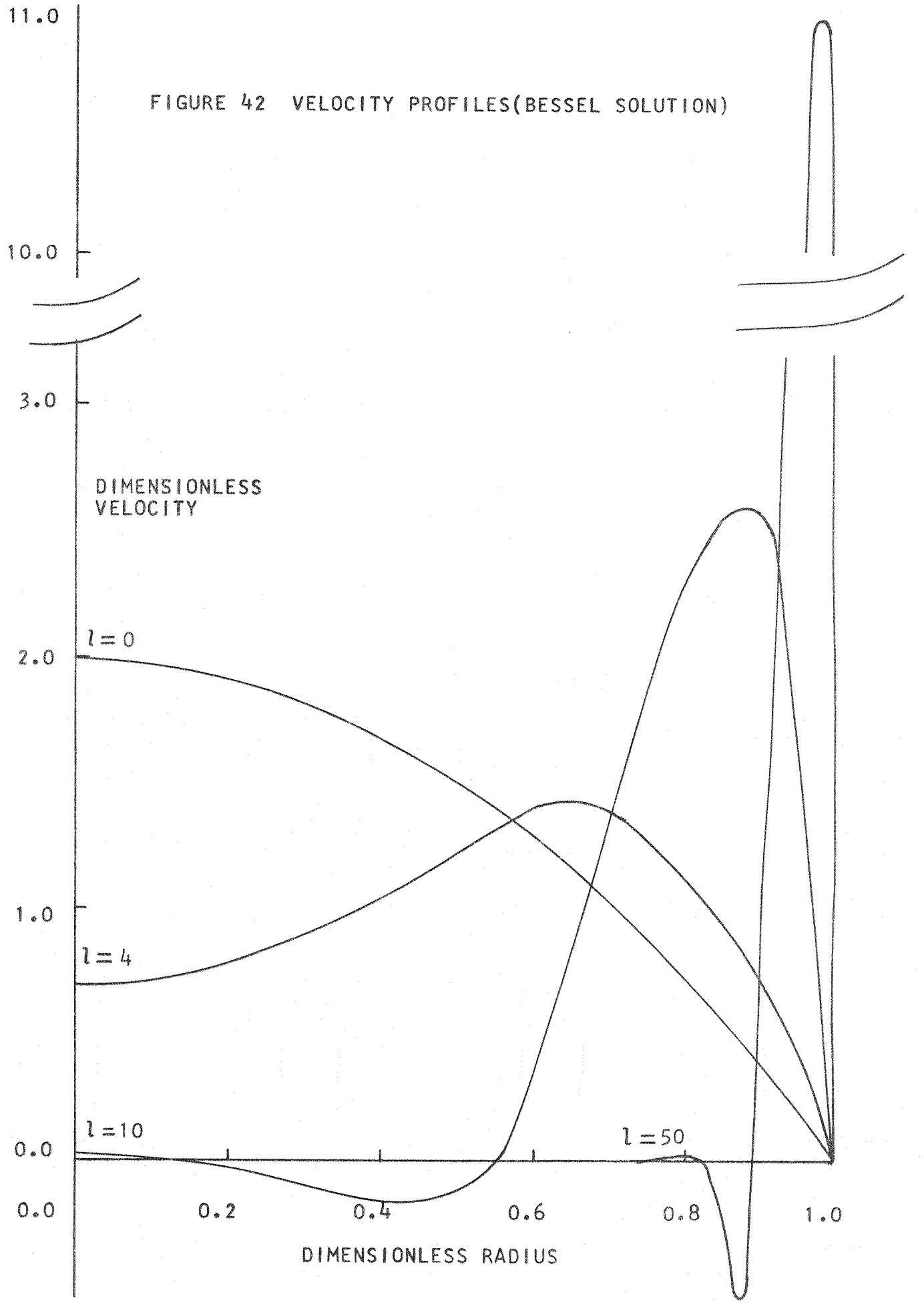

FIGURE 43 EXPONENTIAL DAMPING TERM

$$F(R) = \exp(l.(R-1)/\sqrt{2})$$

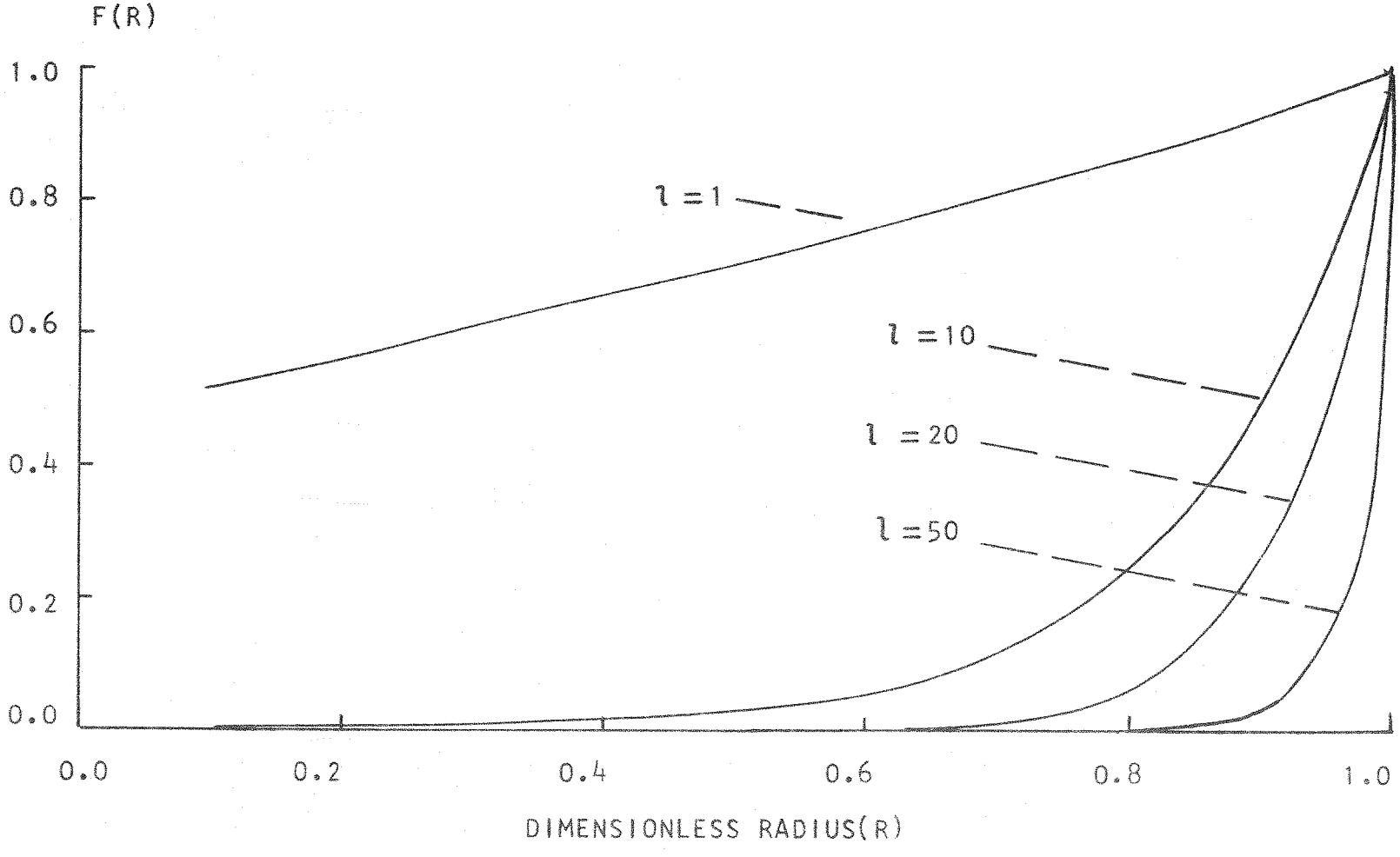

of the theory which characterises this boundary layer formation. The assumption by Hallman that the flow is to be fully developed cannot be immediately reconciled with the generally accepted concept of a free convection boundary layer growing with vertical distance. This is reflected in his Nusselt versus Rayleigh curve as a 0.27 power variation, instead of the usual 0.25 power law of natural convection heat transfer. However similar presumptions have been made previously for free convections in stratified environments.

In an analysis of 'valley winds in stratified air' Prandtl assumes a similar form of differential equation (but one dimensional) to that used by Hallman, Ostroumov, etc, and applies it to a heated inclined plane. The form of solution is assumed and contains both an exponential decay and an oscillatory term. The temperature solution can be compared with Hallman's work and there is agreement in, for example, the position of the maxima and minima, i.e. the temperature solution assumed by Prandtl is

$$T_c = \text{Const.} \exp\left(-\frac{y}{l^*}\right) \cos\left(y/l^*\right)$$

with the relation (linking Hallman's and Prandtl's analyses)

$$l^* = \frac{D\sqrt{2}}{2\,l}$$

This gives turning points at

$$\frac{y}{l^*} = \left(j + \tfrac{3}{4}\right)\pi \qquad j = \text{integer number}$$

i.e. $$\frac{2y}{D} = \frac{\sqrt{2}}{l} \cdot \left(j + \tfrac{3}{4}\right)\pi$$

The agreement between the dimensionless distances (1 - 2y/D) and R is better than 3%.

Prandtl's explanation of the negative portion of the temperature curve is that fluid which has not been heated is carried upwards by frictional forces to a region where the stratification temperature is hotter than the fluid arriving, and hence a dip in the temperature is experienced. Also Schwind and Vliet have observed that under certain

conditions in stratified fluids the boundary layer does not grow, appearing fully developed.

Apart from the fact that similar forms of analysis have been used previously for free convections in stratified flows one of the important effects in boundary layer growth has been shown to be the property variation owing to the large temperature gradients. This effect is indeed large and the natural growth of a free convection boundary layer is small in comparison. Hence there is strong justification in extending the Bessel solution to the free convection limit and applying the 'boundary layer' dimensions, as calculated from a locally applied theory, to the results.

From the relationship

$$R = 1 + \frac{n\pi\sqrt{2}}{l}$$

it is possible to calculate the position of the first zero in the velocity for various values of "l". A plot of the distance of the first zero from the wall is plotted against "l" in Figure 44, and hence the 'boundary layer' thickness at any given Rayleigh number may be determined. These results have been superimposed onto the higher mass flow rate curves where the linear temperature gradient approximation for the theory may be made. The agreement between theory and experiment is not as close at these flow rates as was the case previously, with the results showing a slightly larger growth rate than that predicted by theory.

Convection Velocity

As mentioned previously the maximum velocity at which the tobacco smoke entered the dewar was measured. This is the peak negative velocity and may be compared both in position and magnitude with the results from the Bessel solution. It is also possible to assume a model similar to that proposed by Drake et al where a uniform velocity is assumed

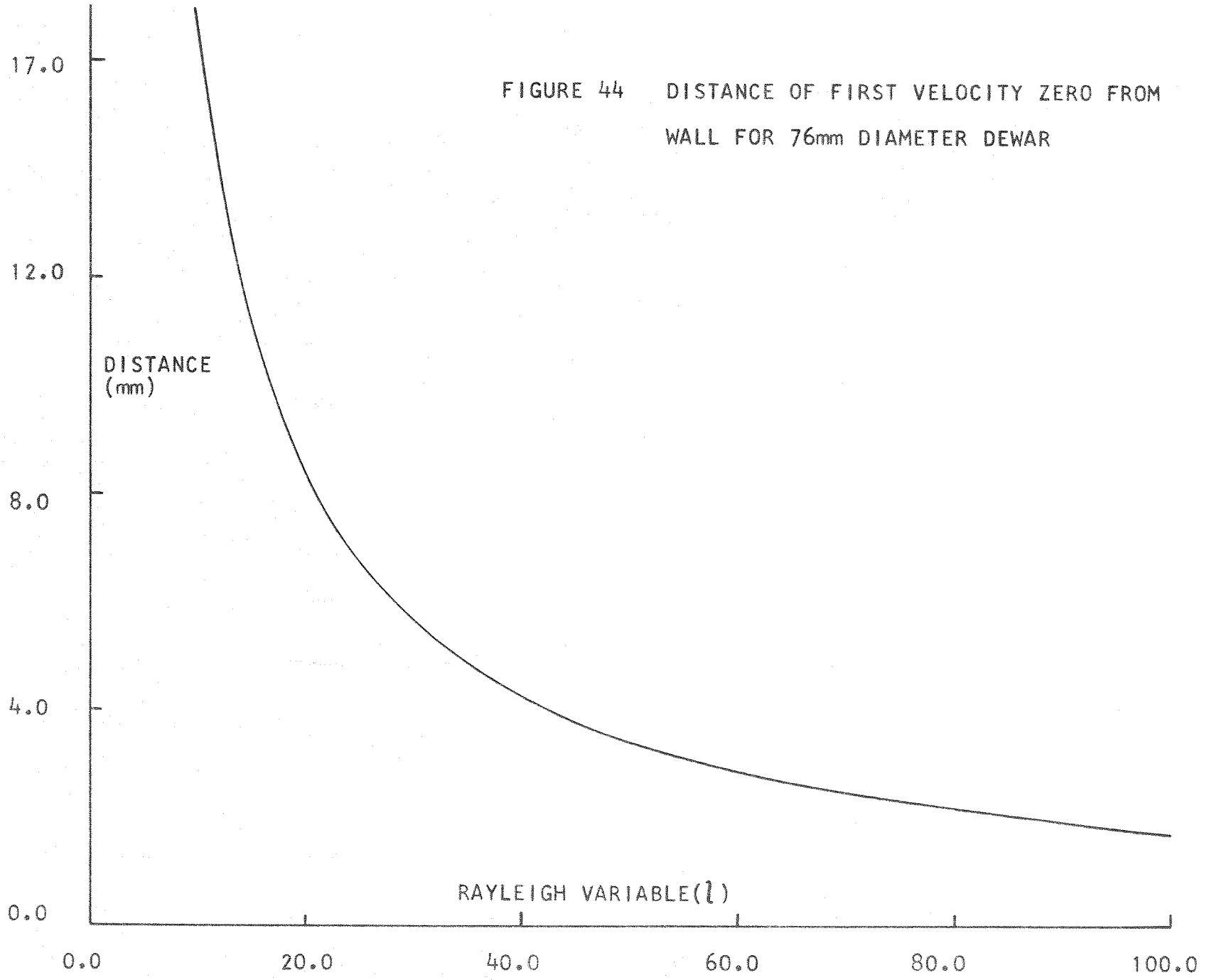

FIGURE 44 DISTANCE OF FIRST VELOCITY ZERO FROM WALL FOR 76mm DIAMETER DEWAR

outside the free convection boundary layer in order to satisfy mass continuity. Unfortunately this latter analysis not only produces rapidly changing velocities with vertical distance ($\approx 1/3$ cm s^{-1} cm^{-1}) but are also of approximately one order of magnitude too large. The assumption that the boundary layer thickness is much smaller than the diameter of the dewar, which is inferred in the analysis, fails in this particular case. It is to be expected from these reports that this analysis will work on larger diameter vessels.

Returning therefore to the Bessel solution, we can calculate the radial position of the first minimum in the velocity profile for various "l" values (see previous modulus and phase equations). The results are plotted in Figure 45. The position of the first minimum can be seen to fall within the region $0.75 < 2r/D < 1.0$ for the Rayleigh numbers encountered in the experiments. This behaviour fits in well with experimental observations. Also we can calculate the magnitude of the dimensionless velocities at these points and the results are presented in Figure 46, plotted against the $\frac{1}{4}$ power of Rayleigh number. The plot is closely linear.

For a given mass flow the average velocity at a given temperature level may be calculated and hence, using Figure 46, the actual velocity. For the two cases considered (where, as before, the limitation is the possibility of approximating the experimental temperature profiles to a linear variation) the results are almost uniform changing over the length of the dewar by about 7%. This is again in general agreement with observations. Figure 47 presents the vertical velocity profiles.

The maximum limit on the negative velocity from the experiments is approximately 6.0 mm s^{-1} and 3.3 mm s^{-1} for overall mass flow rates of 0.078 grm s^{-1} and 0.054 grm s^{-1} respectively. In comparison we have velocities of approximately 3.5 mm s^{-1} and 2.5 mm s^{-1} respectively from the locally applied Bessel solution. The theory produces velocities

FIGURE 45 RADIAL POSITION OF FIRST VELOCITY MINIMUM

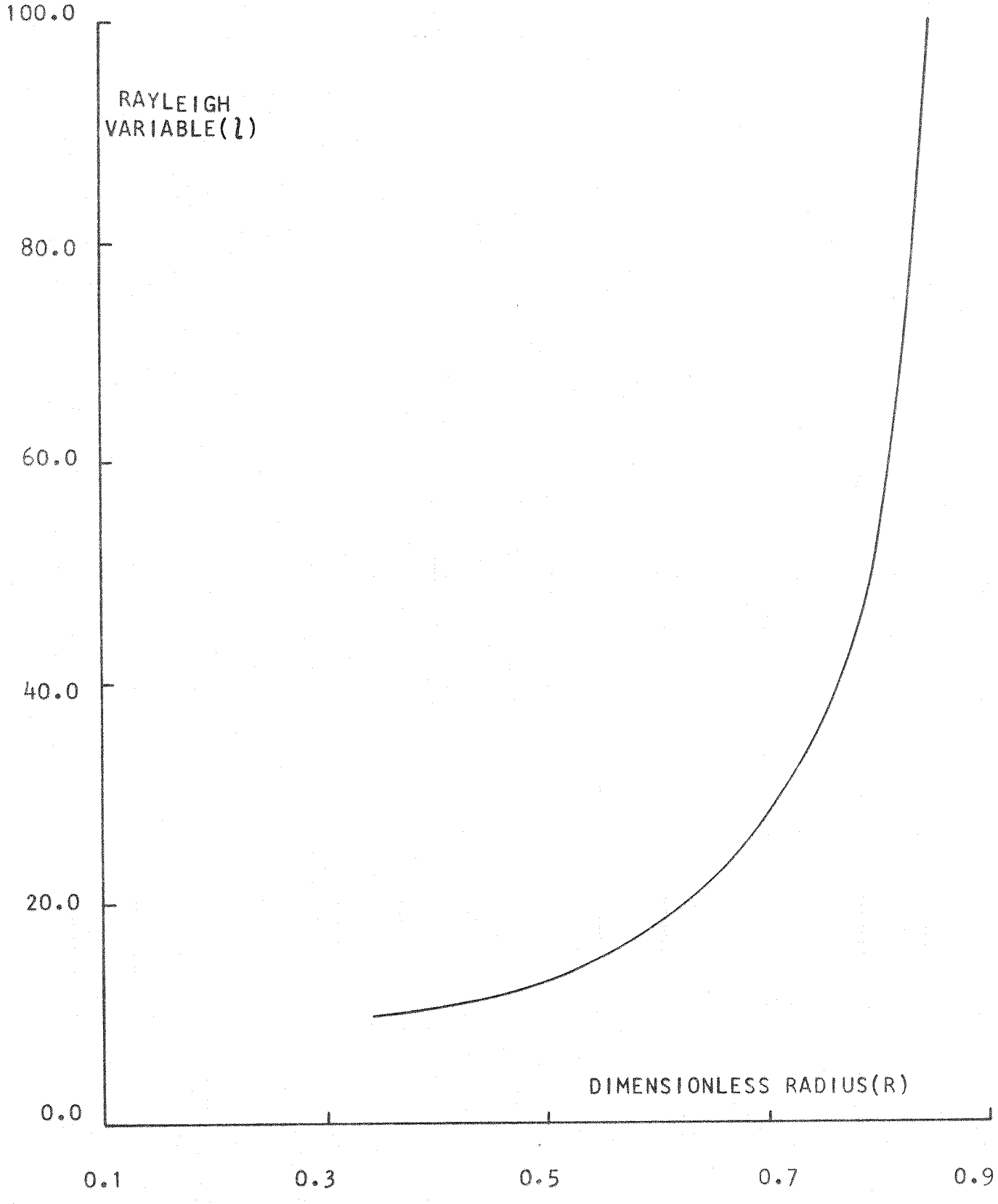

FIGURE 46 DIMENSIONLESS PEAK NEGATIVE VELOCITY

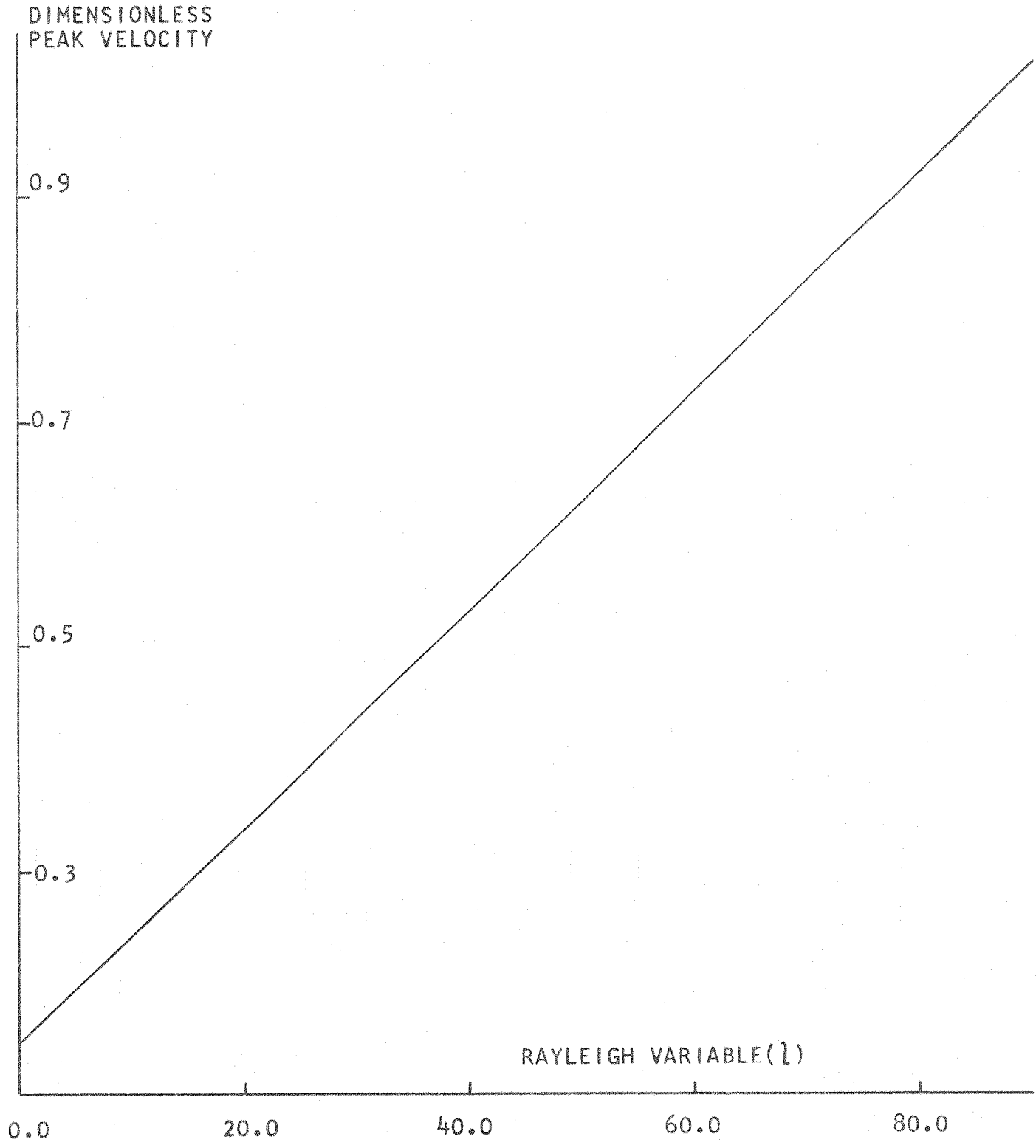

FIGURE 47 PEAK NEGATIVE VELOCITY IN 76mm DIAMETER DEWAR

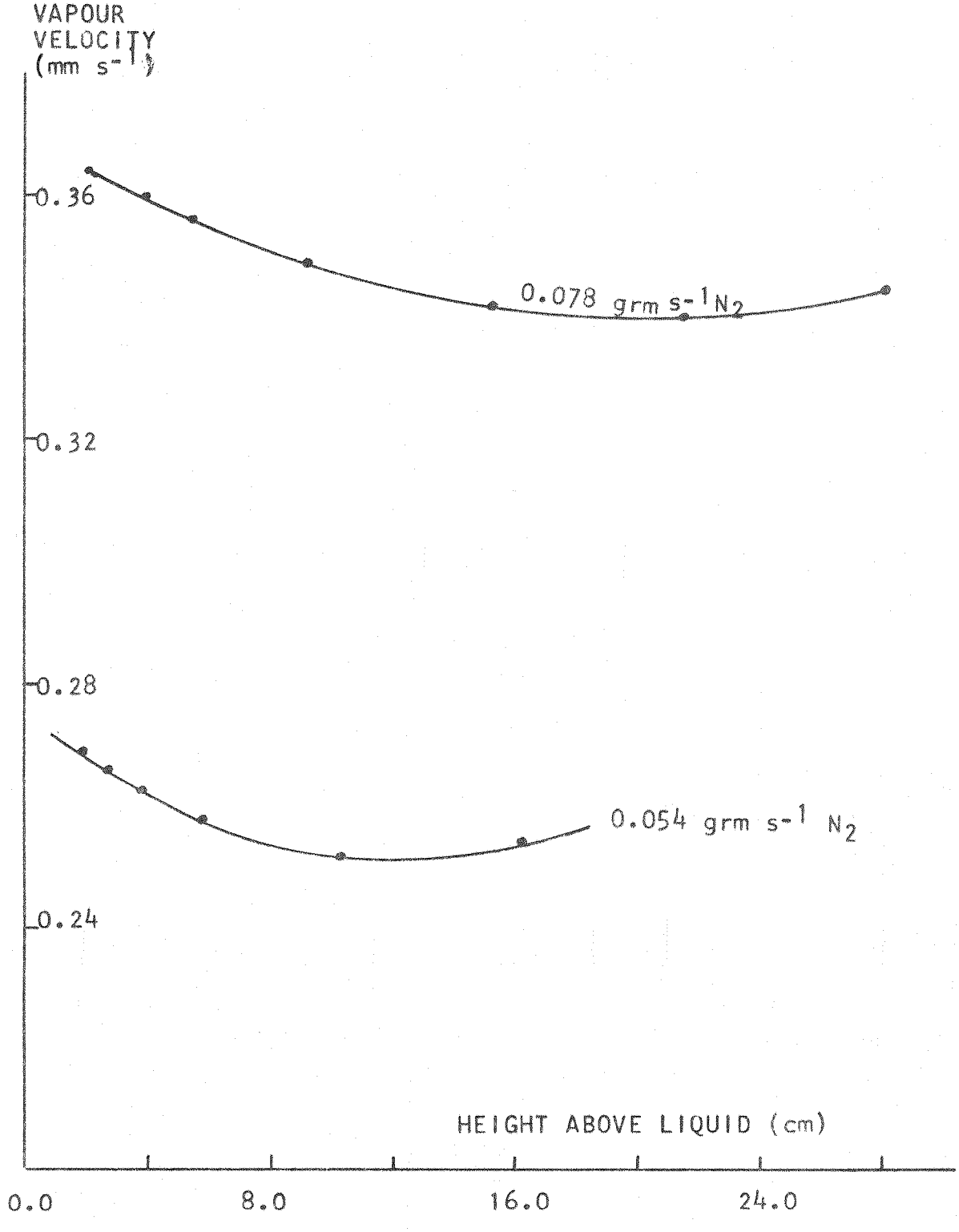

which are of the right order and too small by a factor of 1.5. The influence of the free fall velocity of the tracing element has not been allowed for in the calculations, but this is believed to be very small. For example, the local recirculation generated by an isolated heater maintains a low circulation velocity, and very little tracing element drops below the lowest level of the heater.

In summary, therefore, the theory has generated the correct order of magnitude of negative velocities, being almost uniform vertically despite large temperature gradients, and forming a horizontal velocity profile which suppresses flow in the centre regions, and has an off-axial maximum in the reverse flow. A boundary layer is also seen to form at the wall and grows in an almost linear manner owing to the changing temperature. The theory needs to be refined and expanded not only to produce experimental velocities more accurately, but to incorporate the other observed features of thermosyphoning, and turbulence in the region above the liquid surface.

Accuracy

Absolute Temperature (including reproducibility) $\pm$ 1.0 K

Vertical Position $\pm$ 0.25 mm

Boundary Layer Thickness (including reproducibility) $\pm$ 0.5 mm

Mass Flow Rates $\pm$ 0.001 grms s^{-1}

Time $\pm$ 0.05 secs

CHAPTER 5

And,spite of Pride,in erring Reasons spite
One truth is clear,WHATEVER IS,IS RIGHT

Essay on Man
A.Pope

SUMMARY AND DISCUSSION

Compounded Heat Transfer Graph

The variation of Nusselt number for vertical tubes under free, forced, or mixed convective heat transfer can be seen by reference to Figure 48 where the selected analyses have been arranged. Representative velocity profiles are also superimposed.

It is immediately noticeable that the analyses of free (both open and enclosed) and mixed convections in tubes converge to a similar variation of Nusselt number as the natural convection influence is increased. Both Hallman's mixed convection analysis and Lighthill's thermosyphon analysis behave as a 0.27 power law for intermediate Rayleigh numbers, and Lighthill, Dyer and Elenbaas extend into a purely free convective variation with a 0.25 power law for larger Rayleigh numbers. At this point the temperature profiles have a flat portion in the centre, and the temperature difference with the wall changes within a small distance from the wall. Dyer's relation for the free convection limit has been extrapolated in the graph to cover lower Rayleigh numbers, and it can be seen to closely fit the results of Clarke and Rohsenow as given in Hallman's mixed convection paper. As mentioned previously Colburn's results for water flowing at low velocities in a vertical tube also fit a natural convection law.

The velocity profiles show two main features with either a net positive or net zero flow, and a degree of distortion of the velocity profile dependent on the natural convection influence. These two features are reflected in the characteristic suppression of flow in the core of the fluid for mixed convection, and the high reverse flows in thermosyphoning.

FIGURE 48 HEAT TRANSFER FOR FREE AND MIXED CONVECTIONS IN TUBES

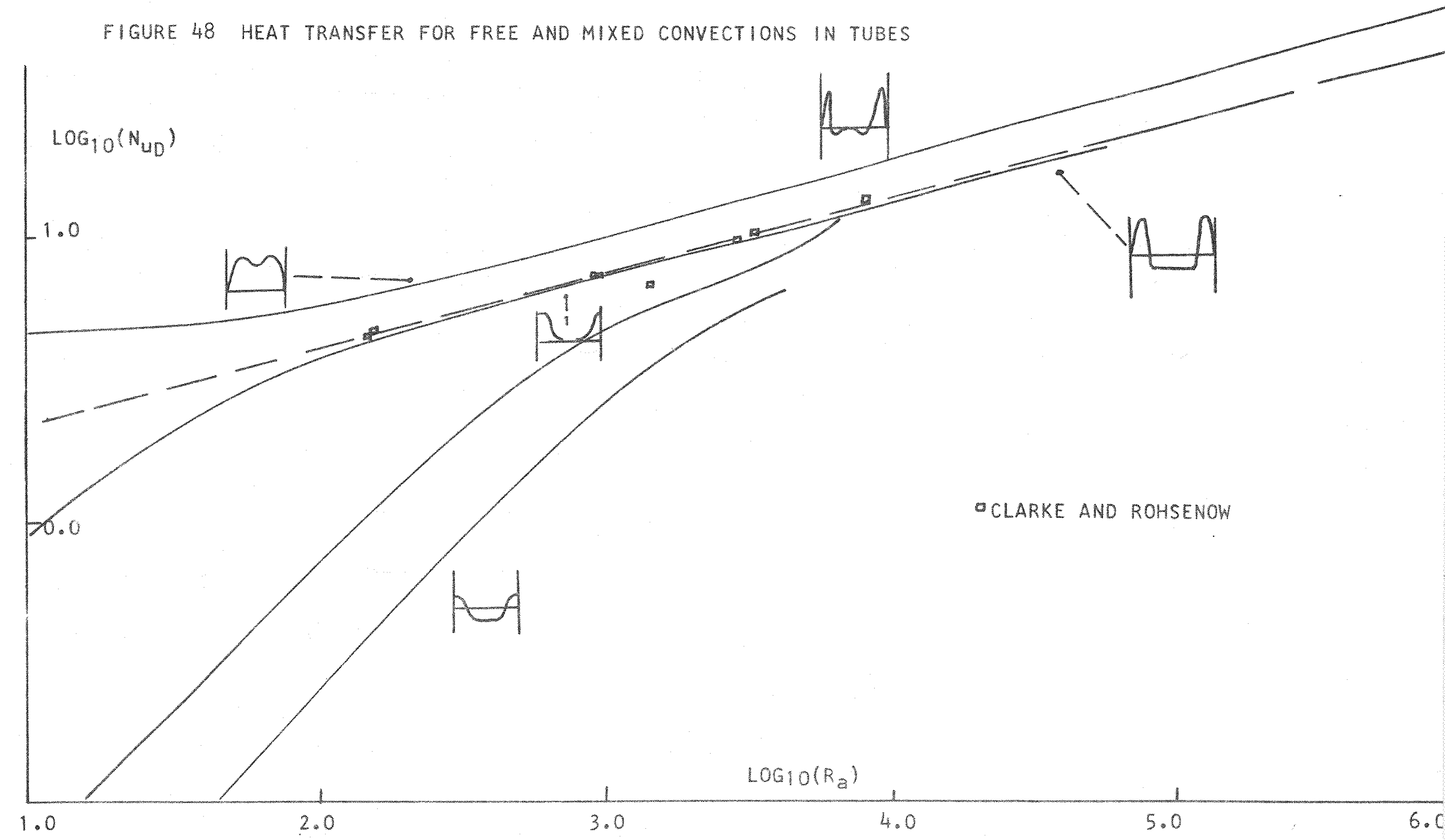

Analysis of Results

(a) Fluid Flow

The mixed convection regime, as we have already seen, is short lived in terms of Rayleigh number variations. The flat plate analyses arranged in the literature survey from the work of Sparrow and Gregg and Eshghy, the work of Acrivos, and the correlation work of Eckert et al, have all amply demonstrated the restricted extent of the mixed convection regime. In the results already presented the Rayleigh number covers the range 10^5 to 10^7. Since we can see that natural convection forces have begun to change the forced convection Nusselt number of 48/11 at a Rayleigh number of approximately 10^2, then we should not expect that the mixed convection influence would extend to the region 10^5 to 10^7. We are led to the conclusion that the interpretation of the results should be based on natural convection considerations. Also the manner in which the flow became turbulent, with waves travelling upwards very close to the wall, suggests a natural convection boundary layer.

Lawrence and Chato have demonstrated the instability of the mixed convection flow in the amplification of disturbances when there is an inflection point in the velocity profile, with the velocity at the centre line less than the velocity at some radial position. Hence there is a tendency at moderately high Rayleigh numbers for the mixed flow to develop into turbulence. At large Rayleigh numbers we should expect a natural convection boundary layer which will eventually itself develop into turbulence. Between these turbulent extremes the Bessel solutions behave in a free convective manner and are stable. A comparison with Prandtl's analysis of the free convection flow in a stratified environment and the Bessel solutions has already shown close similarities.

The flow in a cryogenic vapour column could be considered to consist of a purely free convection boundary layer, and a core which is in reverse flow, satisfying mass continuity demands. The core velocity is assumed

to have a uniform velocity across a given diameter. This type of analysis assumes that the boundary layer thickness is small in comparison with the diameter of the tube. The core velocities obtained from these considerations are not only too large in comparison with experimental results but also decrease away from the mouth of the dewar. The Bessel solutions however produce an off-axial velocity peak in the reverse core flow, and also lead to an almost vertically uniform velocity; both features agreeing with experimental observations. A future extension of this work must be to incorporate a thermosyphoning effect towards the exit of the dewar for low mass flow rates. Dyer has predicted that this flow will be complicated and unstable, yet it appears in practice to be neither.

(b) Heat Transfer

It is possible to incorporate a heat generating term in the equations governing the fluid flow in a vertical tube. Hallman has solved this type of problem and presents the results for various situations. For the case where the fluid gives up heat to the wall a reverse flow next to the wall occurs. In the optimising of leads to superconducting solenoids it would therefore seem necessary to consider the influence of a heat generating lead on its environment, and the resulting fluid flow. Also Donadieu and Damman use a heat transfer coefficient which is determined from pure free convection relationships which would only apply for systems in which the vapour at a distance from the lead is unaffected by the heat flux. This would be the case in large diameter systems, whereas in small systems convection and conduction heat transfer take place. One further point arising from this work is that equilibrium times can be of the order of hours (particularly with respect to the coupling with the nitrogen shield) and for non-continuous operation of solenoids one could possibly not use a steady state solution.

Projected Research

Two features which have not been quantified sufficiently are the effects of thermosyphoning and the extent of the gas-liquid interface. In the former case it is necessary to define an intake temperature and velocity for the thermosyphoned fluid, in order to determine the mixed temperatures. It may even be necessary to measure the wall heat flux and perhaps to try to separate the flows at the exit of the dewar in order to prevent uncontrolled mixing of a discharging boundary layer with incoming fluid. In the case of the gas-liquid interface both the heat transfer and extent of turbulence are required. The effects therefore of gas bubbles discharging from a turbulent surface and temperature profiles and heat flux distributions will have to be determined.

It would be preferable to design a glass system which would permit both the measurement of wall temperatures and radial temperature distributions, and also visual studies. A further feature would be to change the geometry (preferably the diameter) in order to determine the possible different fluid flow regimes.

Finally the heat transfer from a surface in the vapour column should be undertaken for highly symmetrical conditions. This would involve a single extended heated surface down the axis of the dewar with perhaps the return lead being fed through the vacuum space. A more sensitive visual technique would be useful to measure boundary layer growth.

NOMENCLATURE

Roman Characters

A	temperature gradient dt/dx
A_o, A_1	tabulated form of modulus of kelvin functions, order 0, 1 for large argument x (e.g. $x^{\frac{1}{4}} e^{-x/2} M_o(x)$)
A_r	total vertical area
a_n	least squares coefficients of orthogonal polynomials
$B_o(x)$, $B_1(x)$	tabulated forms of value of phase of kelvin functions
$C_o(x)$, $C_1(x)$	order 0, 1 for large argument x (e.g. $\theta_o(x) - x/2$)
C	pressure drop term
C_1, C_2	dimensional factors based on Grashof number. Defined in text.
C_p	specific heat
D	diameter
D_i	partial differential operator with respect to coordinate i e.g. $\partial/\partial i$
E	stream function
E^*	energy parameter (dimensionless)
$f(t)$	general function
$f_o(s)$, $f_1(s)$	functions based on Blasius similarity variable s
G_{r_i}	Grashof number based on dimension i ($\frac{g\beta\Delta T i^3}{\nu^2}$)
g	acceleration due to gravity
$g(t)$	general function
H	total height of plate
h	heat transfer coefficient for free convections from a plane
h_{c_m}	mean heat transfer
h_e	effective heat transfer
I_o	modified Bessel function of first kind order 0
i	$\sqrt{-1}$

J_o Bessel function of first kind order 0

K_o modified Bessel function of second kind order 0

k thermal conductivity

k_c equivalent thermal conductivity combining conduction and convection effects

L a length

l $=R_a^{\frac{1}{4}}$

l_i/l_o ratio of length of unheated starting length l_i to heated length l_o in a tube

$M_o(x)$, $M_1(x)$ modulus of kelvin functions, orders zero and one

M^* momentum parameter (dimensionless)

$\dot{m}$ mass flow of vapour per second

N_{u_i} Nusselt number based on length dimension i = hi/k

N_{u_m} mean Nusselt number

P pressure

P_r Prandtl number $\mu C_p/k$

Q total heat quantity

$Q_n(x)$ approximating polynomial

R dimensionless radius 2r/D

R_{a_i} Rayleigh number (modified) (based on dimension i)

$$\frac{g\rho\Delta T i^3}{\mu^2} \cdot \frac{\mu C_p}{k} \cdot \frac{i}{L}$$

r radial position

s Blasius similarity variable

T absolute temperature

T_o absolute environment temperature

T_s absolute surface temperature

(T_1-T_2) temperature difference between parallel plates

T_c solution of temperature profile from a heated plane in a stratified environment

U, U_o velocity in x (or in polar coordinates z) direction

U_d dimensionless velocity in z polar coordinate direction

U_m mean velocity in z polar coordinate direction

V velocity in y (or polar coordinate r) direction

w distance between plates

X dimensionless distance ($= (G_r \cdot N_u)^{\frac{1}{4}}$)

x vertical coordinate

Y_o Bessel function of second kind, order 0

y horizontal coordinate

Z constant of proportionality

z polar, vertical coordinate

Greek Characters

α thermal diffusivity

β expansivity

δ boundary layer thickness

θ temperature difference

$\theta_o(s)$, $\theta_1(s)$ temperature functions based on Blasius similarity variable s

$\theta_o(R)$, $\theta_o(l\,R)$ phase of kelvin functions, order zero

θ_∞' dimensionless temperature gradient

μ viscosity

ν kinematic viscosity μ/ρ

ρ density

τ time

ϕ dimensionless temperature function

ϕ_n nth orthogonal polynomial

ψ stream function

ω velocity variable

Special Functions

$$\text{erf } x = 2/\sqrt{\pi} \int_0^x e^{-a^2}\, da$$

$$\text{erfc } x = 1 - \text{erf } x$$

$$\text{ierfc } x = \int_x^\infty \text{erfc } a\, da$$

Note: The slash "/" is used to denote division by the variable following. If there is more than one variable then the whole quantity to be divided will be in brackets.

e.g. $(k(T_s - T_o))/2 \,.\, (U_o/\nu.x)^{\frac{1}{2}}$

should be read as

$$\left(\frac{k(T_s - T_o)}{2} \right) \left(\frac{U_o x}{\nu} \right)^{\frac{1}{2}}$$

REFERENCES

Abramowitz and Segun, Handbook of Mathematical Function, p 432, Dover

Acrivos A., Chem, Eng. Sci, Vol 21, p 343-352 (1966)

Barakat H.Z. and Clark J.A., 3rd Int, H.T. Conf, Chicago, Vol II (1966)

Berman R., Brock J.C.F. and Huntley D.J., Cryogenics (August 1964)

Bevans, J.T., Ind. and Eng. Chem., Vol 49, p 114 (1957)

Blasius H.Z., N.A.C.A. T.M. 1256 (1950)

Bodoia J.R. and Osterle J.F., T.A.S.M.E. C 84, pp 40-44 (1962)

Borelius G., Keesom W.H., Johansson C.H. and Linde J.O., Proc. Kon. Akad., Amsterdam, 35 10 (1932)

Carslaw H.S. and Jaeger J.C., Conduction of Heat in Solids, Oxford Clarendon Press, 1947, (1) p 15, (2) p 56

Collins, M.W., Inst. of Mech. Eng. Conf. (1971)

Crooks M.J., Cryogenics (February 1969)

Cryogenics, p 146, March 1961

Donnadieu L. and Damman C., Extrait de la Revue Generale de l'Electricite, February 1968

Dotson J.P., M.S. Thesis, Purdue Univ, Indiana (1954)

Dyer J.R., 4th Int. Heat Transfer Conf, Paris 1970, Vol IV, paper NC2.8

Eckert E.R.G. and Diaguila A.J., T.A.S.M.E. pp 497-504 (1954)

Eckert E.R.G. and Jackson T., N.A.C.A. TN 1015 (1951)

Elenbaas W., Physica 9, p 1 and p 865

Eshghy S., T.A.S.M.E. p 290 (1964)

Evans L.B., Reid R.C. and Drake E.M., Am. Inst. Chem. Eng. Journal, Vol 14, No 2, pp 251-259

Griffiths E. and Davis A.H., Dept of Scientific and Industrial Research Food Investigation, Special Rept No 9, 1931, H.M.S.O.

Hallman T.M., T.A.S.M.E., Vol 78, p 1831 (1956), N.A.S.A. TND-1104 (1961)

Hall W.B. and Price P.H., Institute Mech. Eng. Conf. (1971)

Hamming, R.W., Numerical Methods for Scientists and Engineers, 1962, McGraw Hill

Hanratty T.J., Rosen E.M. and Kabel R.L., Ind. Eng. Chem., Vol 50, p 815 (1958)

Hartnett J.P. and Welsh W.E., T.A.S.M.E., Vol 79(2), p 1551 (1957)

Jakob M., Heat Transfer, Vol I (Wiley and Sons 1957) (1) p 450, (2) p 538

Kalmus H.P., Rev. Sci. Instr. Vol 25, No 3 (1954)

Krondberger H. and Brown A.F., J. Sci. Inst., Vol 24, pp 151-155 (1947)

Kwang-tzu Yang and Nee V.W., 4th Int. Conf, Paris Versailles 1970

Lawrence W.T. and Chato J.C., T.A.S.M.E., p 214 (1966)

Leveque M.A., Annales des Mines, Vol 13, pp 201-300 (1928)

Lighthill M.J., Quart. Jour. of Mech. and Appl. Math., Vol VI, pt 4 (1953)

Lorenz L., Wiedemanns Annalem, 13, 581 (1881)

Lynam P., Ph.D. Thesis, Southampton Univ (1968)

Lynam P. and Scurlock R.G., ICEC2 (1968

Lynam P., Mustafa A. and Scurlock R.G., Cryogenics 9 (1969) 242

Martin B.W., Proc. Roy. Soc. (London) Series A, Vol 230, pp 502-530 (1955)

Martin B.W. and Cohen H., Brit. Journal of Applies Physics, Vol 5, pp 91-95 (1954)

Martinelli R.C. and Boelter L.M.K., Univ. Cal. Pub. in Engin. (1942)

Metais B. and Eckert E.R.G., T.A.S.M.E., pp 295-296 (1964)

Morton B.R., J. Fluid Mech., Vol 8, p 227 (1960)

Mull W. and Reiher H., Gesundh-Ing Beihefte Reihe 1, No 28 (1930)

Ostrach S., N.A.C.A. TN 2635 (1952)

Ostrach S., N.A.C.A. TR 1111 (1953)

Ostroumov G.A., N.A.C.A. TM 1407 (1958)

Perry J.H., Chemical Engineers Handbook 4th Ed, pp 5-31

Pigford R.L., Chem. Eng. Prog. Symp. Series, Vol 51

Pohlhausen E.Z., Angew Math U Mech, Vol 115 (1921)

Prandtl L., Essentials of fluid dynamics, Blackie & Son (1952) p 422

Rohsenow W.M. and Choi H.Y., Heat Mass and Momentum Transfer, Prentice Hall (1961)

Rosen E.M. and Hanratty T.J., A.I.CH.E., pp 112-123 (1961)

Rosenbaum R.L., Rev. Sci. Inst., Vol 39, No 6 (1968)

Seban R.A. and Shimazaki T.T., T.A.S.M.E., Vol 73, pp 803-809 (1951)

Schmidt E. and Beckmann W., Technische Mechanik und Thermodynamik, Vol 1, (1930) pp 341-349 and 391-406

Schwind R.G. and Vliet G.C., Proc. H.T. Fluid Mech. Inst., (1964) Stanford Univ. California

Scorer R.S., Natural Aerodynamics, Pergamon (1958)

Scott R.B., Cryogenic Engineering, Van Nostrand (1966), (1) p 240, (2) p 165, (3) p 333, (4) p 127 (5) p 152

Sparks L.L., Powell R.L. and Hall W.J., NBS Reports 9712, 9721

Sparrow E.M., N.A.C.A. TN 3508 (1955)

Sparrow E.M., Ph.D. Thesis, Harvard 1956

Sparrow E.M. and Gregg J.L., (1956(i)), T.A.S.M.E., Vol 78, pp 435-440

Sparrow E.M. and Gregg J.L., (1956(ii)), T.A.S.M.E., Vol 78, p 1823

Sparrow E.M. and Gregg J.L., T.A.S.M.E., Vol 80, p 879 (1958)

Sparrow E.M. and Gregg J.L., J. of App. Mech, p 133 (1959)

Tatom J.W. and Carlson W.O., 3rd Int. H.T. Conf. Chicago, Vol II, p 163 (1966)

Weise R., Forschung a.d. Geb. d. Ingenieur-wes, 6, 281, (1935)

White G.K., Experimental Techniques in Low Temperature Physics, 2nd Ed., p 148, Clarendon Press

Williams J.E.C., Cryogenics, December 1963, p 234

ACKNOWLEDGEMENTS

I would like to thank my supervisor Dr R.G. Scurlock for his support and encouragement throughout the course of this research.

I would also like to thank many of the staff and students of the Physics Department who in numerous ways have given help and assistance, and in particular:

Professors E.W. Lee, G.W. Hutchinson and K.J. Barnes, for the use of the Physics Department facilities;

Dr I. Morton and Dr K. Kellner for useful discussions and advice;

Dr Morton also undertook the Spline curve fitting computation and with Dr P. Lynam was in part responsible for prompting the author to investigate the natural convection boundary effects;

Dr G. Daniell for valuable advice on mathematical problems;

Mr A. Acton for allowing me to calibrate my thermocouples along with his germanium thermometers and for his efforts in nursing a temperamental refrigerator;

The technical staff, Mr B. Fewell and Mr B. Heath for their assistance in the manufacture and assembly of parts of the apparatus.

The Science Research Council for a maintenance award.

APPENDIX A

CURVE FITTING AND ORTHOGONAL POLYNOMIALS

A four term polynomial is recommended by White for least squares fitting and interpolating thermocouple calibration data. However, in the case of the gold iron thermoelement, this polynomial cannot describe the low temperature maxima and minima in the thermopower. It is necessary to increase the degree of the polynomial and this leads to inherent computational difficulties.

Any additional information which one requires a polynomial to include by adding another term becomes progressively more difficult, since t^n behaves in much the same way as t^{n+1}. This is demonstrated by Schwarz's inequality:

$$\left(\int f(t)\, g(t)\, dt\right)^2 \leqslant \int (f(t))^2\, dt \int (g(t))^2\, dt$$

where the integration is over a given interval. If the two functions are equal the equality holds while if the two functions are orthogonal the left hand side by definition is zero. This is therefore a measure of the "difference" between functions and it can easily be shown that the equality condition is almost met for polynomial terms, of moderately low orders.

e.g. in the interval $0 < t < 1$ we have for t^n and t^{n+1}

$$\left(\frac{1}{2n+2}\right)^2 \leqslant \frac{1}{2n+1} \cdot \frac{1}{2n+3}$$

This similarity is reflected in the determinant of the set of simultaneous, linear, algebraic, equations defining the coefficients of the least squares fitting polynomial. Hamming has shown that this Hilbert determinant rapidly becomes very small, being characteristically unity for order one and 3.7×10^{-12} for order five. It is obvious that with numbers like

these rounding error problems are easily going to arise even for medium powers of polynomials.

A simpler solution is to consider the approximating polynomial as a series of mutually orthogonal functions. The chief advantage of this method is that the coefficients of the functions may be calculated separately rather than having to solve the whole set of simultaneous equations. These coefficients automatically provide a least mean squares fit. A further advantage is that it is a more economical process since there is no need to recalculate all previous coefficients when more are required; it is only necessary to determine the extra functions and coefficients.

The ICL library subroutine F4CFORPL uses orthogonal monic polynomials which are generated on the data points. An explanation of their origin is as follows:

Let the approximating polynomial be

$$Q_n(x) = \sum_{n=0}^{N} a_n \phi_n(x)$$

orthogonality is defined by the dot product

$$(\phi_n, \phi_m) = 0 \qquad n \neq m$$

$$= N_m \qquad m = n$$

now

$$\phi_n = x\,\phi_{n-1} + \sum_{r=0}^{n} C_r \phi_r \qquad (1)$$

forming the dot product with ϕ_{n-1} we have

$$(\phi_{n-1}, \phi_n) = 0 = (\phi_{n-1}x, \phi_{n-1}) + C_{n-1}\,N_{n-1}$$

$$C_{n-1} = -\left(\frac{x\,\phi_{n-1}, \phi_{n-1}}{N_{n-1}}\right)$$

$$\phi_n = x\,\phi_{n-1} + C_{n-1}\,\phi_{n-1} + C_{n-2}\,\phi_{n-2} + \sum_{r=0}^{n-3} C_r \phi_r$$

similarly

$$\phi_{n-1} = x\,\phi_{n-2} + C_{n-2}\,\phi_{n-2} + \sum_{r=0}^{n-3} C_r\,\phi_r$$

subtracting and rearranging we have

$$\phi_n = x\,\phi_{n-1} + C_{n-1}\,\phi_{n-1} + (\phi_{n-1} - x\,\phi_{n-2})$$

forming the dot product with ϕ_{n-1}

$$0 = (x\,\phi_{n-1}, \phi_{n-1}) - (\phi_{n-1}x, \phi_{n-1}) + N_{n-1} - (x\,\phi_{n-2}, \phi_{n-1})$$

$$N_{n-1} = (x\,\phi_{n-2}, \phi_{n-1}) = -\,C_{n-2}\,N_{n-2}$$

hence

$$C_{n-2} = -\frac{N_{n-1}}{N_{n-2}}$$

Considering ϕ_{n-1} and ϕ_{n-2} in a similar way we can show C_{n-3} is zero. In fact all other constants C_{n-3}, C_{n-4} etc can be shown in this way to be zero.

Thus from (1)

$$\phi_n = x\,\phi_{n-1} - \frac{(\phi_{n-1}x, \phi_{n-1})}{N_{n-1}}\,\phi_{n-1} - \frac{N_{n-1}}{N_{n-2}}\,\phi_{n-2}$$

which is the recursion formula for the polynomials.

The coefficients are determined from the condition of minimising the mean square error on the data points. However as mentioned this condition is met in the definition of the approximating polynomial and orthogonality.

$$\frac{\partial}{\partial a_k} \sum_i (y_i - Q(x_i))^2 = 0$$

$$-2 \sum_i (y_i - Q(x_i)) \cdot \phi_k = 0$$

$$2\left(\sum_i y_i\,\phi_k - a_k \sum_i \phi_k\,\phi_k\right) = 0$$

$$\therefore a_k = \frac{\sum_i y_i\,\phi_k}{\sum_i \phi_k\,\phi_k}$$

Assuming

$$\phi_o = 1$$

$$C_1 = 0$$

we can then construct the approximating polynomial $Q_n(x)$. The argument can be extended by considering the minimisation of the weighted mean squares but the form remains the same.

In practice, these polynomials were intrinsically very well behaved, and their apparent instability shown by eventually producing oscillations was due to their highly flexible nature in being able to reproduce the data points. It could be imagined that increasing the number of polynomials would determine the true physical characteristic of a curve to a closer and closer approximation. However, this is not necessarily the case, since the only criteria the mathematics imposes is that the sum of the squares of the residuals be a minimum, and it says nothing of the individual residuals. A systematic variation in residuals can occur particularly if there is a data point with a large deviation. In general it is difficult to define a best fit curve, and one can only select the least complex curve consistent with a low root mean square error and randomised residuals.

The choice of an approximating curve was made, as mentioned in the apparatus section, on the basis of three features of the curves. The root mean square error was seen to decrease rapidly with increasing number of polynomials and then to change abruptly and decrease very slowly. Also the first differential proved to be a very sensitive guide to the behaviour of the fit, far more so than the curve itself. It showed how the fit was progressing and how complex the curve was becoming. Finally a check on the residuals revealed whether the fit had produced a curve with low deviations on the data points and with no systematic variations. In the cases of the three gold iron samples the curves which showed the best features were those which had their

root mean square errors on the knee of the RMS versus number of polynomials curve. Figures 49 to 51 demonstrate these effects as produced on the first sample of gold-iron.

The polynomials were rearranged into the form of a simple power series for convenience. The thermal emf was expressed in terms of temperature, but by the reversion of series (Abramowitz and Segun) the temperature can easily be expressed in terms of the emf.

Coefficients of Polynomials in Series Form

	Spool 1	Spool 2	Spool 3
T^0	0.474523069139 E 01	0.476247161871 E 01	0.466553548054 E 01
T^1	-0.868506174981 E-02	-0.633616122684 E-02	-0.915383541417 E-02
T^2	-0.654279305138 E-03	-0.105606988777 E-02	-0.546711534007 E-03
T^3	0.300990238196 E-04	0.546909770969 E-04	0.247500506814 E-04
T^4	-0.681394260932 E-06	-0.149316375984 E-05	-0.547625950462 E-06
T^5	0.828107842650 E-08	0.238660489897 E-07	0.645979283313 E-08
T^6	-0.521966379564 E-10	-0.225258532842 E-09	-0.393454301571 E-10
T^7	0.134138699967 E-12	0.116241089916 E-11	0.973872013739 E-13
T^8		-0.252675037681 E-14	

FIGURE 49 BEHAVIOUR OF FIRST DIFFERENTIAL OF CURVE FIT

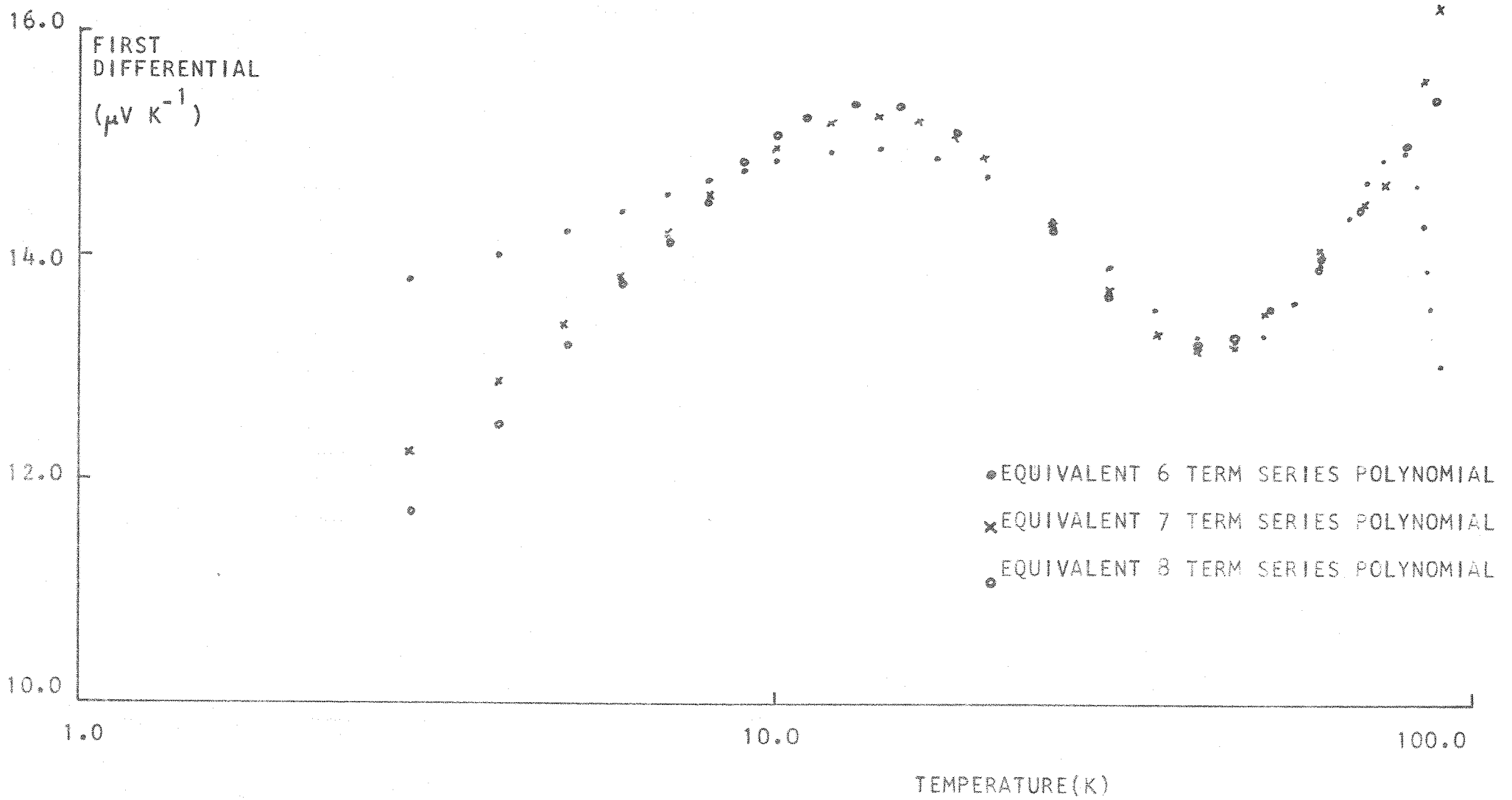

FIGURE 50 BEHAVIOUR OF RMS VALUE OF CURVE FIT

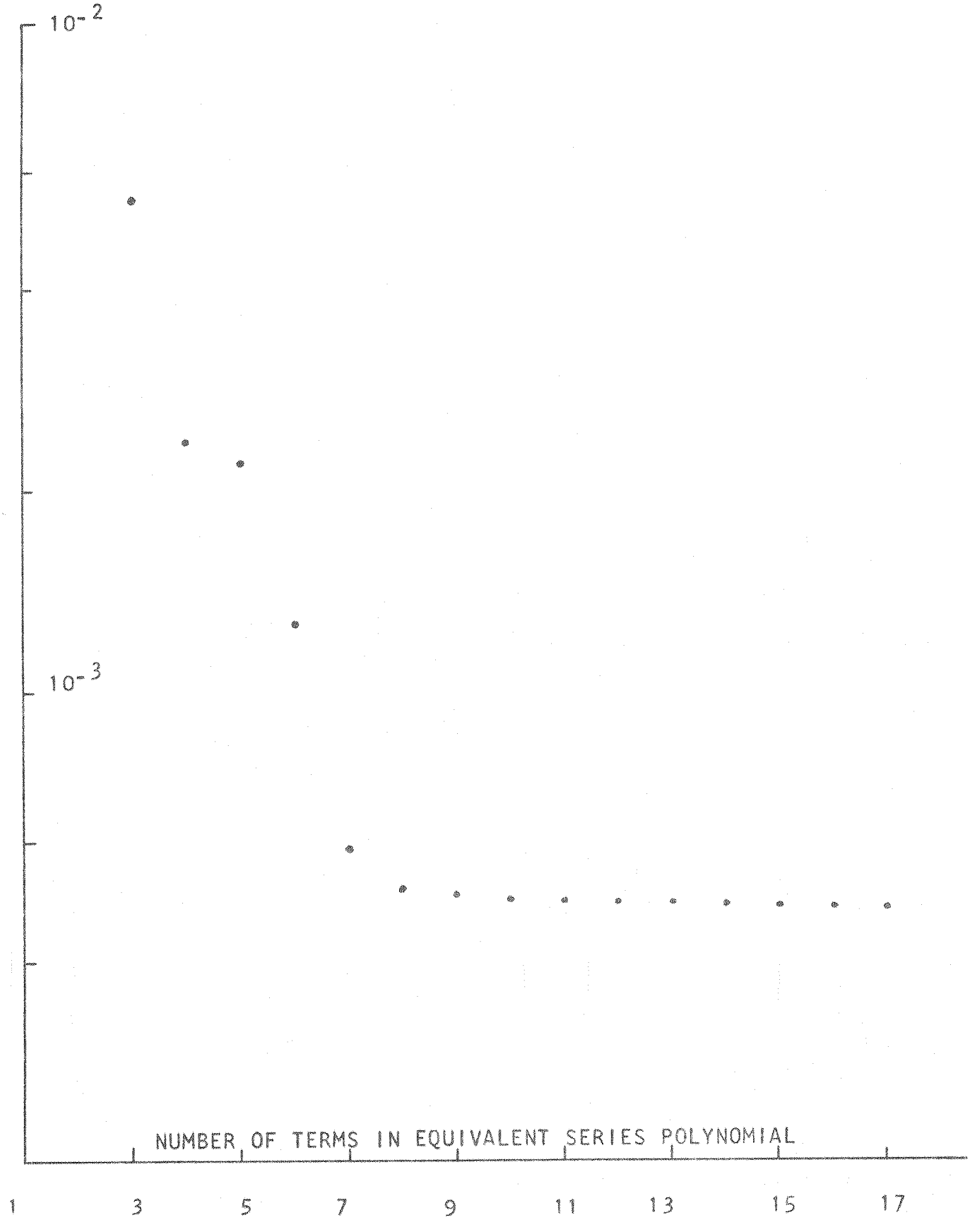

FIGURE 51 PLOT OF RESIDUALS ON DATA POINTS

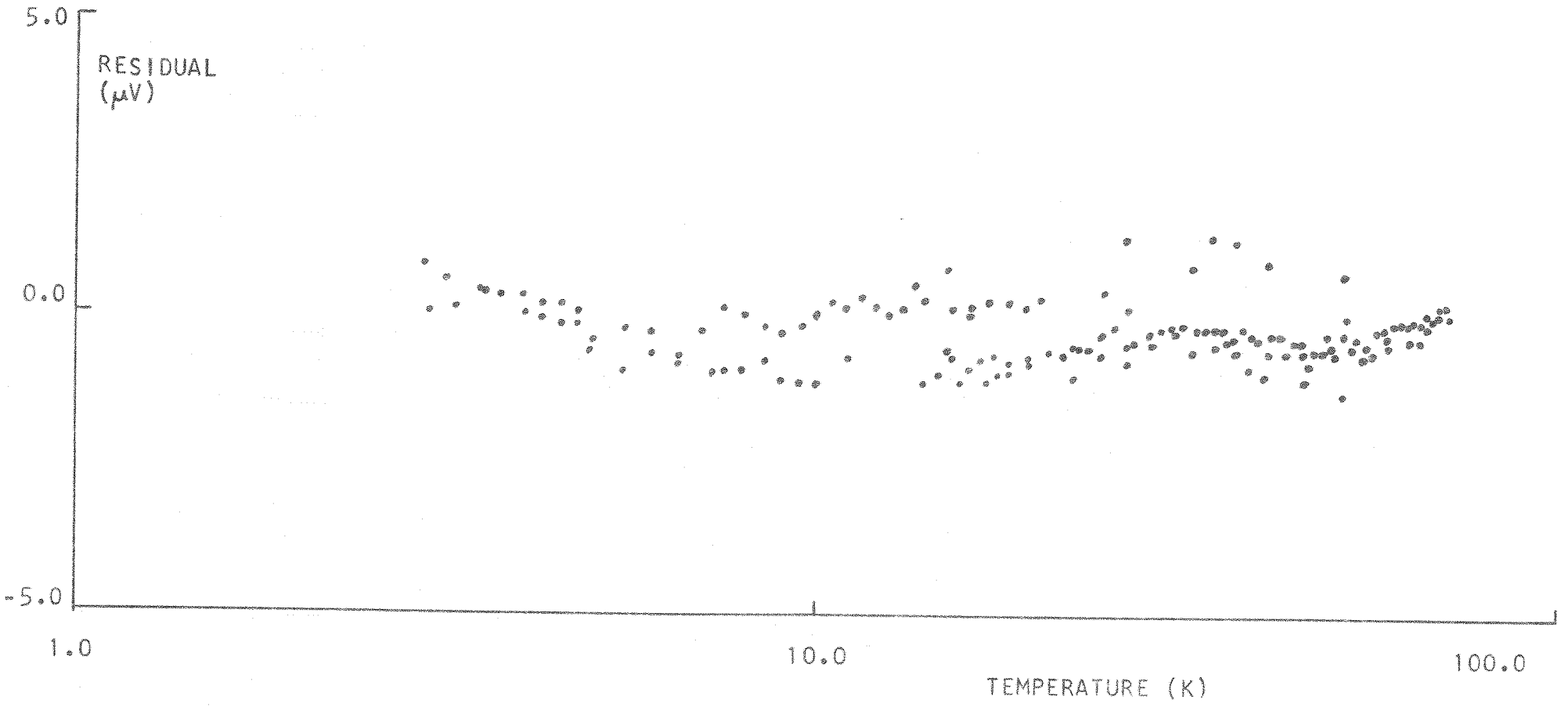

APPENDIX B

NOTE ON PENETRATIVE CONVECTION

It was previously mentioned that the tobacco smoke formed into 'droplets' and that the reason for this behaviour was not originally understood. No experimental work was undertaken to investigate this feature alone since time did not permit it. However an understanding of this phenomenon was sought from published work, and a feasible explanation was found in a book by Dr R.S. Scorer.

In his book Dr Scorer describes the formation of thermals in the atmosphere and also produces experimental evidence to support his theory. In order to simulate the thermals he inverts the buoyancy force and uses a 'heavy' salt solution with a barium sulphate precipitate (to make the cloud white) and allows it to sink into a container of water. The cloud becomes pear shaped with a long tail and either grows or is eroded depending upon the temperature gradient of the environment.

Figure 52 shows the idealised structure of the head of the thermal and with it is a sketch of an actual 'thermal' from his experimental evidence. It is the vortical motion which produces the rounded leading part with a continuous mixing with the environment occurring on this surface.

The similarity between this work and the appearance of the tobacco smoke clouds is very striking, and the explanation seems readily applicable to the stratified nitrogen vapour and the slightly denser tobacco cloud.

FIGURE 52 PENETRATIVE CONVECTION "THERMALS"

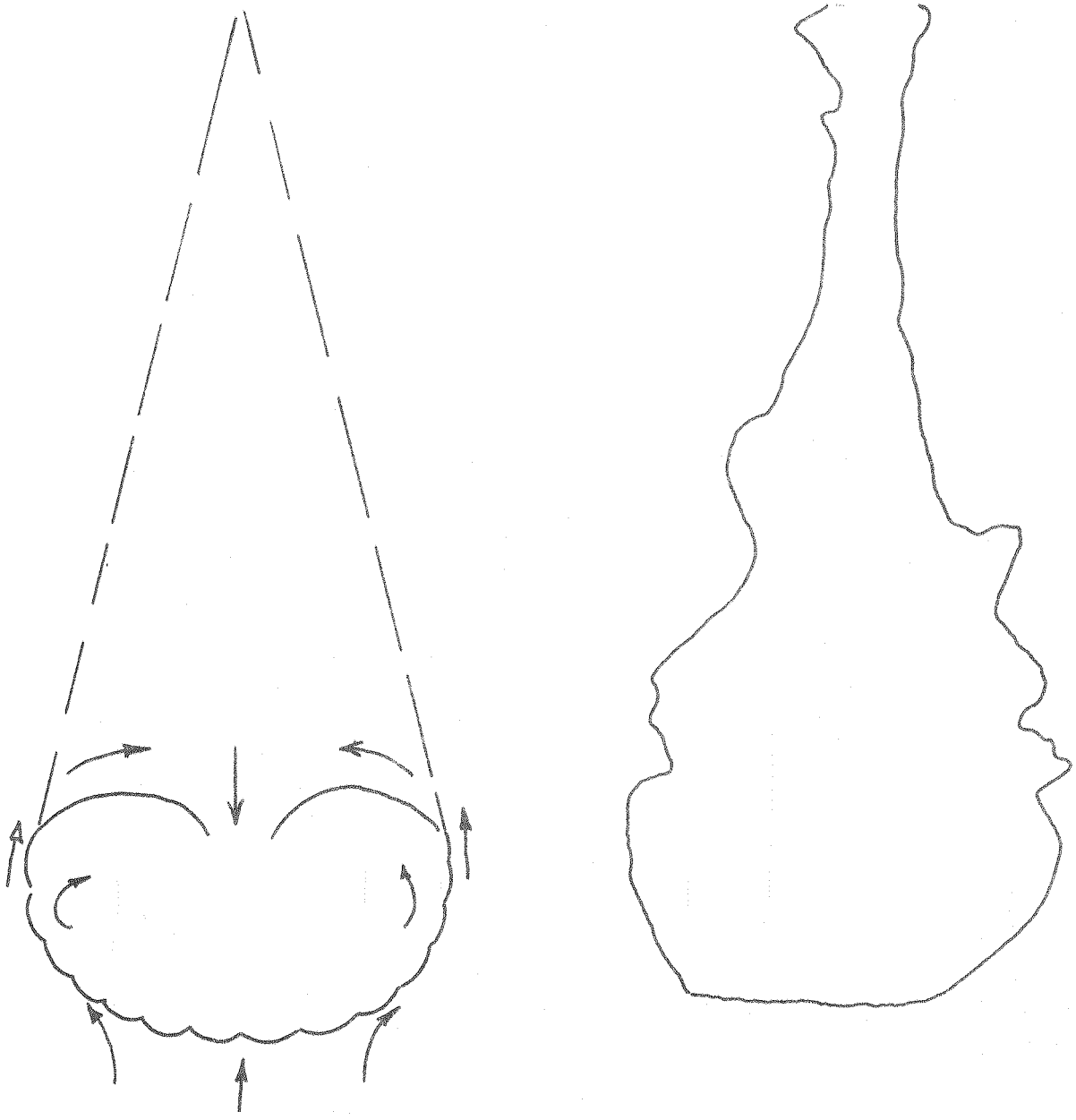

APPENDIX C

The following published papers were included in the bound thesis. These have not been digitised due to copyright restrictions, but the links are provided.

J.Boardman, P.Lynam, R.G. Scurlock (1970) “Reduction of evaporation rate of cryogenic liquids using floating hollow polypropylene balls.” Proc.ICEC3 Cryogenics Vol. 10, pp 133

APPENDIX D

The following published papers were included in the bound thesis. These have not been digitised due to copyright restrictions, but the links are provided.

J.Boardman, P.Lynam, R.G. Scurlock (1972) “Solid/vapour heat transfer in helium at low temperatures” *Inernational Cryogenic Engineering Committee*; Eindhoven, Netherlands, 24 May, 1972

APPENDIX E

The following published papers were included in the bound thesis. These have not been digitised due to copyright restrictions, but the links are provided.

J.Boardman, P.Lynam, R.G. Scurlock (1973) “Complex flow in vapour columns over boiling cryogenic liquids.” Cryogenics Vol. 13 Issue: 9, pp.520-523

J.Boardman, P.Lynam, R.G. Scurlock (1973) “ 50 kG gas cooled superconducting solenoid operated at 13 K.” Cryogenics Vol. 13 Issue: 9, pp. 524-525